DESIGN, SYNTHESIS, AND BIOLOGICAL EVALUATION OF NOVEL HETERO-BIVALENT LIGANDS TARGETING KINASES

by
Samanthreddy Kedika

A Dissertation Submitted to
The Department of Pharmacological and Pharmaceutical Sciences
College of Pharmacy
University of Houston

In Partial Fulfillment of the Requirements for the Degree of

Doctor of Philosophy

in Pharmacology/Medicinal Chemistry

Chair of Committee: Dr. D. Gomika Udugamasooriya

Committee Member: Dr. Gregory D. Cuny

Committee Member: Dr. Ke-He Ruan

Committee Member: Dr. James M. Briggs

Committee Member: Dr. Damian W. Young

University of Houston
April 2020

DEDICATED TO MY FAMILY AND FRIENDS

ACKNOWLEDGMENTS

First of all, I would like to thank my supervisor Dr. D. Gomika Udugamasooriya for continuously supporting throughout all these years. This dissertation would not have been possible without your encouragement, guidance, and belief in me. Thank you for providing honest feedback on my weak areas and suggestions on how to overcome them. With your training, I learned how to solve problem, not only in science but in real life too! You were available all the time whenever I needed and addressed all the issues. I really appreciate your patience. Thank you for providing me excellent support and making my scholarly journey more meaningful.

I would like to thank my committee members, Dr. Gregory D. Cuny, Dr. Ke-He Ruan, Dr. James M. Briggs, and Dr. Damian W. Young for your scholarly suggestions during my proposal defense and in the follow-up meeting. Thank you for honest criticism and giving me a prompt but valuable feedback that helped me to craft my research and dissertation.

I would also like to thank my lab members. Satya, most of the lab techniques I learned from you. I appreciate your time and effort in explaining the minute things and make me understand. Tanvi, I learned a single experiment but the most crucial one from you. Thank you for teaching with extreme care. I would also like to thank my other lab members Vineeta, Aaron, Jaspal, Joseph, and Haowen for your company and scholarly discussions.

I also want to thank my cohorts; Youngki, Yan Li, Pavan; my departmental friends Ananthalakshmi, Raghavendra, Anumitra, Sandeepan, Sanket, Kevin

and Mohan; my seniors, Sameer and Saleem; my master's friends Chandu Sekhar, Praveen for their friendship and support. Thank you for making this journey memorable.

Finally, I would like to thank my family (mom, dad and brother) for providing unconditional emotional support during all these years. I am here today just because of you.

ABSTRACT

Hetero-bivalent ligands consist of two copies of monomers that are connected through a linker. They show improved affinity towards their target through an avidity effect and can also enhance specificity, as part of the binding pocket may be absent in a similar target. This strategy was successful in yielding potent and specific kinase inhibitors by simultaneously targeting ATP and secondary peptide binding pockets. We innovatively apply this concept in two different kinase systems where we link low-affinity ATP binding pocket targeted small molecule PP2 with natural peptides that recognize secondary binding sites to produce potent and or specific hetero-bivalent ligands.

In the first application, we targeted Extra-cellular Regulated Kinase5 (ERK5) that is known to play key roles in maintaining cancer stem cell signaling in a variety of cancers. The conventional ATP binding site inhibitors have not yet yielded expected levels of anti-cancer effects, due to complexities in converting ERK5 activation into Cancer Stem Cell (CSC) biological effects. Therefore, we hypothesized that designing a hetero-bivalent ligand, which simultaneously blocks a unique regulatory peptide interaction involved in upstream ERK5 kinase activation, and the conventional ATP binding pocket, produces stronger CSC biological effects. The active hetero-bivalent ligand ERK5.1 (i). inhibited ERK5 activation and kinase activity (IC_{50}~8.5 μM) simultaneously, in two independent assay systems (ii). inhibited CSC activities, such as colony formation, migration and cell proliferation (IC_{50}~6.5 μM)

In the second application, we expanded the idea of using peptide sequences belonging to the same protein as the non-ATP binding site moiety in hetero-bivalent ligand design. Typically, these secondary peptide sequences are derived from substrate peptides from interacting proteins or structure based or combinatorial methods. The use of an already existing natural peptide sequence of the same kinase that uniquely interacts with a binding pocket within the same kinase as the non-ATP binding moiety in hetero-bivalent ligand design has never been investigated. We selected EphA3 kinase as a model system because of known natural peptide sequence in the SAM domain linker region, which turns back and binds to the bottom of EphA3. We connected this unique sequence to a PP2 analogue. Using a combination of structure and combinatorial approaches, we optimized the much longer linker (57 Å) to yield potent hetero-bivalent ligand EPHB2.3 (K_d~250 nM). We also report our effort to the convert the linker part of EPHB2.3 to gain additional binding affinity.

TABLE OF CONTENTS

LIST OF FIGURES

LIST OF SCHEMES

1. HETERO-BIVALENT LIGANDS TARGETING KINASES

1.1. Multivalent ligands and concept of avidity:

Multivalent interactions of biological molecules play a crucial role in biochemical events.[1-2] Synthetic multivalent ligands were designed to understand and mimic these interesting interactions of biological molecules, and proved to be successful in designing probes and inhibitors for various cellular applications.[3-5] These ligands consist of multiple copies of monomers that are tethered onto a linker scaffold. They exhibit significant improvement in binding affinity towards the target when compared with constitutive weak binding monomers.[6-8] Based on the type of interacting monomers, multivalent ligands are further divided into two types: (i). homo-multivalent ligands exhibiting multiple copies of similar monomers (ii). hetero-multivalent ligands consisting of multiple copies of different monomers. While homo-multivalent ligands can only exhibit improved affinity towards the target, hetero-multivalent ligands also exhibit a high degree of specificity as they engage different interaction sites at the same time. As a result, hetero-multivalent ligands received much attention in designing molecules targeting proteins with very similar homologous structures.

The enhancement of affinity incrementally using multivalent ligand design is usually termed “avidity”. Simultaneous binding of these monomers likely produces this marked increase affinity.[9-10] For example, when a hetero-bivalent ligand binds to a target, binding of one monomer forces the second monomer in proximity to

that target, which increases its local concentration in target surroundings. As a result, the second monomer binds to the target more easily. If the second monomer dissociates from the target, the partially bound monomer is forcefully enhances rebinding. As a result of binding and rebinding, the hetero-bivalent ligands can exhibit exponential gains in affinity and selectivity towards the target.[11-12]

Thermodynamically, the binding free energy ($\Delta G_{binding}$) of a typical hetero-bivalent ligand binding with a target is equal the sum of the individual binding free energies of two monomers (ΔG_1, ΔG_2) and the binding free energy associated with linking two monomers (ΔG_{other}).[13] It can be expressed using the following equation:

$$\Delta G_{binding} = \Delta G_1 + \Delta G_2 + \Delta G_{other} \quad \text{.....(1)}$$

The equation is a simple model explaining the binding free energy of hetero-bivalent ligand with the target. In this model, ΔG_1 and ΔG_2 remain constant as they are intrinsic properties of monomers. ΔG_{other} corresponds to different energetic effectsincluding the entropic gain or loss, obtained due to the linking of two monomers. If the two monomers are connected with a rigid linker, the hetero-bivalent ligand may not interact properly due to restrictions imposed by the linker. If a flexible linker is employed in the design, then increased flexibility of the linker negatively affects the ΔG_{other}. However, this is not always the case because the flexible linker may allow for the formation of additional interactions with the target, and most importantly, recent reports suggest that avidity effects such as rebinding

positively contribute to free energy of binding, which indicates that linker flexibility benefits the binding.[14-15]

1.2. Protein kinases as a model system:

Protein kinases are the enzymes that catalyze phosphorylation, a major signal transduction event inside the cell.[16-17] By performing a simple phosphate transfer, protein kinases affect many characteristics of their partner proteins such as subcellular localization, tertiary structure, and activity that ultimately decides the fate of signal transduction. The human genome encodes more than 518 protein kinases that are well known to regulate the majority of the signaling pathways involved in maintaining normal cellular processes.[18] However, dysregulated kinase activity hampers this normal cell signaling and is implicated in the progression of major diseases ranging from autoimmune diseases to cancers.[19] Therefore, developing kinase inhibitors to inhibit dysregulated kinase activity and thereby inhibit disease progression has been a major area of research focus for decades in pharmaceutical drug discovery.[20]

The majority of kinase inhibitors developed so far are small molecules that are focused on designing molecules that fit into the ATP binding pocket. Not surprisingly, most of these inhibitors exhibit poor selectivity due to similar ATP binding pockets shared among the kinome.[21-22] Besides, this design requires repeating the synthesis of small molecules and optimizing the reaction conditions,

which consumes a lot of time and effort to yield more potent drugs. Therefore, alternative strategies are required that can be applied to the whole kinome or at least to the majority of kinases, producing the most potent and selective kinase inhibitors without much synthesis effort.

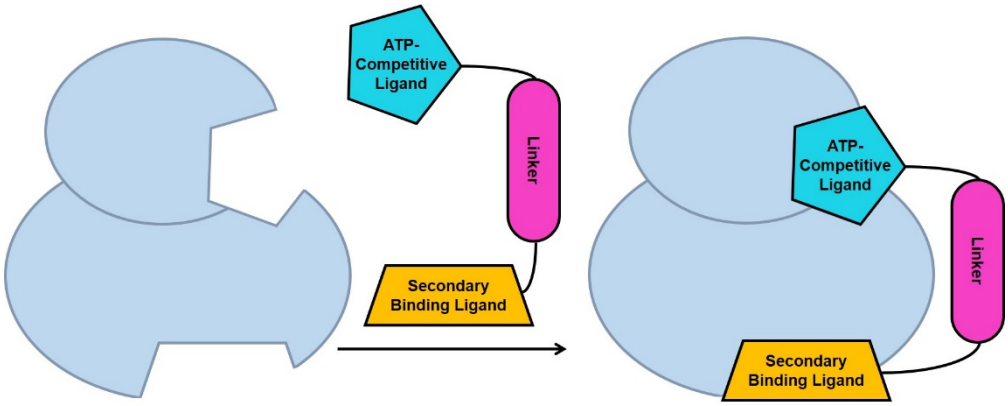

Figure 1. Schematic diagram showing hetero-bivalent kinase inhibition. Hetero-bivalent ligand consists of ATP competitive ligand and secondary binding ligand connected using linker (*on arrow*) and they target corresponding ATP and secondary peptide binding pockets on a kinase (*on left panel*) simultaneously to yield hetero-bivalent kinase inhibition (*on right panel*).

Though kinases share a similar ATP binding pocket, they exhibit unprecedented selectivity in phosphorylating one substrate over another. Kinases evolved to gain this exquisite selectivity using the specific secondary binding pockets outside the ATP binding sites.[13, 23] These specific peptide pockets can recognize peptide sequences that belong to substrate proteins binding to the catalytic or regulatory sites involved in recognizing specific binding partners. However, when such short peptide sequences targeting these regions are developed as drug-leads, they usually display very weak affinities (often in the micromolar to millimolar level). Typically, longer peptide structures are needed to achieve desired nanomolar

potency where cell permeability is considered to be a significant problem. The hetero-bivalent strategy is particularly beneficial here. Targeting two different binding sites (ATP and a specific secondary regulatory peptide binding site) will increase the affinity and selectivity towards the targeted kinase. Since the specific peptide sequences exist for the majority of kinases, it is possible to generate a hetero-bivalent ligand for most kinases. Attaching an organic moiety onto these peptides would increase their serum stability and cell permeability as well.

Hetero-bivalent inhibitors can be divided into two types based on the specific peptide binding pocket they target within kinase. The first type involves bisubstrate kinase inhibitors that target a substrate peptide binding pocket in addition to the ATP binding site while the second type consists of hetero-bivalent inhibitors that a target specific peptide pocket outside of the kinase active site along with the ATP binding pocket.

1.2.1. Bisubstrate inhibitors targeting protein kinases:

Ricourt, et al. first reported the design of bisubstrate inhibitors targeting protein kinase C (PKC), a serine-threonine protein kinase having ten highly homologous isozymes.[24] In this report, they used a pseudosubstrate peptide (SRRRRRR) targeting the substrate-binding pocket of PKC and connected to a 5-isoquinyllsulfonyl moiety that binds to the ATP binding site. In this report, they used a crystal structure of phosphoglycerate kinase, a relevant kinase reported at that

time, to predict the distance between N9 of adenine of ATP and a hydroxyl side-chain of serine. The distance was found to be 16.3 Å.To cover this distance, an amino ethylene glycol-based linker was utilized. The resultant bisubstrate compounds inhibited PKC with an IC_{50} of 0.3 μM, which is almost 67 times more potent compared with 5-isoquinyllsulfonyl moiety (IC_{50}~20 μM) alone. This study demonstrated that structure-based design can improve the affinity of a bisubstrate inhibitor towards a kinase. The same bisubstrate inhibitor also potently inhibited PKA (IC_{50}~0.003 μM), another close family member of PKC that shares a similar peptide binding pocket.

Alternatively, Kruse, et al. reported bisubstrate inhibitors targeting Abelson tyrosine kinase (Abl).[25] In this report, the authors evaluated the role of linker and tyrosine substrate effective recognition by Abl kinase. Here, the authors hypothesized that the presence of tyrosine increases the affinity of bisubstrate inhibitors towards protein tyrosine kinases. To study this, tyrosine or tyrosine mimics were connected to 5'-[4-(fluorosulfonyl)benzoyl]adenosine (5'-FSBA), which act as ATP binding site ligand. The linker distance between 5'-FSBA and tyrosine was changed by altering the number of phosphate groups (varying from 2-3). All derivatives modestly inhibited Abl kinase (IC_{50}~19-150 μM) and similar IC_{50} values between different panels of compounds, having the difference in linker length and tyrosine or tyrosine mimics, suggested that there is no effect of linker length and tyrosine substrate recognition. These results emphasized the need for

structural information beyond the tyrosine residue for the design of potent bisubstrate inhibitors. Based on the similar design several other bisubstrate inhibitors targeting other kinases were reported, with very weak inhibitory activities, explaining the critical impact of knowing structural information in bisubstrate inhibitor design.[26-29]

Next, Paranang, et al. reported a structure-based approach to design a bisubstrate inhibitor, using the crystal structure of insulin receptor kinase (IRK) with its substrate peptide.[30] The design was based on the dissociative mechanism of phosphate transfer from the ATP to the substrate peptide. According to this mechanism, in the transition state, the ADP group departure precedes the nucleophilic attack of the tyrosine hydroxyl group on gamma phosphate. During this transition state, the distance between incoming nucleophilic oxygen of tyrosine and the gamma phosphate of ATP was predicted to be around 5 Å. In addition, the hydroxyl group of tyrosine must be present to form aan H-bond with the catalytic Asp during the transition state that is necessary to hold the substrate peptide firmly. So, these two critical parameters must be necessary to design a potent bisubstrate inhibitor. An acetyl linker that was predicted to cover the necessary distance of 5 Å and aniline group was employed to mimic the hydroxyl group in tyrosine. With these changes, a bisubstrate inhibitor was developed, which potently inhibited the IRK with a K_i~370 nM. Interestingly, an analogue, having only the aniline in place of tyrosine and remaining peptide portion weakly inhibited the kinase ~300 fold.

This explains the importance of the remaining amino acid contribution to the potency of bisubstrate inhibitors. In addition, another analogue, in which tyrosine hydroxyl group was replaced with ether linkage that cannot form an H-bond with catalytic Asp, 80 times weakly inhibited IRK, indicating the importance of hydrogen bonding during the transition state. These results further highlighted the importance of structural information of the peptide beyond tyrosine and also the critical requirement of the hydroxyl group of tyrosine in the transition state to design potent bisubstrate inhibitors. Using a similar inhibition mechanism, a few additional bisubstrate inhibitors were reported.[13, 31-32]

1.2.2. Hetero-bivalent inhibitors targeting protein kinases:

Stebbins, et al. first reported hetero-bivalent inhibitors targeting c-jun N-terminal kinase (JNK) kinase. In this design, they employed docking site (D-site) peptide, a peptide sequence that MAPK substrates or interacting proteins specifically use to interact with the docking site motif on MAPK.[33] The minimal peptide sequence (RPTTLNL) from JNK1 interacting Protein (JIP1) that is essential for recognizing D-site region on JNK1 was used as a secondary binding ligand (pepJIP), and it was connected to SP600125, a potent kinase inhibitor that is known to inhibit JNK1 and other kinases.[34-35] When these two monomers were connected with a glycine-glycine-diaminopropane linker, the resultant hetero-bivalent inhibitor exhibited sub-nanomolar potency (IC_{50}=0.9 nM) towards JNK1 kinase. The hetero-bivalent

inhibitor showed a more than 20,000 fold increase inincreased inhibition when compared with ATP competitive inhibitor SP600125. Further, the selectivity of this hetero-bivalent ligand towards JNK1 when compared to a very closely related family kinase P38alpha was evaluated using a cell-based assay that measure specific cellular inflammatory responses regulated by these two kinases. JNK1 is known to induce TNF-α in response to lipopolysaccharide (LPS), a pro-inflammatory agent, while the P38alpha increases TNF-β levels. To improve the cell permeability, the TAT sequence (GRKKRRQRRR) was inserted. The resultant cell penetrable hetero-bivalent inhibitor selectively inhibited JNK1 mediated TNF-α secretion without elevating the TNF-β levels, which was mediated by P38alpha. Recently, Johnson, et al. reported a hetero-bivalent inhibitor targeting two different domains of c-src receptor tyrosine kinase.[36] In their report, they attached an aminopyrazole based kinase inhibitor to a pentapeptide (NQpYEEI) sequence that binds to the SH2 domain of c-src kinase. As only a few kinases possess the SH2 domain, the authors hypothesized to gain selectivity by simultaneously targeting this domain along with the ATP binding site. Hetero-bivalent inhibitor with a 33 atom PEG linker between ATP and peptide binding site ligands potently inhibited the c-src kinase with an IC_{50} value of 0.16 μM. Later, the hetero-bivalent inhibitor was screened against a panel of 10 kinases and exhibited average IC_{50} of 3.5 μM, about 22 folds more selective towards c-src kinase. Using the similar design

principles, many hetero-bivalent inhibitors targeting protein kinases were reported.[37-39]

2. HETERO-BIVALENT LIGANDS TARGETING EXTRACELLULAR REGULATED KINASE5 (ERK5) KINASE

2.1. Literature review:

2.1.1. Cancer Stem Cells (CSCs) and ERK5 role in CSC signaling:

Cancer is highly heterogeneous and consists of a subpopulation of cells called Cancer Stem Cells (CSCs) along with non-stem cancer cells in a tumor bulk (Fig. 2).[40-44] These CSCs drive the tumor progression by self-renewal, metastasis and show high resistance to treatments.[45-46] Conventional anti-cancer drugs can kill non-stem cancer cells, but not CSCs. As a result, CSCs remain after therapy and cause tumor relapse. Therefore, CSC targeted drugs are needed that can specifically kill CSCs and aid in total cancer regression.

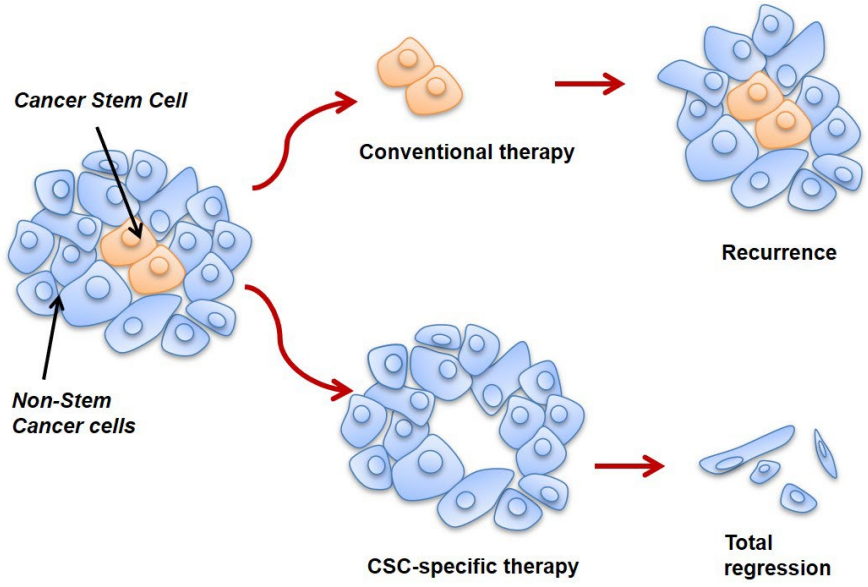

Figure 2. Hypothetical model of targeting Cancer Stem Cells (CSCs) in a tumor. Conventional therapy kills non-stem cancer cells (blue color), leaving the CSCs behind (orange color – *above panel*), which causes tumor recurrence or relapse. CSC targeted drugs kill the CSCs and cause total tumor regression (*bottom panel*).[47]

Currently, major CSC-targeted drug discovery efforts are focused on inhibiting growth signaling pathways such as Hedgehog, Notch, and Wnt that are known to regulate CSC signaling.[40] Recently, mitogen-activated protein kinase 5-extracellular signal-regulated kinase 5 (MEK5-ERK5) pathway emerged as a key player in maintaining CSC signaling.[48-49] MEK5: ERK5 signal axis shows a prominent role during development, as evidenced by defective blood vessel and cardiac formation in transgenic mice engineered without MEK5 or ERK5 kinase.[50-51] In particular, the ERK5 kinase role is well established in maintaining the "stemness" of stem cells during development by promoting transcription factors such as krüppel-like factor 2 (Klf2), estrogen-related receptor beta (Essrb), and reduced expression 1 (Rex1). Also, dysregulated ERK5 activity has been reported in the progression of several cancers.[52-53] Moreover, genetic knockdown studies further supported the notion that ERK5 must be needed for maintaining the stem-like characteristics such as tumorigenicity, migration, and resistance to chemotherapy.[53-55]

2.1.2. Structure of ERK5 and the mechanism of activation:

ERK5 known as big mitogen-activated protein kinase 1 (BMK1) as it has a large mol wt ~130K (~816 amino acid or aa) compared with other classical MAPKs - namely P38, c-jun N-terminal kinase (JNK) and ERK1/2. Structurally, ERK5

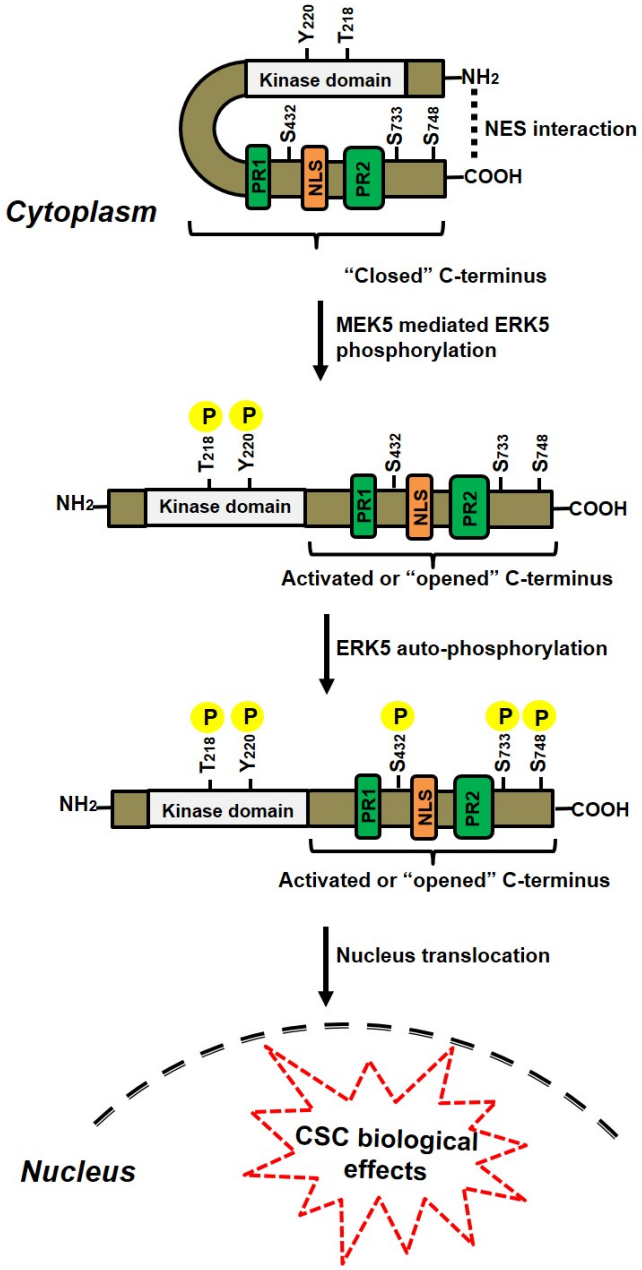

Figure 3. ERK5 activation mechanism. In the unphosphorylated state, ERK5 exists in a closed conformation where both N and C termini interact with each other to form nuclear export signal (NES) interaction that sequesters ERK5 in the cytoplasm. Upon MEK5 mediated phosphorylation at Thr218: Tyr220, ERK5 unfolds to open conformation. Subsequently, ERK5 auto-phosphorylates its own C-terminal tail and translocates into the nucleus to exert CSC biological effects.[56]

consists of N- terminal kinase domain and unique C-terminus, which further divided into nuclear localization signal (NLS) domain, two proline-rich (PR) domains named PR1 and PR2, and additional domains such as a myocyte enhancer factor 2 (MEF2) interacting region and transcriptional activation domain (TAD). The N-terminal kinase domain is mainly responsible for catalytic activity while the C-terminus tail regulates ERK5 kinase activity, nuclear localization, interaction with other transcription factors, and transcriptional activity of ERK5 in the nucleus.[48, 57] Under normal conditions, ERK5 exists in a closed conformation in which both C and N terminus closely interacts and forms a nuclear export signal (NES) that sequesters inactive ERK5 in the cytoplasm (Fig. 3).[57-58] However, when MEK5 kinase specifically phosphorylates ERK5 at Thr-218: Tyr-220 on the activation loop, ERK5 undergoes conformation change from a “closed” state to an open state, which destabilizes the NES interaction that is known to retain ERK5 in the cytoplasm. MEK5 can only phosphorylate ERK5 when it recognizes ERK5 using two interacting domains, namely Phox and Bem1 (PB1) and D-site motif.[59] These two domains hold the MEK5 kinase domain closer to the ERK5 activation loop and aid the phosphorylation. This phosphorylation is also known as MEK5 mediated ERK5 phosphorylation, activates ERK5, which then auto-phosphorylates the C-terminus. This phosphorylation is referred to as ERK5 auto-phosphorylation. It strengthens NLS signal which translocate ERK5 into the nucleus where ERK5 regulates transcription factors such as NF-κB, interleukin8 (IL-8), and MYC that

are involved in maintaining the CSC like characteristics.[48-49, 60-62] In other words, both MEK5 mediated ERK5 phosphorylation and subsequent ERK5 auto-phosphorylation translocate ERK5 into the nucleus, which directly translates to CSC activity. However, recent evidence suggests that ERK5 can translocate into the nucleus without MEK5 involvement or MEK5 independent manner.[63-65] As per these reports, ERK1/2 or cyclin-dependent kinase1 (CDK1) phosphorylates ERK5 on the C-terminus, and this phosphorylation is enough to transport the ERK5 into the nucleus. Recently, Tusa, et al. report further evidence about the MEK5 independent ERK5 nuclear translocation.[66] According to this report, in melanoma, both i). MEK5 dependent, ii). MEK5 independent ERK5 phosphorylation produced proliferation and xenograft formation. Notably, both ERK1/2 and CDK1 mediated phosphorylation on C-terminus ERK5 directly translated to proliferative effect. They also reported that inhibiting MEK dependent ERK5 phosphorylation also produced an anti-proliferative effect. However, they employed pharmacological inhibitors that targeted only MEK5 or ERK5, which showed a weak growth inhibition effect.

2.1.3. Pharmacological inhibitors targeting MEK5: ERK5 signaling:

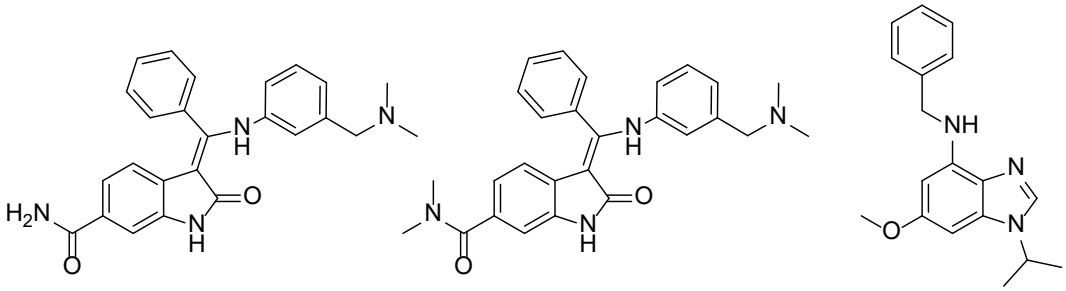

Figure 4. Chemical structures of published MEK5 inhibitors.[67-68]

Several small molecules inhibitors targeting the ATP binding pocket of ERK5 or its upstream kinase MEK5 were developed.[66-72] The first reported compounds were 6-indolinecarboxamide based inhibitors targeting the ATP binding pocket of MEK5 kinase.[67] The two compounds, BIX02188 and BIX02189, inhibited MEK5 kinase activity with IC_{50} values, 4.3 nM and 1.5 nM, respectively, and also inhibited ERK5 at higher concentrations, 810 nM and 59 nM, respectively. However, both BIX02188 and BIX02189 also inhibited colony stimulating factor 1 receptor (CS1FR) kinase at 280 nM and 46 nM, respectively. However, undesired pharmacokinetic properties of these molecules further limited their pharmacological use to inhibit the MEK: ERK5 pathway.

Later, Flaherty, et al. reported benzimidazole based inhibitors of the MEK5 kinase activity.[68] Among these compounds, only compound 6 inhibited the EGF induced ERK5 phosphorylation in western blot. However, this compound also inhibited

ERK1/2 phosphorylation as well, indicating the compound 6 cross reactivity towards MEK1/2, upstream kinases known to activate ERK1/2.

Next, small molecules targeting the ATP binding pocket of ERK5 kinase were reported.[66, 69-72] This first series of molecule were based on pyrido[2,3-d]pyrimidine core scaffold, a privileged moiety in regards to inhibiting ATP binding pocket of many kinases.[73-74] This scaffold was further derivatized to yield a seven member macrocycle, benzo[e]pyrimido-[5,4-b]diazepine-6(11H)-one, that reported to be well accommodated in larger ATP binding pocket of ERK5 kinase.[70, 72] Among all compounds in this series, XMD8-92 inhibited ERK5 kinase activity with an IC_{50} of 240 nM, exhibit selectivity towards ERK5, and inhibited growth of many cell lines including H1299 cells.

Conversely, Lin, et al. reported contradictory findings, proving that XMD8-92 anti-proliferative effects were due to off target inhibition of unrelated class of proteins called bromodomains (BRDs), in particular BRD4 subtype.[71] In this study, they synthesized compounds, as shown in Fig. 5A, having a core benzo[e]pyrimido-[5,4- b]diazepine-6(11H)-one scaffold, with varying degrees of selectivity towards ERK5, BRD4 or both and compared their anti-proliferative activity along with selective BRD4 inhibitor: I-BET762. Surprisingly, ERK5 selective inhibitor AX15836 did not show anti-proliferative activity. The dual inhibitor AX15839, XMD8-92 and selective BRD4 inhibitor I-BET762 inhibited cell proliferation. Interestingly, all these compounds (except I-BET762) were confirmed for target

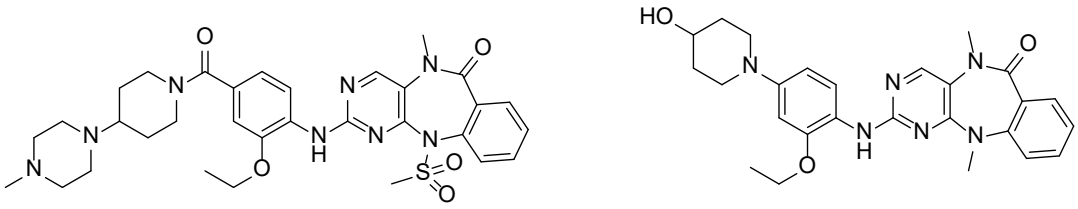

AX15836

ERK5 IC_{50}= 8 nM
BRD4 K_d= 3600 nM

XMD8-92

ERK5 IC_{50}= 190 nM
BRD4 K_d= 170 nM

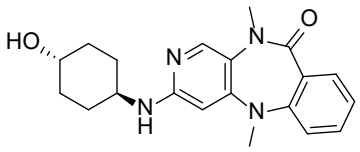

AX15839

ERK5 IC_{50}= 170 nM
BRD4 K_d= 130 nM

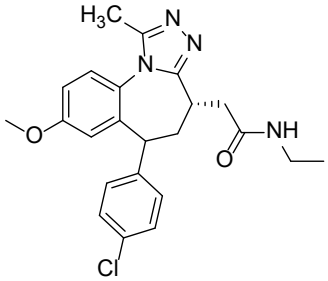

I-BET762

ERK5 IC_{50}= >10000 nM
BRD4 K_d= 31 nM

Figure 5A. Chemical Structures of published ERK5 inhibitors (except I-BET762 which is a BRD4 inhibitor).[71]

engagement using western blot where they proved to inhibit ERK5 auto-phosphorylation. They clearly concluded that inhibiting ERK5 auto-phosphorylation alone did not translate to anti-proliferation activity. These results further raised questions about using XMD8-92 as a probe for studying ERK5 in cell-based studies.

Recently, Ngyuen, et al. reported another compound BAY-885, having a pyrido[3,2-d]pyrimidines scaffold as a selective ERK5 kinase inhibitor.[69] Interestingly, this compound potently inhibited ERK5 catalytic activity (IC_{50}~0.035 μM), and showed no binding with BRD4 (up to 20 μM) and confirmed for inhibiting

ERK5 auto-phosphorylation using MEF2 luciferase reporter gene assay. However, it failed to exhibit anti-proliferation activity.

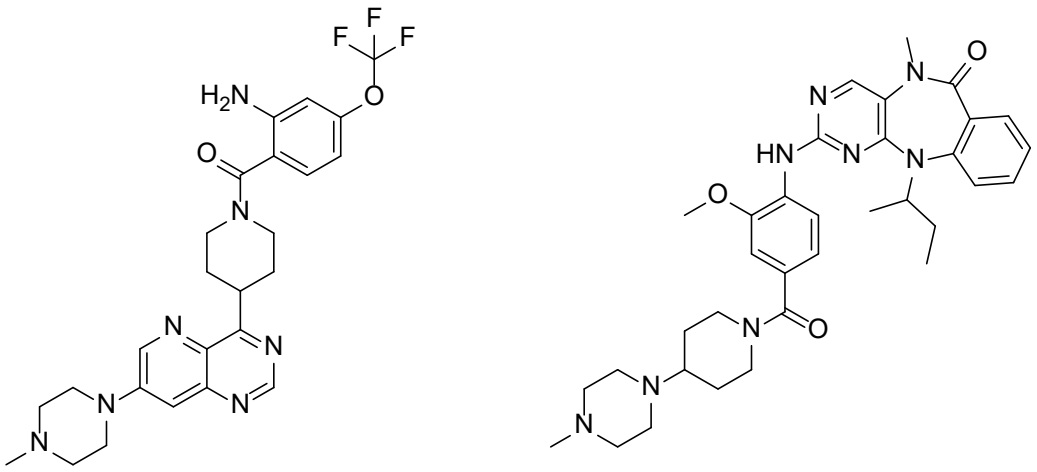

Figure 5B. Chemical structures of remaining published ERK5 inhibitors.[69, 75]

Later, wang, et al. reported selective ERK5 inhibitors JWG-045 (the structure was not published) and JWG-071 (IC_{50}~0.088 μM) with increased selectivity towards ERK5 compared to BRD4 (IC_{50}~6.31 μM).[75] Among these two compounds, only JWG-045 was further tested on melanoma cell lines, which inhibited ERK5 auto-phosphorylation and, surprisingly, melanoma cell proliferation with an IC_{50} value of 5.81 μM.[66] So far, JWG-045 was the only ERK5 selective compound that exhibited antiproliferative activity. It is quite unclear about the exact reason behind such a discrepancy in ERK5 kinase inhibition and achieving anti-CSC activity. Overall, the mutually conflicting reports of ERK5 selective inhibitors AX-15836, BAY-885 and

JWG-045, further questions the validity of targeting ERK5 ATP binding pocket for inhibiting CSC biological activity.

2.2. Statement of problem:

Over the past few years, there has been a significant interest in targeting CSCs to support the complete eradication of tumors. MEK5: ERK5 is a pathway reported to be one of the promising signaling systems that regulate several signal mediators involved in maintaining cancer stem-like characters. Further genetic knockdown studies confirmed the ERK5 role in maintaining tumorigenicity, migration, and proliferation. The majority of researchers chose to inhibit the ERK5 kinase activity as a starting point to pharmacologically target this pathway. The initial ERK5 ATP competitive inhibitor XMD8-92 proved to be effective at inhibiting CSC signaling in several cancers. However, subsequent reports attributed the anti-CSC activity of this compound to the off-target effects. A recent report suggests that pharmacological inhibition of either MEK5 or ERK5 kinase produces weaker anti-proliferation effect.REFERENCE Seemingly contradictory results of subsequent ERK5 selective kinase inhibitors, such as BAY-885 and JWG-071, raised doubts about inhibiting kinase activity alone to achieve the ultimate anti-CSC biological effect. This suggests that, stronger inhibitors with additional mechanisms need to be explored for complete inhibition of ERK5 signaling. Therefore, developing alternative design strategies that can specifically inhibit this pathway is of

paramount importance as it enables the opening of avenues for novel therapeutics to combat CSCs effectively.

2.3. Hypothesis:

We hypothesize that designing a hetero-bivalent inhibitor that can simultaneously blocks: (i) MEK5 mediated ERK5 phosphorylation as well as (ii) ERK5 auto-phosphorylation may result in stronger anti-CSC effects. We plan to achieve this (i) by blocking D-site peptide interaction that MEK5 kinase critically requires for binding, which will then block the activation of ERK5. To achieve this (ii), we will attach a weak ATP binding site molecule, that then binds the ATP binding pocket to yield a hetero-bivalent inhibitor that simultaneously blocks both D-site and ATP binding pockets of ERK5 kinase. The rationale for choosing a weaker ATP binding site molecule is to reduce non-specific binding to other kinases, but since it is within the hetero-bivalent ligand, it will strongly bind to EKR5 active site.

2.4. Materials and methods

2.4.1. General

NovaSyn TGR resin was used for solid phase synthesis reactions (MilliporeSigma, Darmstadt, Germany). All chemical reagents and solvents were obtained from the commercial sources and used without further purification. 2-azidoacetic acid, 3-azidopropionic acid and 4-azidobutanoic acid were purchased from MilliporeSigma (Darmstadt, Germany). Disposable reaction syringes (5 ml) (Intavis AG) were used as reaction vessels for solid-phase synthesis.

All compounds were purified using Waters HPLC and analyzed by Applied Biosystems Voyager De-Pro mass spectrometer using alpha-Cyano-4-hydroxycinnamic acid as matrix. NMR spectra were recorded at room temperature using a JEOL ECA-600 instruments (^{1}H NMR at 600 MHz and ^{13}C NMR at 150 MHz).

2.4.2. Chemical synthesis:

2.4.2.1. PP2 analogue:

Compound was synthesized as previously described.[76]

^{1}H NMR (600 MHz, DMSO-d_6): δ 8.39 (s, 1 H), 8.36 (s, 1 H), 8.24-8.22 (m, 1 H), 7.75-7.73 (m, 2 H), 7.61-7.59 (m, 2 H), 7.56-7.53 (m, 1 H), 7.43-7.42 (m, 1 H), 4.30 (s, 1H);^{13}C NMR (150 MHz, DMSO-d_6): δ 158.07, 156.14, 154.83, 145.65, 139.13,

134.62, 131.17, 130.81, 130.32, 130.07, 129.77, 124.16, 123.03, 121.93, 99.31, 83.30, 82.22.

2.4.2.2. Biotinylated PP2 monomer:

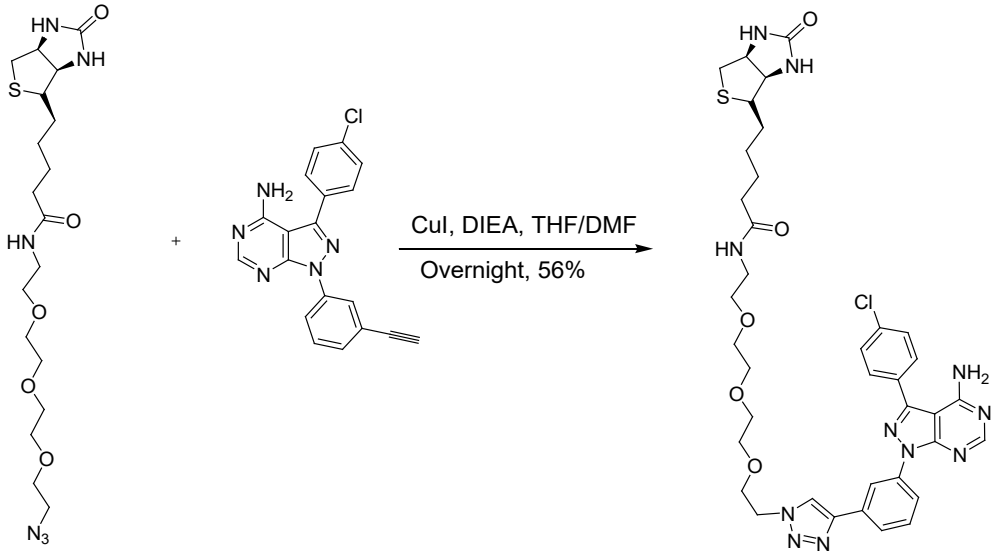

Scheme 1. Synthetic scheme of biotinylated PP2 monomer.

The compound was synthesized by following the similar conditions as previously discussed.[37]

PP2 analogue was dissolved in 200 uL of THF and DMF (1:1). Then CuI (0.004 mmol), DIPEA (0.089 mmol) and azide-PEG3-biotin (0.045 mmol) were added and stirred at room temperature for overnight. The crude was mixed with water and extracted with DCM. The organic layer was dried over anhydrous Na_2SO_4, evaporated and purified using column chromatography to yield yellow color solid (21 mg, 56%).

2.4.2.3.D-site peptide monomer (biotinylated and non-biotinylated):

Compounds were synthesized on Novasyn TGR resin (MilliporeSigma, with a 0.20-0.30 mmol/g loading, 90 μm diameter) using previously established solid phase peptide synthesis protocols in our lab.[37, 77]

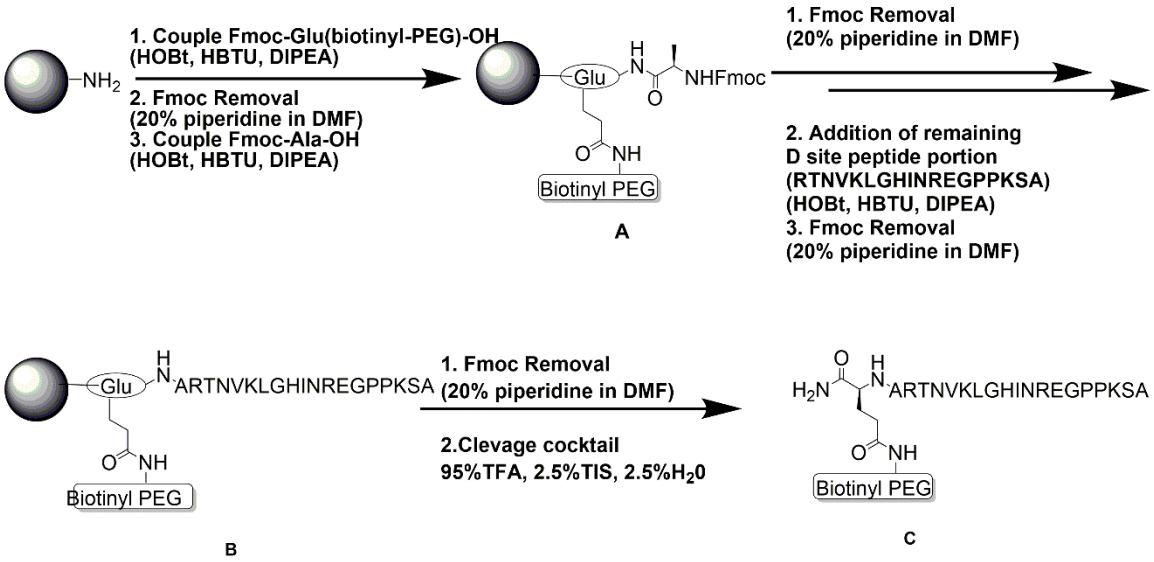

Scheme 2. Synthesis scheme of D-site peptide.

The synthesis procedure involves following steps.

Step 1: The resin (100 mg per each synthesis) was added to each peptide reaction syringe (5 mL) and allowed to swell in 2 ml of dimethylformamide (DMF) for 1 hr. Then DMF was removed.

Step 2: The resin was treated with Glu(biotinyl-PEG)-OH (5n mol) (n = loading capacity of resin x quantity of resin used per reaction), HBTU (5*n* mol) and HOBT (5*n* mol), DIPEA (10*n* mol) in DMF (2 ml) at room temperature for overnight. This step was avoided in case of non-biotinylated D-site peptide synthesis.

Step 3: The resin was washed with DMF (10 x 2 ml), and 20% piperidine solution in DMF [2 x (2 ml x 10 min)] was added to achieve Fmoc deprotection. The resin was again washed with DMF (10 x 2 ml).

Step 4: After achieving Fmoc deprotection, Fmoc-ala-OH was coupled to resin using reagents [HBTU (5*n* mol) and HOBT (5*n* mol)] and base [DIPEA (10*n* mol)] in DMF (2 ml) for 2 hrs to get compound A.

Step 5: Fmoc group was deprotected as described in *step 3*, and the remaining amino acids in D-site peptide sequence (RTNVKLGHINREGPPKSA) were subsequently introduced by repeating the conditions in *step 3* and *step 4*, repeatedly to get compound B.

Step 6: The Fmoc group was deprotected by following *step 3*.

Step 7: The resin was washed with DCM (10 x 2 ml) and treated with cleaving cocktail [95% TFA, 2.5% water, 2.5% triisoproylsilane (TIS)] (3 ml) for 2 hrs to get compound C. The cocktail was collected in a tube and TFA was evaporated to get both biotinylated and non-biotnylated derrivates of D-site peptide around 19% (12.3 mg) and 21% (10.7 mg) in yields the obtained crude was analyzed using MALDI-TOF and purified using HPLC.

2.4.2.4.Synthesis of ERK5 series hetero-bivalent ligands (biotinylated and non-biotinylated):

The synthesis procedure involves following steps.

Step 1,2,3, and 4 were followed as described in 2.4.2.3.

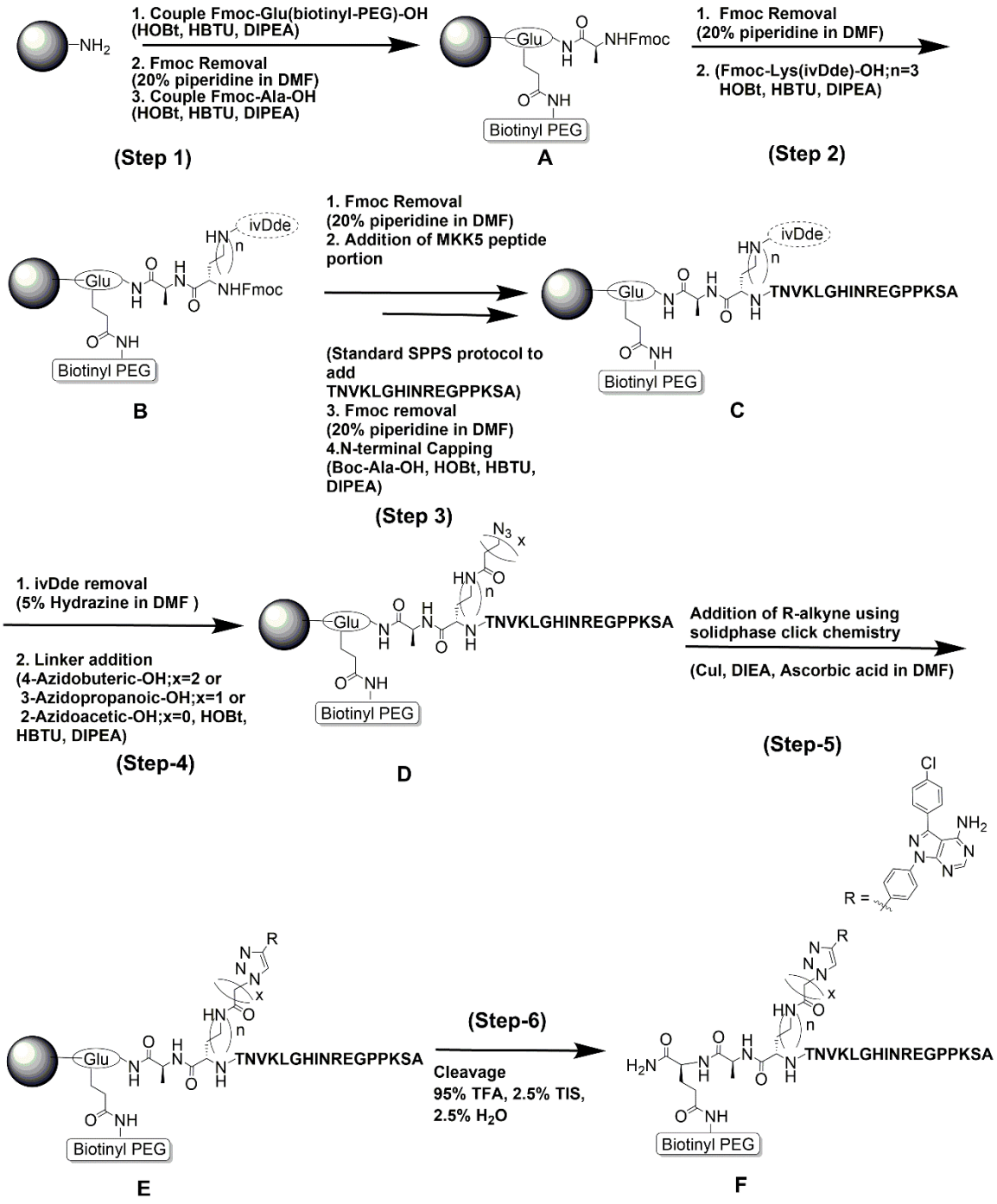

Scheme 3. Synthesis scheme of ERK5 series hetero-bivalent ligands.

Step 5: Fmoc-Lys-IvDde-OH was coupled to resin using the coupling conditions mentioned in 2.4.2.3 to get the compound B. Then, Fmoc group was deprotected and remaining amino acids were coupled (TNVKLGHINREGPPKSA) using conditions mentioned in *step 3* and *step 4* of 2.4.2.3.

Step 6: N-terminus was capped with Boc-Ala-OH (replacing N terminus Fmoc-ala-OH) using the conditions described in *step 4* of 2.4.2.3 to get compound C.

Step 7: IvDde group was deprotected by treating the resin with 5% hydrazine [3 x (2 ml x 10 min)]. The resin was again washed with DMF (10 x2 ml).

Step 8: The corresponding azidoalkanoic acid [2-azidoacetic acid (~3.5 Å) or 3-azidopropanoic acid (~4.7 Å) or 4-azidobutanoic acid (~5.9 Å)] was coupled to the resin using the conditions described in *step 3* of 2.4.2.3 to get compound D.

Step 9: The resin was treated with Copper Iodide (3 *n*) and PP2 analogue (3 *n*), Sodium-L-ascorbate (5 *n*) in DMSO: Pyridine (7:3 v/v) for overnight at room temperature to get compound E. The reaction vessel was drained and washed with Cu scavenger cocktail [ascorbic acid (0.02 gmL^{-1}) in DMSO: Pyridine (6:5)].[78]

Step 10: Compounds were cleaved from the resin using the procedure described in *step 7* of 2.4.2.3. synthesis to get both biotinylated and non-biotnylated derivates of compound F in following yields: Bt- ERK5.1 (17%, 12.7 mg), ERK5.1 (18%, 11 mg), Bt-ERK5.2 (21%, 15.8 mg), Bt-ERK5.3 (24%, 18.1 mg), ERK5.3 (23%, 14.2 mg).

2.4.3. NMR spectra of PP2 analogue:

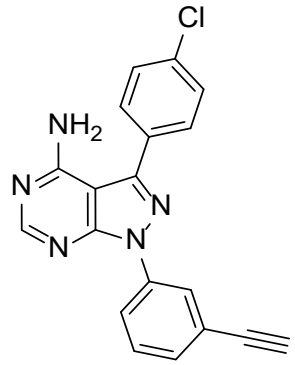

PP2 analogue

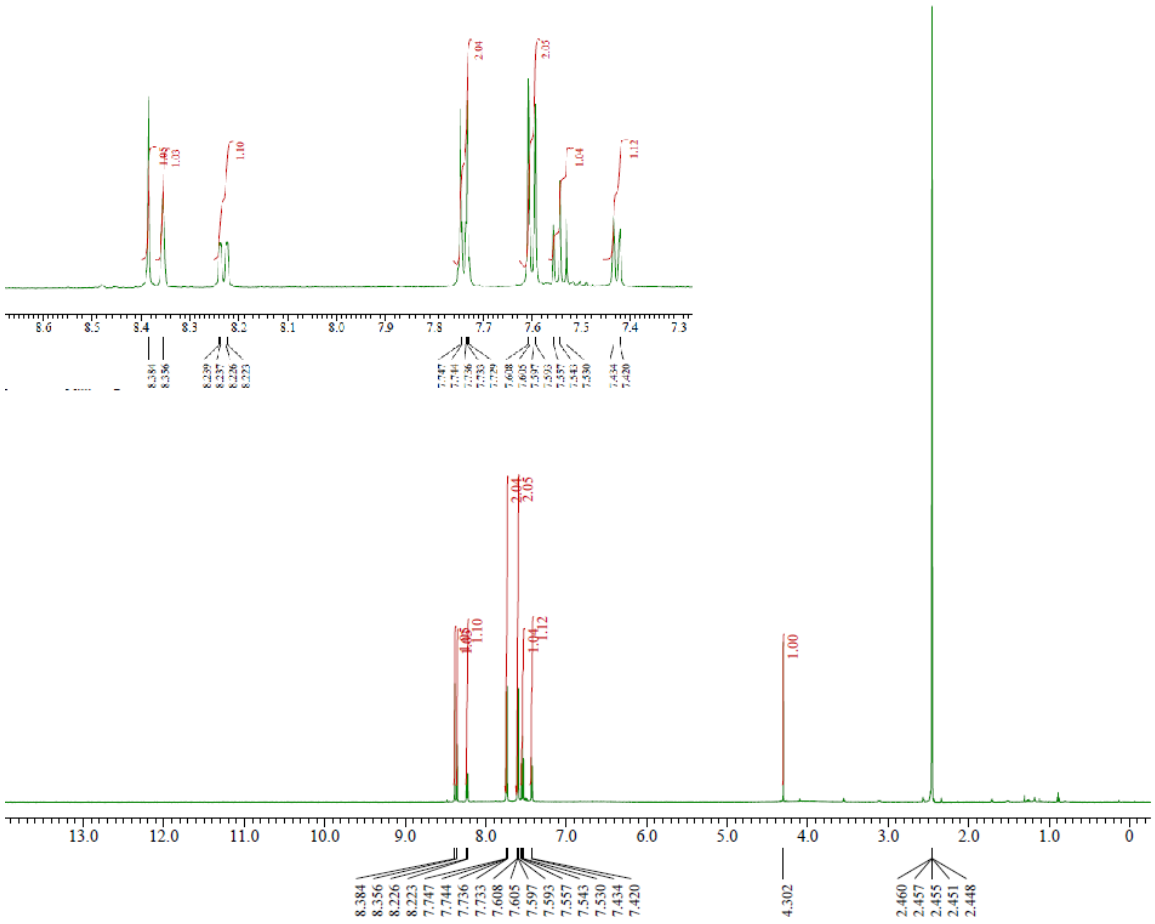

^{1}H NMR (600 MHz, $CDCl_3$)

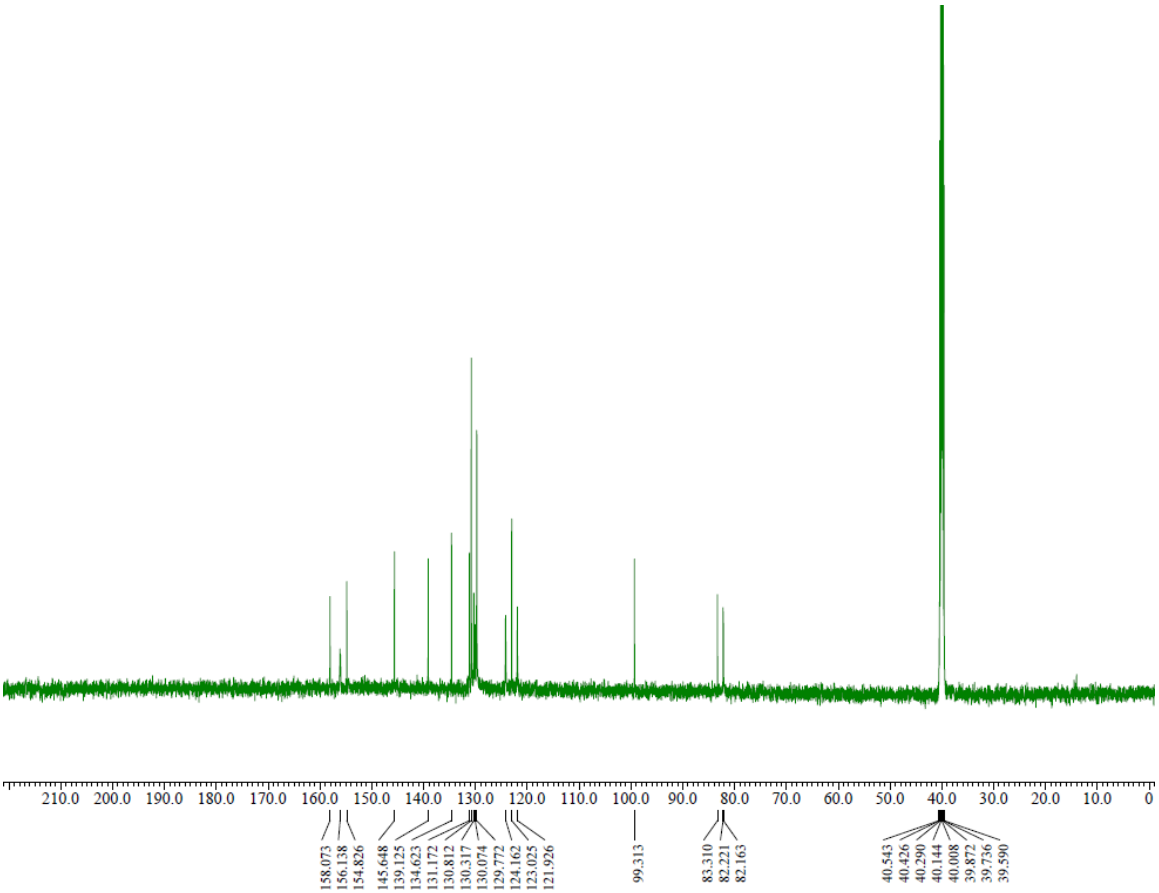

^{13}C NMR (150 MHz, $CDCl_3$)

2.4.4. Structure, Mass spectrum, and HPLC analysis of Compounds:

2.4.4.1. Structure, Mass spectrum, and HPLC analysis of biotinylated PP2 monomer:

(A)

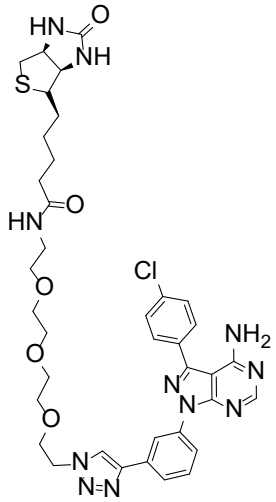

Biotinylated PP2 monomer

Exact Mass – 789.29

(B)

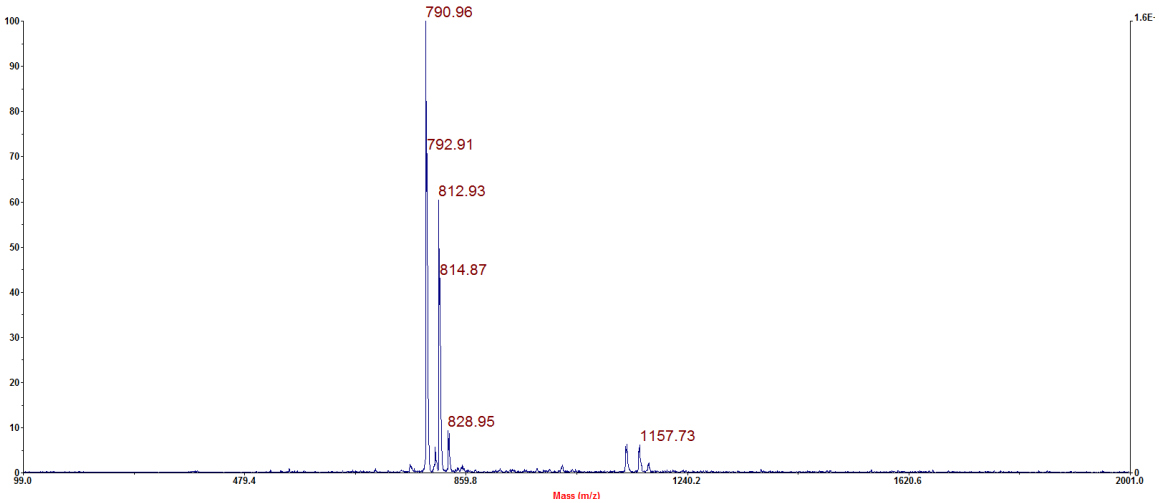

Characterization of biotinylated PP2 monomer: (A). Chemical structure. (B). MALDI-TOF spectrum

(MALDI-TOF+) m/z = 790.96$[M+H]^+$, 792.91$[M+3H]^+$ 812.93$[M+Na]^+$,

828.95$[M+K]^+$

2.4.4.2. Structure, Mass spectrum, and HPLC analysis of biotinylated D-site peptide monomer:

(A)

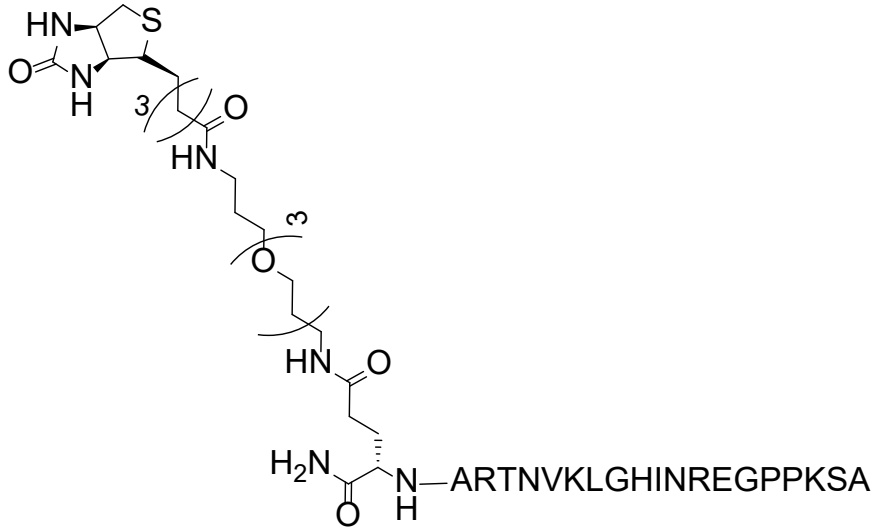

Biotinylated D-site peptide monomer

Exact Mass – 2600.43

(B)

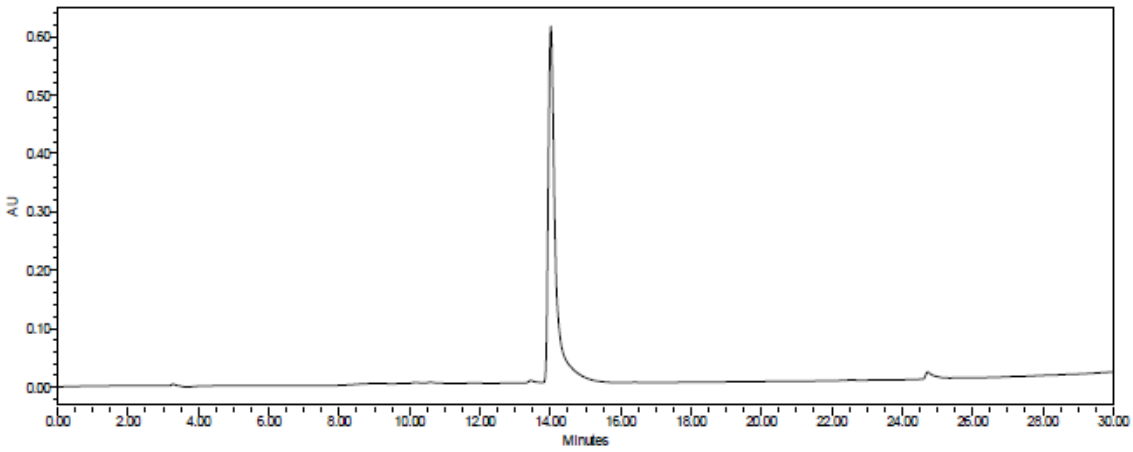

(C)

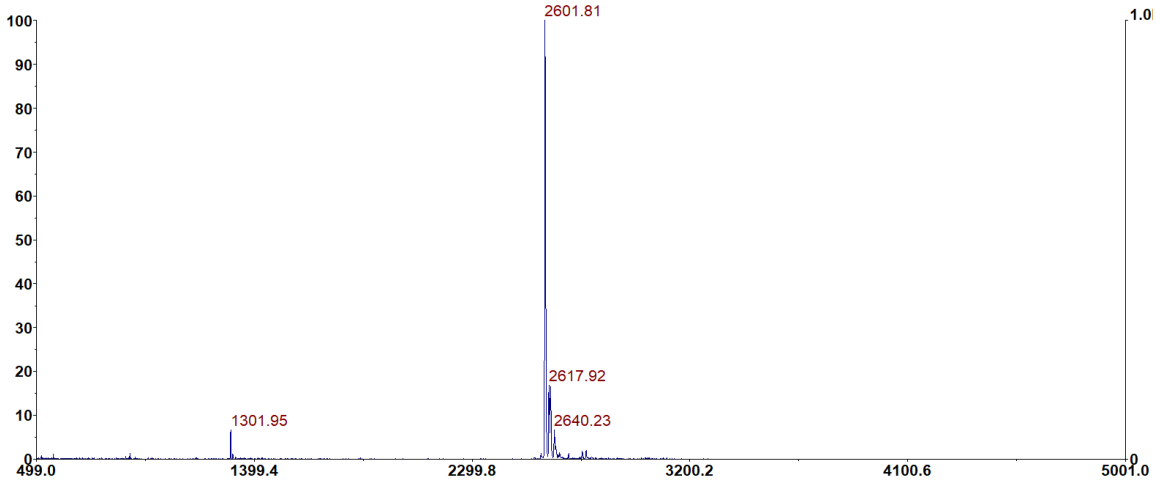

Characterization of biotinylated D-site peptide monomer: (A). Chemical structure. (B). Analytical HPLC. (C). MALDI-TOF spectrum.

(MALDI-TOF+) m/z = 2601.81 $[M+H]^+$, 2624.00 $[M+Na]^+$, 2640.23 $[M+K]^+$

2.4.4.3. Structure, Mass spectrum, and HPLC analysis of non-biotinylated D-site peptide monomer:

(A)

H_2NOC—ARTNVKLGHINREGPPKSA—NH_2

D-site peptide monomer

Exact Mass-2044.13

(B)

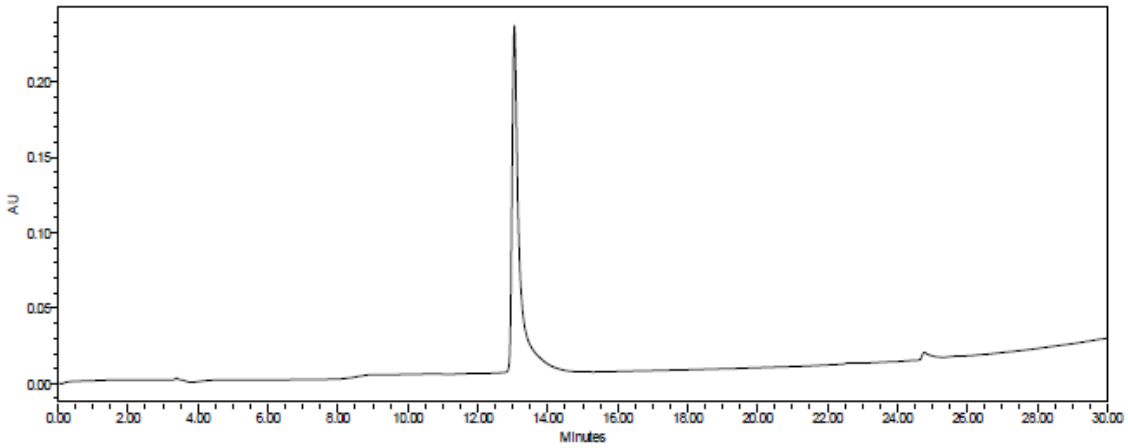

(C)

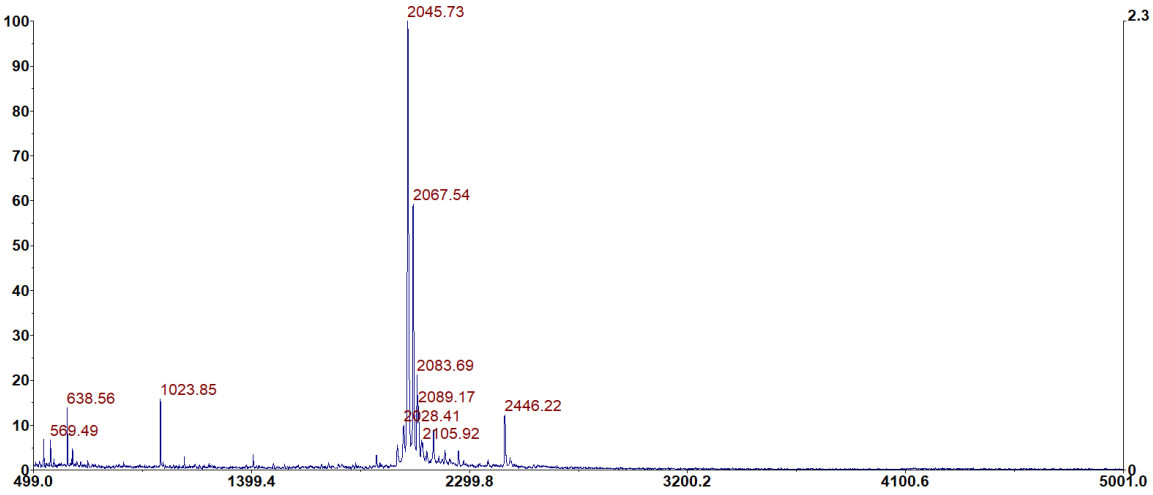

Characterization of non-biotinylated D-site peptide monomer: (A). Chemical structure. (B). Analytical HPLC. (C). MALDI-TOF spectrum.

(MALDI-TOF+) m/z = 2045.73 $[M+H]^+$, 2067.54$[M+Na]^+$, 2083.69$[M+K]^+$

2.4.4.4. Structure, Mass spectrum, and HPLC analysis of biotinylated ERK5 series compounds:

(A)

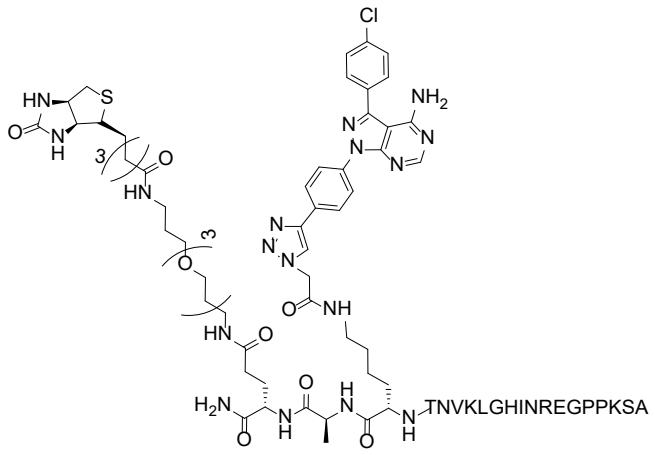

Bt-ERK 5.1

Exact Mass 3000.51

(B)

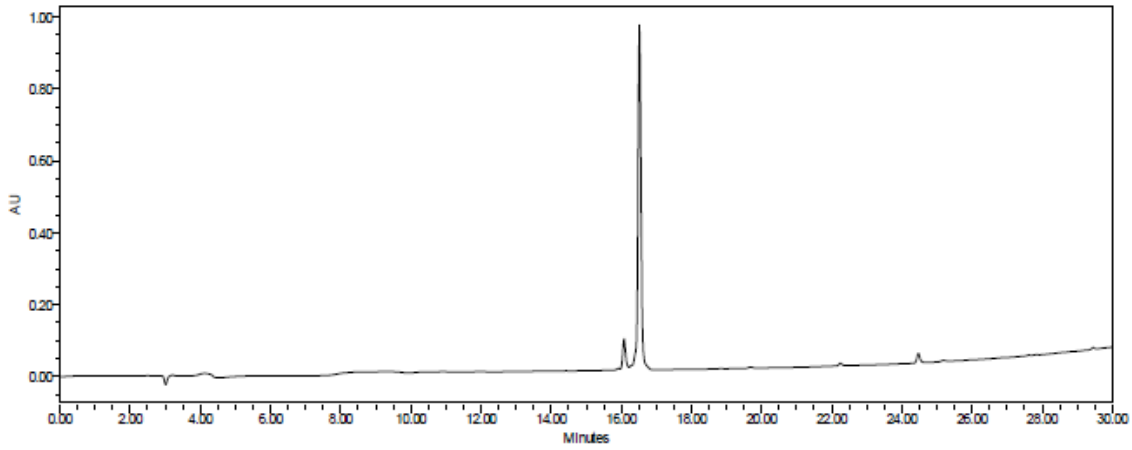

(C)

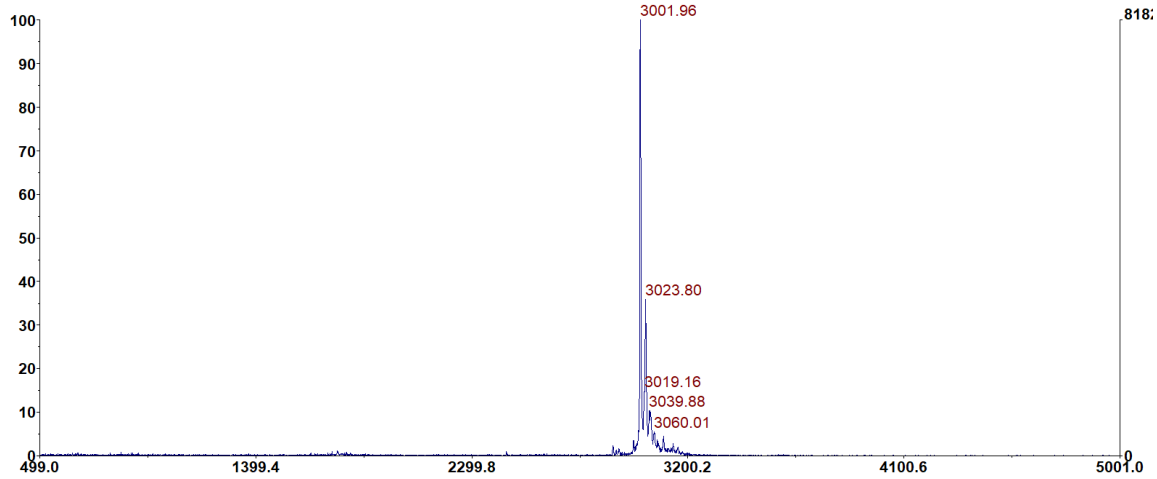

Characterization of Bt-ERK5.1: (A). Chemical structure. (B). Analytical HPLC. (C). MALDI-TOF spectrum.

(MALDI-TOF+) m/z = 3001.96$[M+H]^+$, 3023.00$[M+Na]^+$, 3039.88$[M+K]^+$

(A)

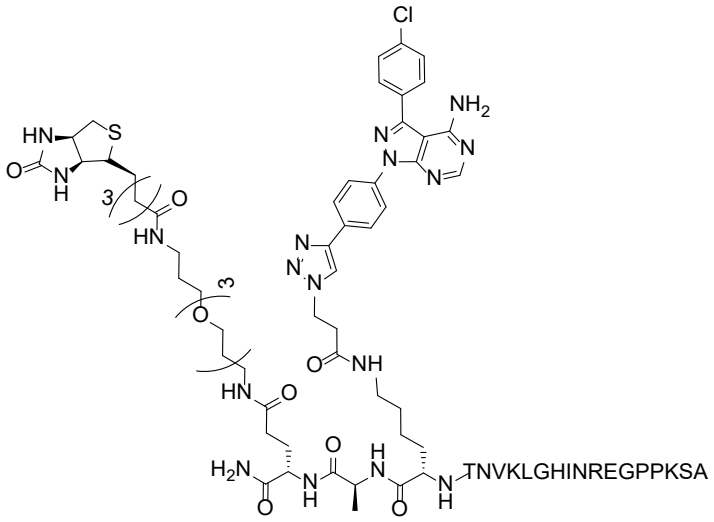

Bt-ERK 5.2

Exact Mass 3014.53

(B)

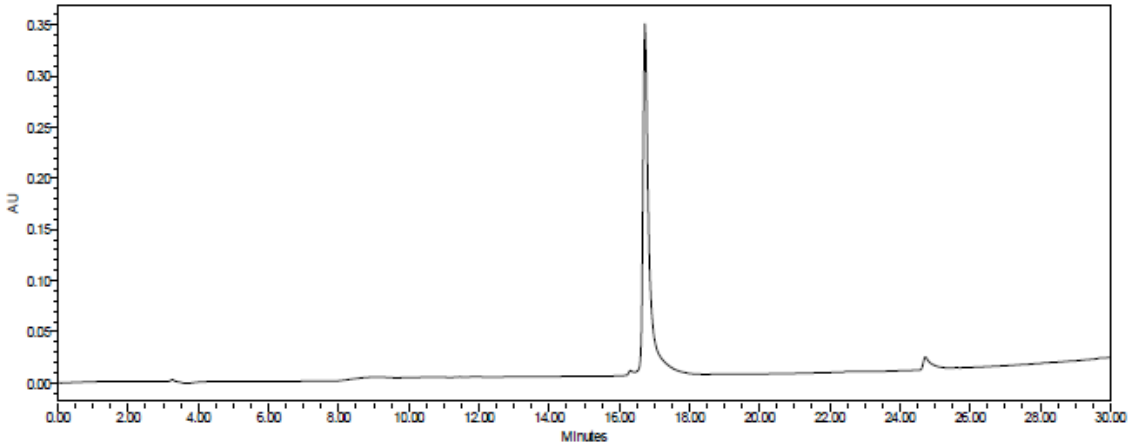

(C)

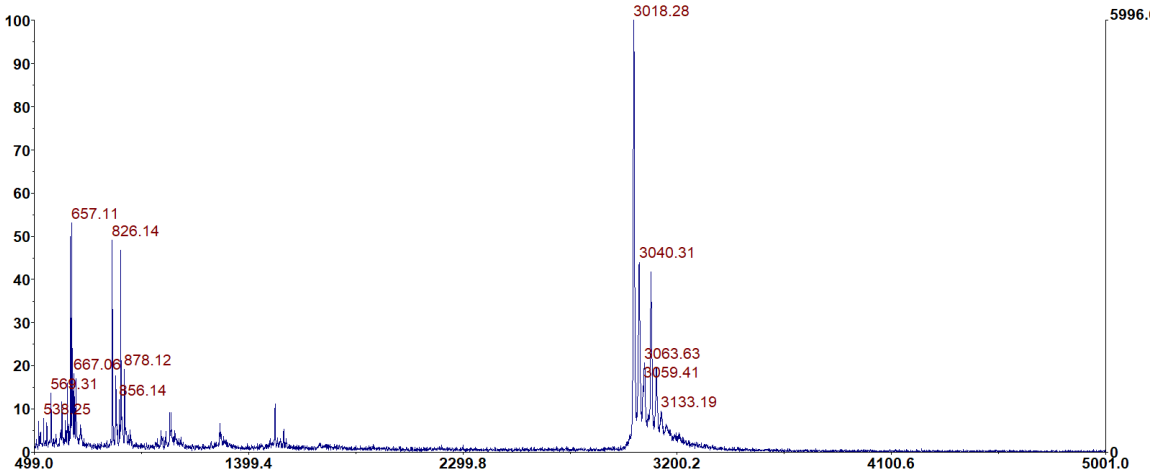

Characterization of Bt-ERK5.2: (A). Chemical structure. (B). Analytical HPLC. (C). MALDI-TOF spectrum.

(MALDI-TOF+) m/z = 3018.28$[M+H]^+$, 3040.31$[M+Na]^+$, 3059.41$[M+K]^+$

(A)

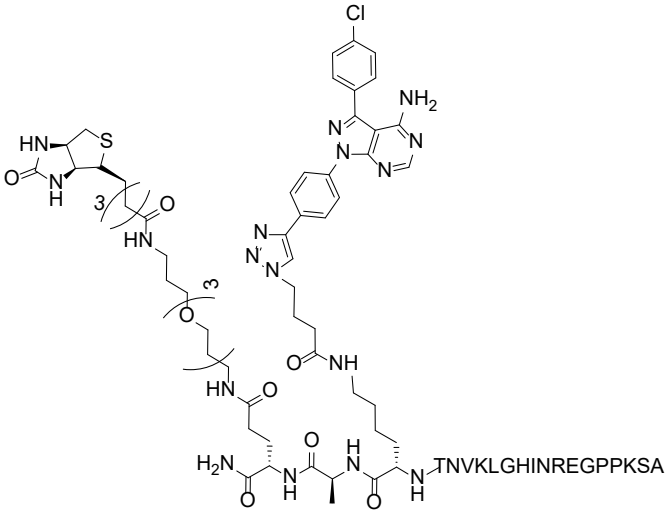

Bt-ERK 5.3

Exact Mass 3028.55

(B)

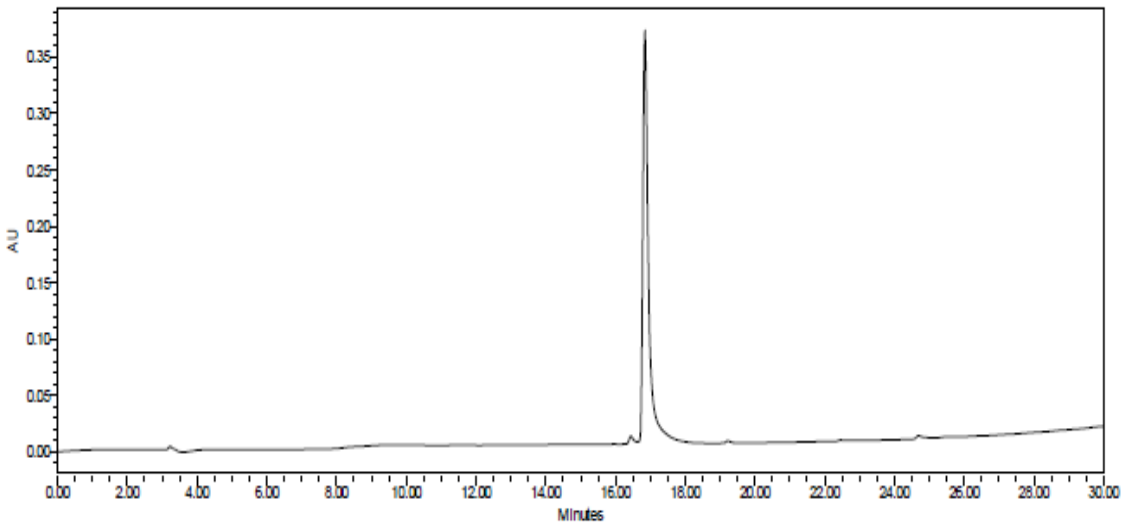

(C)

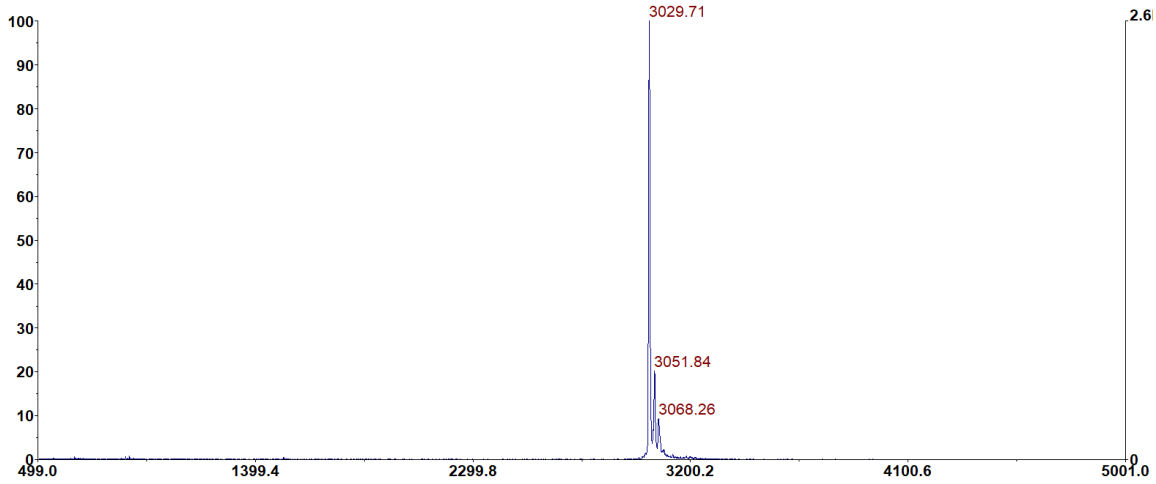

Characterization of Bt-ERK5.3: (A). Chemical structure. (B). Analytical HPLC. (C). MALDI-TOF spectrum.

(MALDI-TOF+) m/z = 3029.71$[M+H]^+$, 3051.84$[M+Na]^+$, 3068.26$[M+K]^+$

2.4.4.4. Structure, Mass spectrum, and HPLC analysis of non-biotinylated ERK5 series compounds

(A)

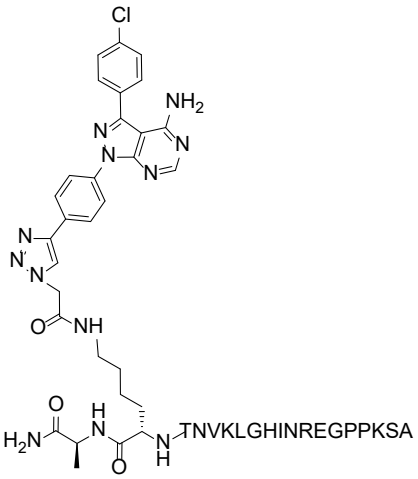

ERK 5.1

Exact Mass 2443.23

(B)

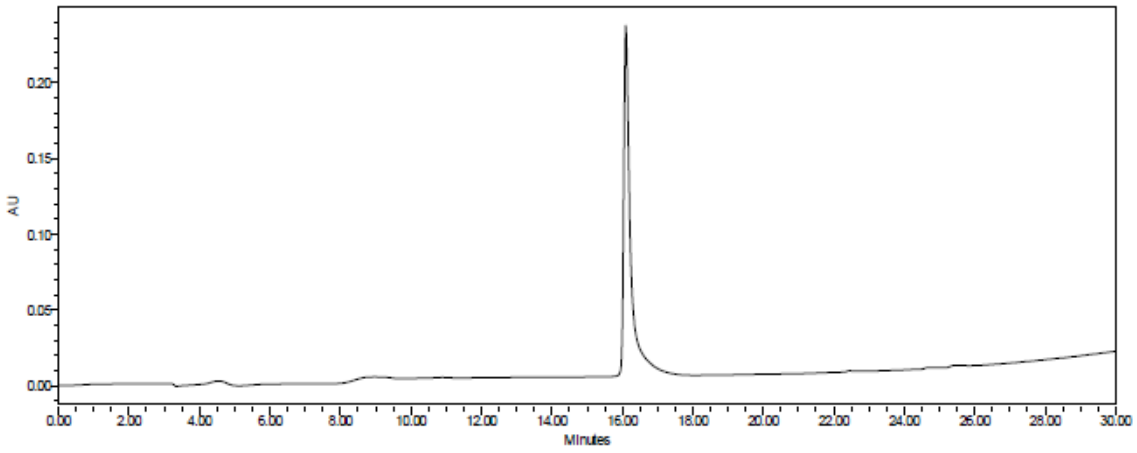

(C)

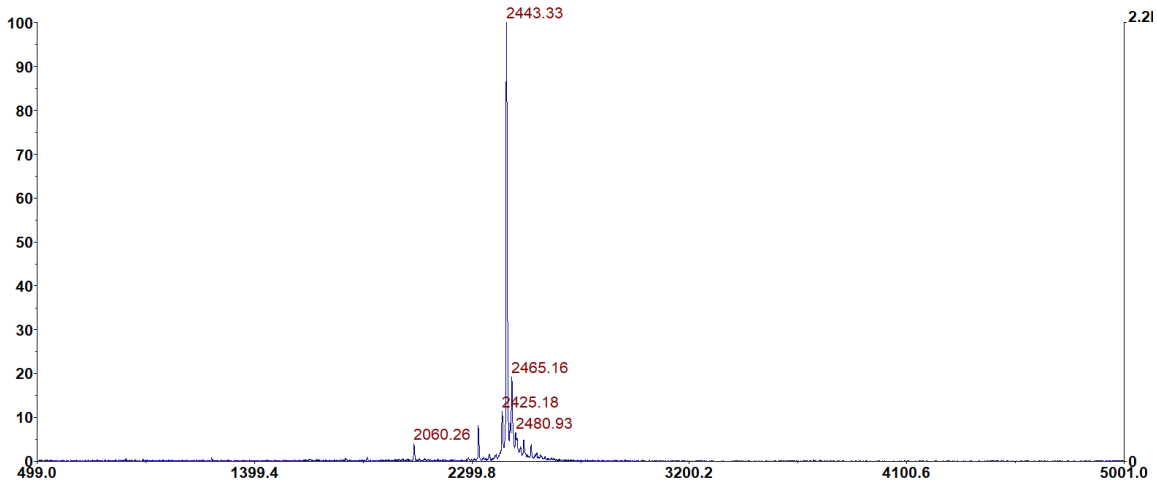

Characterization of ERK5.1: (A). Chemical structure. (B). Analytical HPLC. (C). MALDI-TOF spectrum.

(MALDI-TOF+) m/z = 2443.33$[M+H]^+$, 2465.16$[M+Na]^+$, 2480.93$[M+K]^+$

(A)

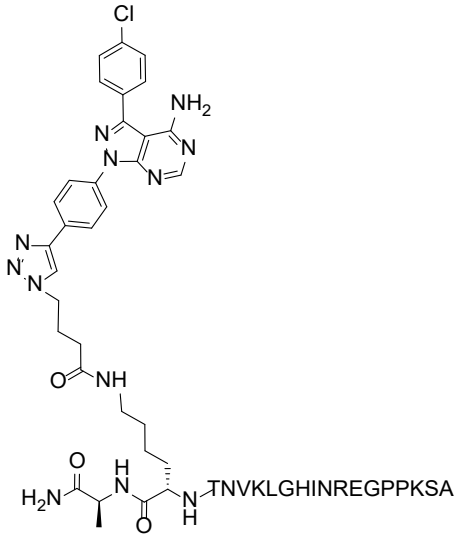

ERK 5.3

Exact Mass 2471.27

(B)

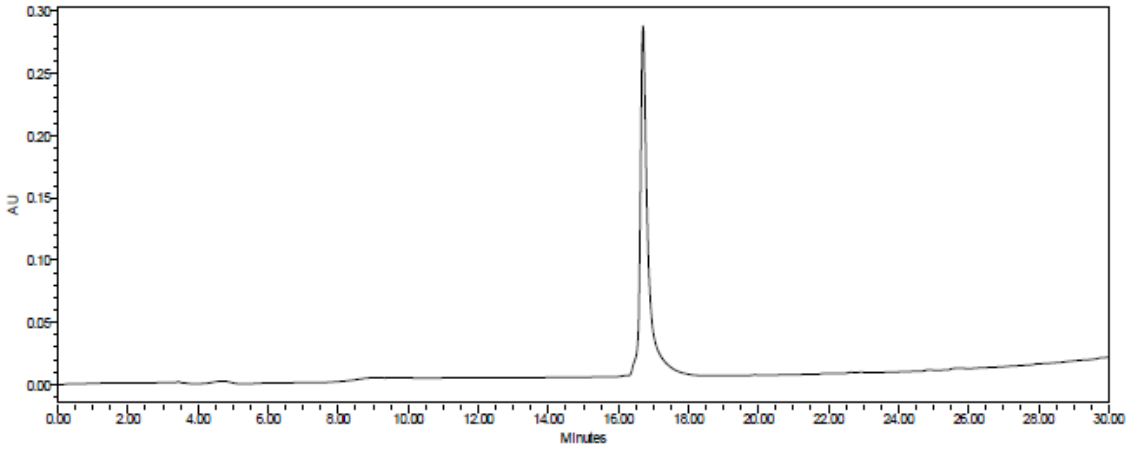

(C)

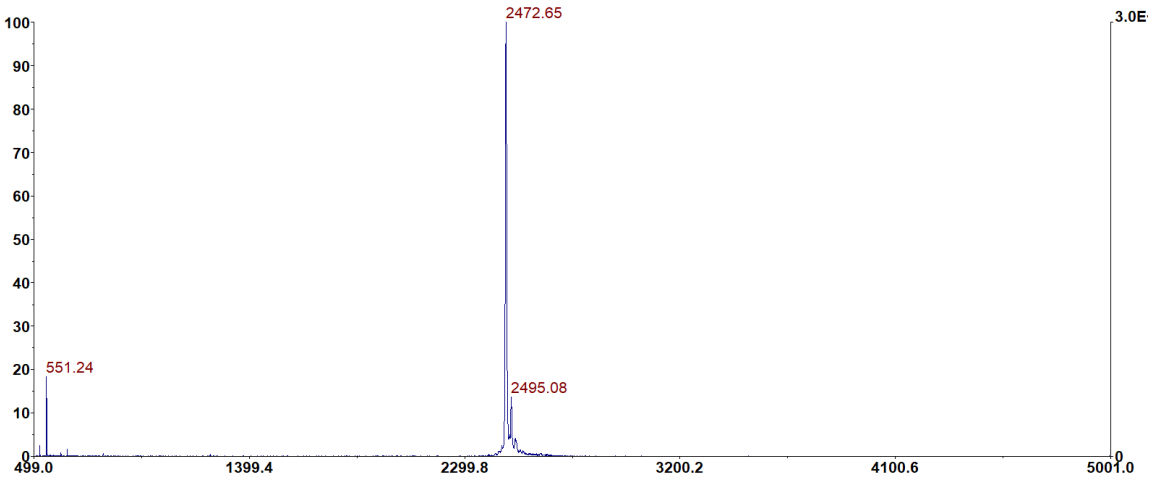

Characterization of ERK5.3: (A). Chemical structure. (B). Analytical HPLC. (C). MALDI-TOF spectrum.

(MALDI-TOF+) m/z = 2472.65$[M+H]^+$, 2495.08$[M+Na]^+$

2.4.5. Molecular modelling and docking studies:

MOE (Molecular Operating Environment, chemical computing group) software used for docking studies.[79] The crystal structure of ERK5 kinase in complex with MEK5 and ANP (PDB: 4IC7) was used for docking the PP2 analogue. First, the receptor (ERK5 kinase) was prepared by (i). removing the co-crystallized ligand (ANP) and MEK5 kinase (ii). correcting the structural issues in the crystal structure using the “structure preparation tool” (iii). adding and optimizing the H-bond network using protonate 3D tool. In a separate window, the ligand (PP2 analogue) was prepared for docking by (i). drawing the structure using “build” tool (ii). assigning atom types and charges using MMFF94x force field (iii). minimizing ligand energy. Next, the PP2 analogue was docked with ERK5 kinase and visualized.

Molecular modelling and docking results were visualized using either MOE or Discovery Studio (BIOVIA).

2.4.6. Biochemical Characterization:

2.4.6.1.ELISA-like binding assay:

White, 96 well Nickel coated plates (Pierce™) were coated with 50 µL of His tagged recombinant ERK5 protein (ProQinase GmbH, Freiburg, Germany) at a concentration of 1 µg/mL (diluted with Tris buffered Saline or TBS) for 1 hr at room temperature. All wells were washed with 3 X 100 µL of TBS and blocked with

starting block buffer (Thermo Fisher Scientific, Waltham, MA). Fifty microliters of biotinylated compounds in starting block buffer (PP2 monomer, D-site peptide monomer, Bt-ERK5.1, 5.2 and 5.3) were added to each well at 1, 3, and 10 μM concentrations and incubated for 1 hr. All wells were again washed with TBS (3 x 100 μL). Then all wells were incubated with fifty microliters of streptavidin-horse radish peroxidase (HRP) (Novus biologicals, Littleton, CO) in starting block buffer (at 1:800 dilution) for 1 hr. Next, all wells were washed as discussed before and treated with 50 μL of SuperSignal ELISA Pico Chemiluminescent Substrate (Thermo Fisher Scientific, Waltham, MA). The obtained luminescence signal was measured at all wavelengths using a Spectramax i3 microplate reader (Molecular Devices, San Jose, CA).

2.4.6.2. FRET based kinase assay:

Z'- lyte activity assay offered by SelectScreen Kinase profiling service (Thermo Fisher Scientific, Waltham, MA) has been used to determine the IC_{50} values of compounds. The same service was being utilized to investigate the selectivity profile of ERK5.1 against two closely related MAPKs: ERK1 and ERK2.

Z'- lyte assay is a fluorescence based coupled enzyme format. In this assay, substrate peptide is labelled with two different fluorophores coumarin and fluorescein at N and C terminus, respectively - that forms FRET pair. After a kinase reaction, the phosphorylated peptide incubated with a protease that specifically

cleaves the phosphopeptide which disrupts the FRET pair. The following protocol was used by Thermo Fisher (http://assets.ThermoFisher.com/TFSAssets/BID/Methods&Protocols/20180123_SSBK_Customer_Protocol_and_Assay_Conditions.pdf) according to their literature. 10 µL of kinase reaction mixure [100 nL of 100X compound in 100% DMSO + 2.4 µL of kinase buffer (50 mM HEPES pH 7.5, 0.01% BRIJ-35, 10 mM MgCl2, 1 mM EGTA) + 5 µL 2X peptide/kinase mixture + 2.5 µL 4X ATP solution] was incubated in a low volume Non Bonding Surface (NBS), black 384-well plate for 60 minutes. Five microliter of development reagent A solution at 1:1024 dilution was then added and incubated for another 60 minutes. The fluorescence was recorded using plate reader and analyzed as per their protocol. The analyzed data was reported as % kinase inhibition from company which was plotted against compound concentration using GraphPad Prism software using non-linear regression analysis to calculate IC_{50} values.

The same protocol was used for all three kinases (ERK1/2 and ERK5) which basically differs in the peptide/kinase mixture composition and ATP concentration which were detailed below:

ERK1: 5.94 - 94.5 ng MAPK3 (ERK1) and 2 µM Ser/Thr 03 in 50 mM HEPES pH 7.5, 0.01% BRIJ-35, 10 mM MgCl2, 1 mM EGTA, ATP (45 µM).

ERK2: 2 - 45.5 ng MAPK1 (ERK2) and 2 µM Ser/Thr 03 in 50 mM HEPES pH 7.5, 0.01% BRIJ-35, 10 mM $MgCl_2$, 1 mM EGTA, ATP (100 uM).

ERK5: 1.51 - 12.7 ng MAPK7 (ERK5) and 2 µM Ser/Thr 04 in 50 mM HEPES pH 7.5, 0.01% BRIJ-35, 10 mM MgCl2, 1 mM EGTA, ATP (17 µM).

2.4.7. Cellular Characterization:

2.4.7.1.Cell culture:

NCI-H1299 (male) lung cancer cell line was obtained from the cell collection of Dr. John Minna's research group at the UT Southwestern Medical Center. It was grown in RPMI-1640 supplemented with 10% FBS under 37°C and 5% CO_2.

2.4.7.2.MTS cell viability assay:

H1299 cells (800 cells) were plated per well in clear bottom 96-well plates. On 2nd day of plating, eight different concentrations of non-biotinylated derivatives of PP2 analogue, D-site peptide and ERK5.1 were prepared between 0.1 to 40 µM in RPMI medium in presence of 10% FBS and 1% BSA. All the three compounds and each concentration were tested in triplicate. The same treatment was repeated on 4th day of the cells plating. Next, 20 µl of CellTiter 96® Aqueous One Solution MTS reagent (Promega, WI) was added to each well on day 5 and were incubated for 2 hrs. Absorbance was measured from each well at 490 nm wavelength using the plate reader (Spectramax i3, Molecular Devices, CA).

2.4.7.3.Colony formation assay:

H1299 cells were seeded at in a 6-well plate (300 cells per well) and allowed to attach for overnight. On following day, cells were treated with non-biotinylated derivatives of PP2 analogue, D-site peptide, ERK5.1 and ERK5.3 as a negative control (RPMI + 10% FBS + 1% BSA). Each compound was tested at three different concentrations (0, 5, 10 μM). On day 9 of cells plating, colonies were washed with PBS, fixed with 10% formalin and stained with 20% crystal violet solution in methanol (EMD Millipore Sigma, Danvers, MA) for 10 minutes followed by washing with distilled water to remove the excess stain.

2.4.7.4. Wound healing assay:

H1299 cells were plated in 24 well plates (100,000 cells per well) and cells were allowed to grow a monolayer. A cross section scratch was made in each well and subsequently washed with PBS for one time to remove the cell debris. Then cells were treated with non-biotinylated derivatives of PP2 analogue, D-site peptide, ERK5.1 and ERK5.3 at three different concentrations (0, 5, 10 μM) diluted in growth medium (RPMI + 10% FBS + 1% BSA). After 24 hours, cells were stained with 20% crystal violet solution in methanol and photographs were taken at 10X microscope.

2.4.7.5. Western blot:

H1299 cells were grown to get 70-90% confluence and treated with 40 μM of non-biotinylated PP2 analogue, D-site peptide, ERK5.1 and ERK5.3 for 2:15 hours at 37 °C. Then culture medium was removed and lysis buffer (Thermo Fisher Scientific, Waltham, MA) premixed with protease and phosphatase inhibitor cocktail (Thermo Fisher Scientific, Waltham, MA) was added and incubated for 30 mins at 4 °C. Cell debris was scrapped and centrifuged in 1.5 mL tube for 15 mins (at 10,000 g). Supernatant layer of cell lysate was collected and separated using SDS-PAGE gel (Mini-PROTEAN TGX Gels) (Bio-Rad, Hercules, CA) and transferred on to nitrocellulose membranes. Membranes were then probed with anti-phospho-BMK1/ERK5(Tyr218/Thr220) (EMD Millipore Sigma, Danvers, MA) (1:1000) and anti-ERK5 (big-MAPK, BMK 1) (EMD Millipore Sigma, Danvers, MA) (1:4000) primary antibodies and visualized using appropriate secondary antibody: anti-rabbit IgG, HRP-linked antibody (1:1000) (Cell Signaling Technology, Danvers, MA) followed by enhanced chemiluminescent detection using Pierce ECL western blotting substrate (Thermo Fisher Scientific, Waltham, MA).

2.4.7.6.Statistical analysis:

Statistical analysis has been performed using GraphPad prism 6 software. The fluorescence and luminescence readings were first normalized to negative controls

and then analyzed. Dose-response curves were generated according to best fit model and IC_{50} values were calculated using non-linear regression analysis.

2.5. Results and Discussion:

2.5.1. Design of hetero-bivalent inhibitors targeting ERK5 kinase:

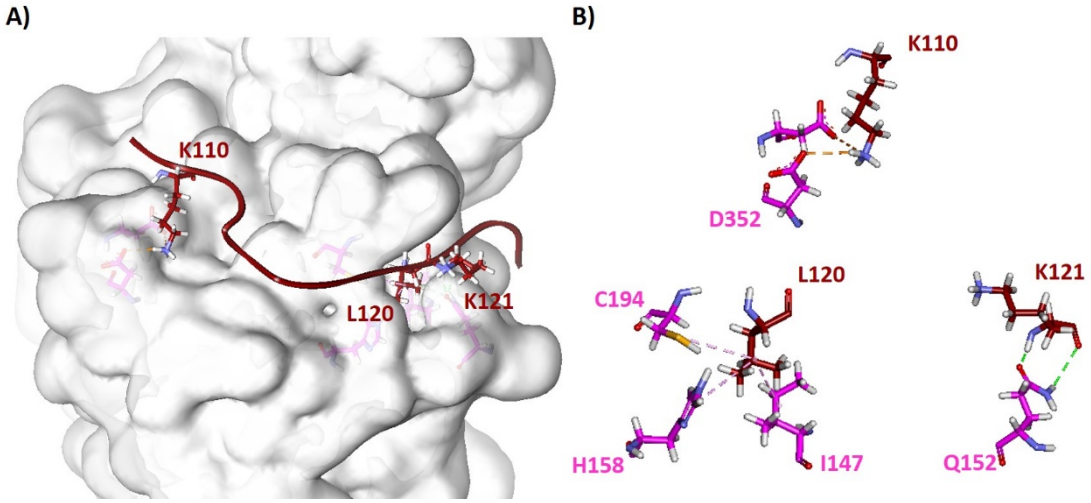

Figure 6. Crystal structure of MEK5:ERK5 complex. For simplicity, only D-site motif of MEK5 (C-terminus 19 amino acids or D-site peptide) are shown. Only the amino acid residues that are mainly involved in interactions were highlighted in stick type representation. (A) Surface view (B) Atomic view of non-covalent interactions between D-site peptide and ERK5 kinase (pink-blue color: ERK5 kinase and brown-blue color: D-site peptide). Hydrophobic, ionic and hydrogen bond interactions were highlighted in light pink, red and green color, respectively.

The hetero-bivalent inhibitor design consists of two components: (a) peptide that targets specific secondary binding pocket outside of the ATP binding site, (b) ATP binding site ligand. We selected the D-site peptide, a 19 aa portion from the C-terminus docking site of MEK5 that is previously known to interact with ERK5, as the secondary binding moiety because (i) it is critical for binding of MEK5, as deletion of this sequence leads to loss of binding[59] (ii). it imparts specificity to ERK5 when compared with closer family kinases ERK1/2.[59] Most importantly, the availability of the MEK5: ERK5 complex crystal structure facilitates the design of optimal linkers necessary for the design of hetero-bivalent inhibitors. In this structure, the D-site peptide interacts with docking groove of ERK5 kinase through

several non-covalent interactions which include (i). salt bridge between Lys-110 and Asp-352 from ERK5 (ii). hydrophobic interaction between Leu-120 and Ile-147, His-158 & Cys-194 from ERK5 (iii). backbone H-bond between amine of Lys-121 and carbonyl group of Asn-152 from ERK5 (Fig. 6). These contacts project the Arg-125 towards the ATP binding site, providing a naturally existing linker path on the kinase surface.

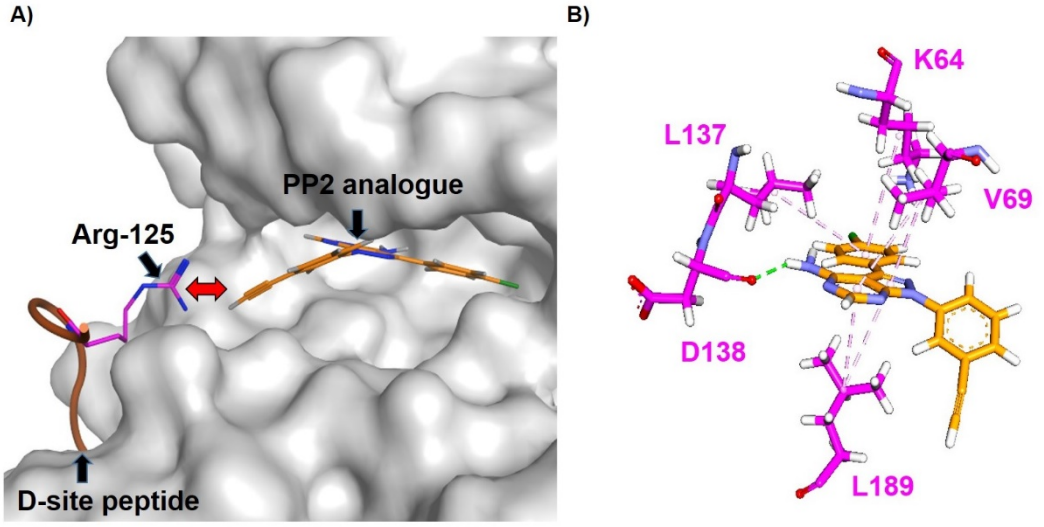

Figure 7. Proposed hetero-bivalent ligand design. (A) Envisioned linker path connecting the D-site peptide and docked structure of PP2 analogue. (B) The amino acids mainly involved in interaction with PP2 analogue are highlighted. (pink-blue color: ERK5 kinase and orange blue color: PP2 analogue). H-bond interactions and hydrophobic interactions are highlighted in green and light pink color, respectively.

Next, we selected a PP2 analogue, a phenyl alkyne derivative of pyrazolopyrimidine analogue (PP2), a previous src kinase inhibitor that was later reported to promiscuously inhibit multiple kinases among the kinome.[76] The core pyrazolopyrimidine scaffold mimics the adenine ring of ATP, providing the common structural feature necessary to interact with ATP binding cleft of kinases. Moreover,

the presence of the alkyne group aids the chemo-selective incorporation of PP2 analogue into peptide sequences containing azide linkers using Cu(I)-catalyzed azide-alkyne cycloaddition (CuAAC).

Next, as the crystal structure of PP2: ERK5 complex has not been reported, we employed molecular docking to visualize PP2 analogue binding into the ATP binding pocket of ERK5 using Molecular Operating Environment (MOE) software.[79] PP2 analogue bound in a typical type-I inhibitor mode (Fig. 7). Typical interactions include (i). H-bond interaction between the carbonyl of Asp-138 in the hinge region of kinase and 6-amino group of the adenine ring (ii). hydrophobic interactions between core adenine ring and side chains of Lys-64, Val-69, Leu-137, and Leu-189. Most importantly, in a low energy pose, the aryl alkyne group of PP2 analogue oriented towards the Arg-125 in the D-site peptide. In this pose, the distance between the guanidine carbon in Arg-125 and the terminal carbon of the aryl alkyne in PP2 analogue was found to be ~4 Å. Here, we used hydrophobic azidoalkanoic acid derivatives that can cover distances between 3.5–6 Å, as linkers.

Next, we modified our previously published complete on bead synthesis protocol to synthesize the hetero-bivalent ligands.[37, 77] The NovaSyn TGR resin with low loading (0.20–0.30 mmol g^{-1}) capacity was selected for the synthesis because it provides enough space which can accumulate the larger complex molecules without steric hindrance.

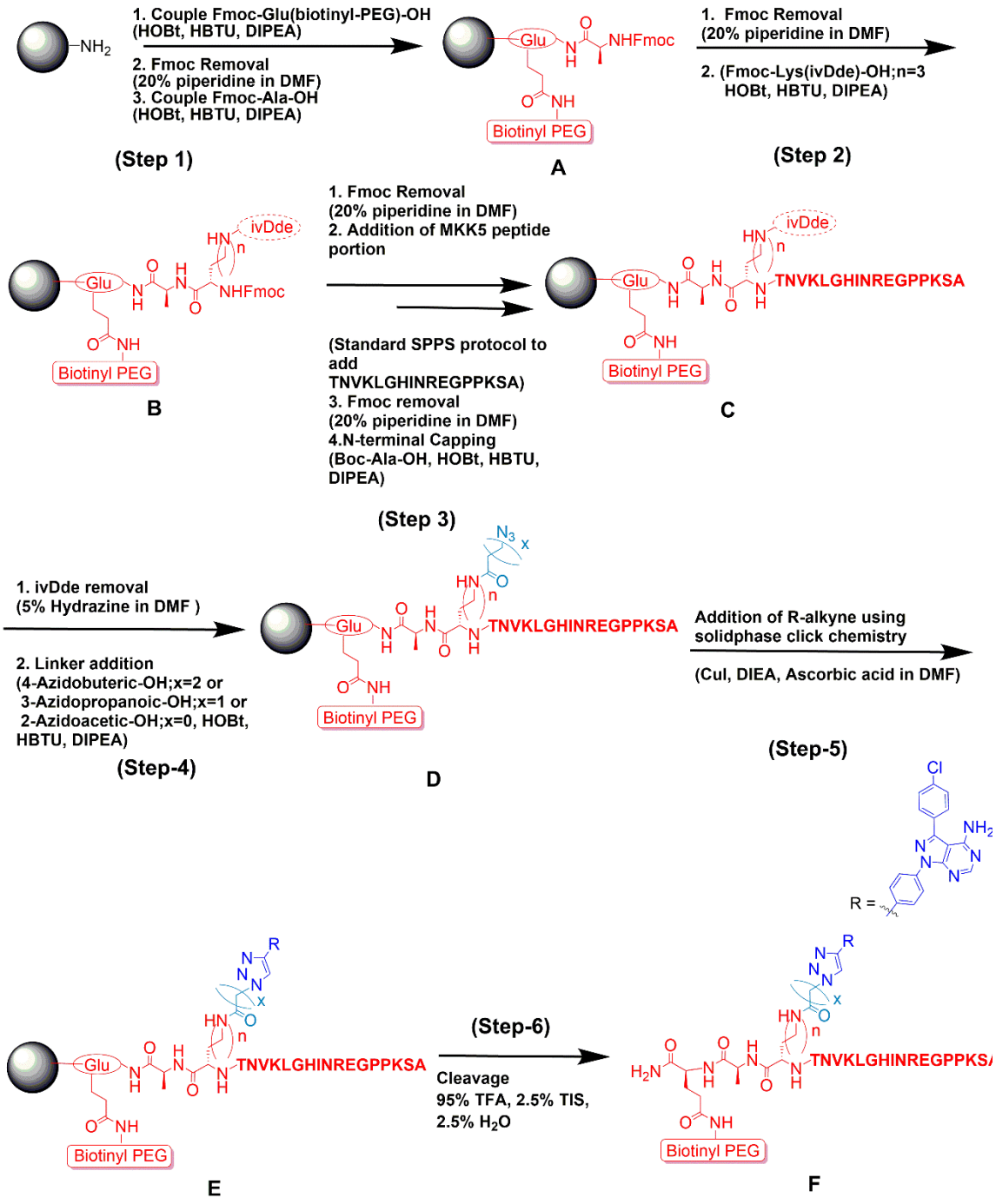

Scheme 3. Synthesis Scheme for ERK5 series of hetero-bivalent ligands.

The first amino acid residue coupled was Fmoc-Glu(biotinyl-PEG)-OH, which provides biotin moiety necessary for detecting the binding event. Next, 20% piperidine in dimethylformamide (DMF) was employed to remove the fluorenylmethyloxycarbonyl (Fmoc) protection, followed by coupling of the second residue Fmoc-Ala-OH to yield compound A (Scheme 3, step 1). Again, Fmoc was deprotected using 20% piperidine (in DMF) and coupled the next residue Fmoc-Lys(ivDde)-OH (*N*-α-Fmoc-*N*-ε-1-(4,4-dimethyl-2,6-dioxocyclohex-1-ylidene)-3-methylbutyl-L-lysine) to get compound B (Scheme 3, step 2). In our design, we replaced the Arg-125 with Lys (Fmoc-Lys-IvDde-OH) as the central linker to connect the D-site peptide and PP2 analogue because (i). arginine is not the critical basic amino for typical D-site binding [59, 80] (ii). the Lys can as a central linker having two orthogonal protecting groups, Fmoc and IvDde, on two different terminal amines which enable to chemoselectively control the synthesis. First, we deprotected the Fmoc using 20% piperidine (in DMF) and built the next amino acids TNVKLGHINREGPPKSA sequentially (except alanine). At the end, Boc variant of alanine, Boc-Ala-OH was coupled to block the N-terminus to get compound C (Scheme 3, step 3). Next, IvDde group was deprotected using 5% hydrazine in DMF and azidoalkanoic acids of different lengths (n=1,2,3) were coupled (compound D) (Scheme 3, step 4). The PP2 analogue was introduced into the sequence using CuAAc in a solvent mixture of dimethylsulfoxide (DMSO): pyridine (3:2) to get compound E (Scheme 3, step 5). Finally, the resin was treated

with cleaving cocktail [95% trifluoroacetic acid (TFA), 2.5% triisopropylsilane (TIS), and 2.5% H_2O], which removes all side chain protecting groups in the synthesized compounds and cleaves it from the resin (compound F) (Scheme 3, step 6). All three hetero-bivalent ligands were synthesized with and without C-terminal biotinylation for *in vitro* binding and activity studies, respectively.

2.5.2. Identification of optimum ERK5 binding hetero-bivalent ligands:

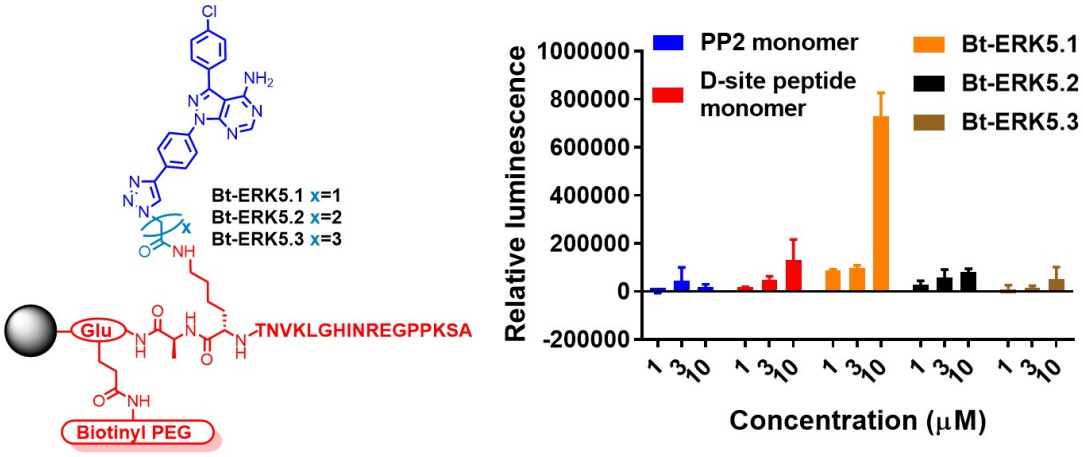

Figure 8. Binding of the ERK5 series of hetero-bivalent ligands. (A). The common chemical structure of the hetero-bivalent ligands. (B). ELISA-like assay results of biotinylated hetero-bivalent ligands binding to the ERK5 kinase domain at three different concentrations (1, 3, and 10 μM). Only Bt-ERK5.1 showed high affinity.

To find the optimal hetero-bivalent ligand, we employed previously established ELISA-like binding assay in our lab.[37] Briefly, nickel coated plates were first coated with His tagged ERK5 kinase domain, and then biotinylated ERK5 derivatives were added to each well at three different concentrations (1, 3 and 10 μM). The binding event was visualized using streptavidin – horseradish peroxidase (HRP) enzyme, which converts the substrate to the luminescent light that is measured at all

wavelengths. In this assay, the shortest linker containing hetero-bivalent ligand Bt-ERK5.1 has shown high affinity towards the ERK5 kinase domain when compared with two longer derivatives Bt-ERK5.2, 5.3 and monomers – PP2, D-site peptide monomers (Fig. 8). It indicates that Bt-ERK5.1 has correct linker length that allows it to simultaneously occupy both PP2 and D-site peptide binding pockets. The longer linker length containing Bt-ERK5.2 and 5.3 exhibited weaker binding similar to the monomers indicating that they were ineffective.

Having confirmed binding results, next activity assays were performed to check the phosphorylation inhibition activity of the compounds. As our design strategy highlights inhibition of (i). MEK5 mediated ERK5 phosphorylation (ii). ERK5 auto-phosphorylation using a single molecule, we employed two assay systems, namely, (i). cell-based western blot (ii). FRET-based kinase system to prove these phosphorylation events, independently.

2.5.3. Hetero-bivalent ligand blocks MEK5 activated ERK5 kinase activity:

First, we employed a cell-based western blot assay to prove MEK5 mediated ERK5 phosphorylation. Here, we utilized native MEK5 mediated phosphorylation in live cell settings and probed this phosphorylation event using anti-BMK1/ERK5(Tyr-218: Thr-220) antibody that specifically detects phosphorylation at Tyr-218 and Thr-220 residues of ERK5. Here, we employed non-biotinylated versions of PP2 monomer, D-site peptide, ERK5.1, and weaker derivative ERK5.3 for this purpose. Briefly, H1299 lung cancer cells were treated with 40μM of indicated compounds

and incubated for one hour. Then cells were lysed, proteins present in cell lysate were separated using western blot and probed with anti-BMK1/ERK5(Tyr-218: Thr-220) antibody.

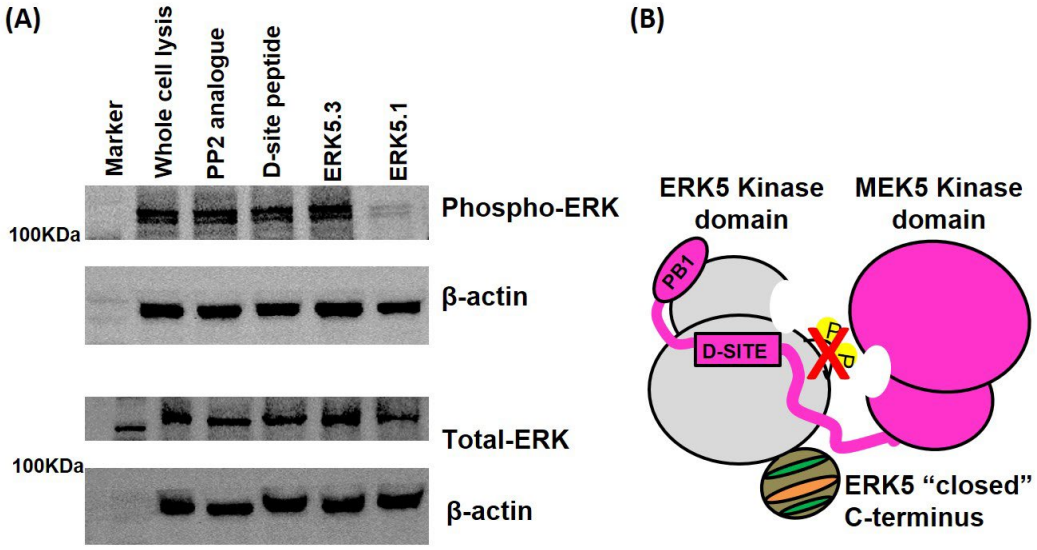

Figure 9. Results of *in vitro* cell based western blot detection to measure MEK5 mediated ERK5 phosphorylation. (A). H1299 cells were untreated or treated with indicated compounds and whole cell lysates were analyzed by Western blot. Only ERK5.1 inhibited MEK5-mediated phosphorylation. (B). Cartoon showing inhibition of MEK5 mediated ERK5 phosphorylation (red "X" mark indicates the blocking phosphorylation site).

As shown in Fig. 9(A), ERK5.1 completely inhibited the phosphorylation, as evidenced by the loss of the corresponding band in western blot. However, the phosphoERK5 bands corresponding to monomers and ERK5.3 still present, indicating that they did not interfere with the MEK5 mediated ERK5 phosphorylation or cell permeable.

Interestingly, this finding is congruent with a previous report where D-site peptide alone failed to inhibit the binding of MEK5 to ERK5.[59] In their report, pull down

experiments were utilized to find out which segment of MEK5 kinase is necessary for MEK5: ERK5 interaction. As per their results, the D-site peptide alone did not pulldown ERK5 kinase, but when it was combined with other MEK5 segments, either N-terminus or PB1 domain, ERK5 kinase was pulled down. It suggested that D-site peptide is critical for binding of MEK5 but not alone, only when combined with another part of MEK5 (either PB1 domain or N-terminus), which indicates that synergistic binding behavior of the D-site peptide with any other segment of MEK5 while binding. Our bivalent strategy employs the similar synergistic binding principle but using ATP binding site partner thePP2 analogue instead of other parts of MEK5 kinase. However, the correct linker length is necessary for this synergism as the incorrect linker containing hetero-bivalent ligand, ERK5.3, failed to inhibit the MEK5 mediated ERK5. Certainly, it is still possible that both the D-site peptide and ERK5.3 alone may not be cell permeable, but the weak binding behavior of these two compounds in ELISA-like assays suggests the absence of synergism could be the reason for the inactivity of those individual monomers. However, direct cell permeability studies need to be performed to further confirm this finding.

2.5.4. Hetero-bivalent ligand blocks ERK5 auto-phosphorylation:

To investigate the effects on ERK5 auto-phosphorylation, a commercially available FRET-based phosphorylation assay was used to measure the compound's ability

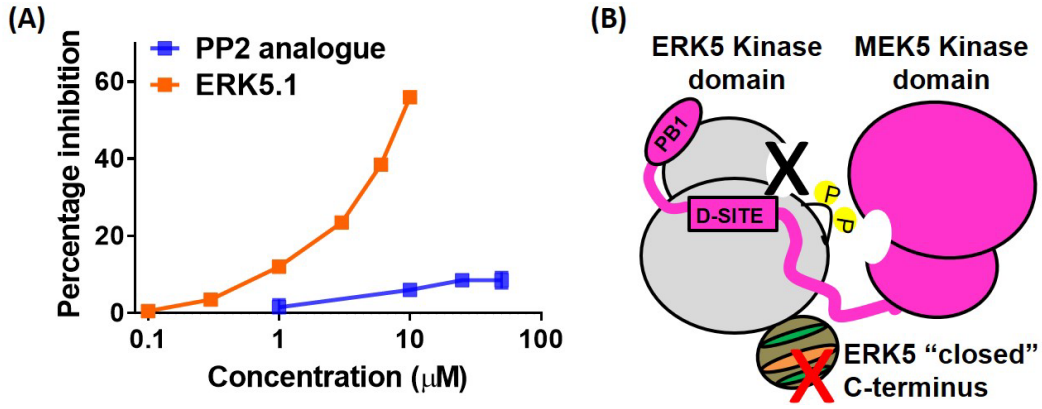

Figure 10. Results of in vitro ERK5 kinase activity assay to measure auto-phosphorylation. (A) The FRET-based ERK5 kinase inhibition assay was performed with varying concentrations of ERK5.1 or the PP2 analogue. ERK5.1 inhibited ERK5 auto-phosphorylation (IC_{50}~8.5 μM). (B). Cartoon representation of ERK5 auto-phosphorylation (black and red "X" marks on the cartoon indicate the blocking site and the affected phosphorylation site, respectively).

to inhibit the ATP binding pocket that represents the substrate phosphorylation. This assay employs activated ERK5 or phosphorylated ERK5, which avoids the need for MEK5 kinase. This uniquely allows us to investigate how MEK5 independent ATP binding pocket inhibition alone affects ERK5 auto-phosphorylation. The active hetero-bivalent ligand-ERK5.1 and PP2 analogue were tested to inhibit the ATP pocket using this assay. As shown in Fig. 10(A), the PP2 analogue alone did not inhibit ERK5 kinase auto-phosphorylation (up to 50 μM), which indicates it is a very weak inhibitor. Interestingly, ERK5.1 has inhibited the auto-phosphorylation in concentration dependent manner with an IC_{50} of 8.5 μM. It suggests that PP2 analogue gained increased access to ATP pocket upon D-site peptide conjugation. As a result, it inhibited the ERK5 kinase auto-

phosphorylation. It also proves that ERK5.1 can still bind to active ERK5, even after activation phosphorylation mediated by MEK5.

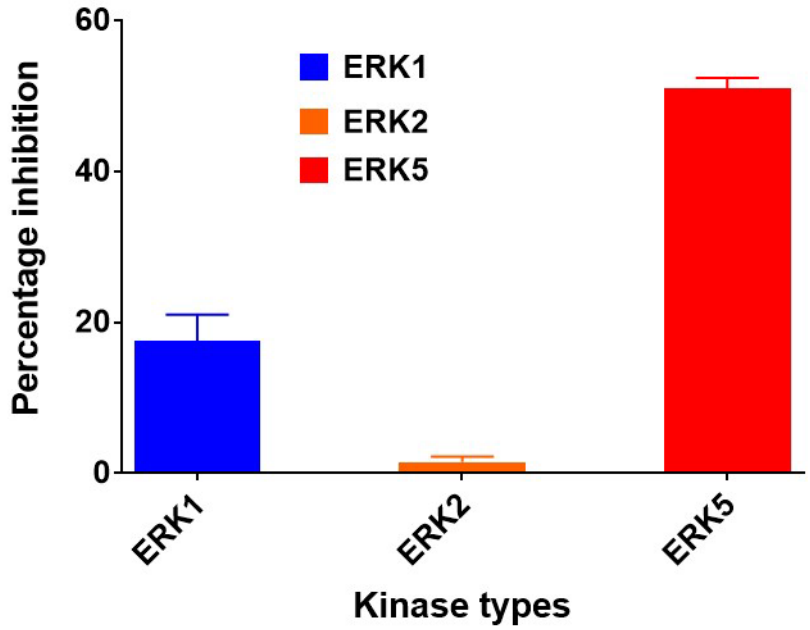

Figure 11. Selectivity results ERK5.1 using kinase activity assay against ERK1/2 and ERK5. The FRET-based ERK5 kinase inhibition assay demonstrated that ERK5.1 specifically inhibited ERK5 when compared to ERK1/2.

We also assessed the selectivity of ERK5.1 against two closely related kinases ERK1/2 using the same FRET-based phosphorylation assay. The hetero-bivalent inhibitor did not inhibit ERK2, slightly inhibited ERK1, and selectively inhibited ERK5 at the measured concentration (8.5 μM), which indicates the selective inhibition ERK5 (Fig. 11) when compared with closer family kinases ERK1/2.

Next, to study whether ERK5.1 can interfere with ERK5 signaling in CSCs, two specific CSC phenotype assays were performed using H1299 cells that are known

to have a significantly higher subpopulation of CSCs. Those assays are (i) colony formation assay (ii) wound healing assay.

2.5.5. Hetero-bivalent ligand inhibits CSC colony formation:

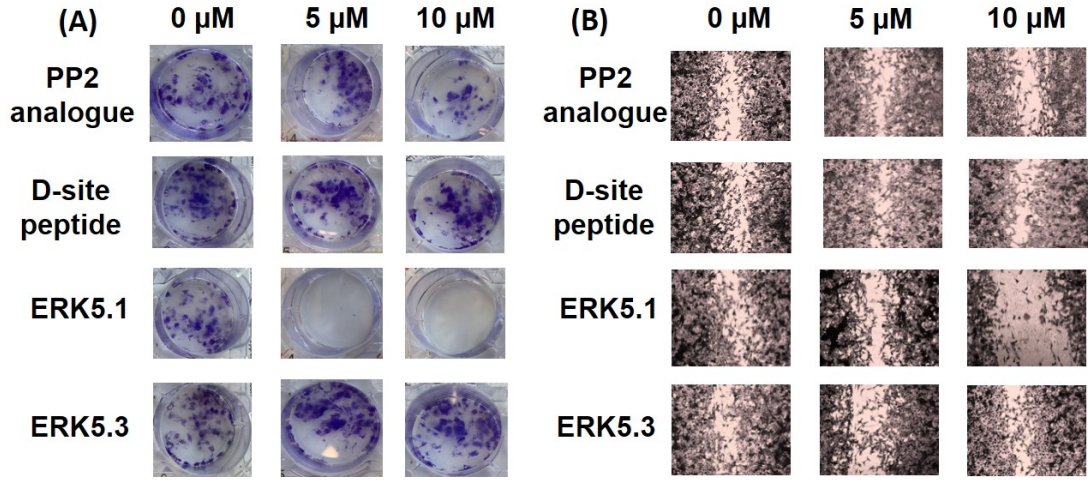

Figure 12. ERK5.1 inhibits CSC signaling in H1299 cells. Treatment with ERK5.1 (A). inhibited colony formation (the self-renewal phenotype) (B). reduced wound healing (the migration phenotype) when compared to treatment with PP2 analogue, D-site peptide, or ERK5.3.

Here, we employ colony formation assay, which tests the ability of CSCs to form colonies in the presence and absence of compounds. CSCs do not require cell to cell contact for their survival, but normal cancer cells do. So, when the cancer cells were seeded at very low number that does not allow cell to cell contact, only CSCs remain and form colonies in media but not normal cells. The compounds are considered to be active against treated H1299 cells with active hetero- bivalent ligand ERK5.1 and weaker ERK5.3, PP2, D-site peptide that can act as controls. As shown in Fig. 12A,Fig. 12(A), only ERK5.1 inhibited colony formation at both 5 µM and 10 µM when compared to 0 µM treatment, which indicates that ERK5.1

specifically kills CSCs. This finding is consistent with previous reports where ERK5 knockdown showed to inhibit colony formation.[48, 81] The two monomers PP2 analogue, D-site peptide, and non-optimal weaker bivalent ligand ERK5.3 did not show any inhibition as indicated by the presence of colonies even at high concentrations (10 μM). Here, ERK5.1 completely inhibited CSC proliferation even at 5 μM concentration, which is below the IC_{50} obtained in the kinase assay (8.5 μM). The reason for such discrepancy may be double attacking mechanism of ERK5.1 inhibiting the MEK5: ERK5 axis in CSC signaling. ERK5.1 acts by not only inhibiting the ERK5 kinase activity but also blocks the upstream MEK5 binding to ERK5 for its activation , which is also responsible for the CSC proliferation phenotype. By simultaneously inhibiting both upstream and downstream phosphorylation events, the hetero-bivalent ligand exhibits greater potency than molecules targeting only the ERK5 kinase activity as measured using the kinase assay.

2.5.6. Hetero-bivalent ligand blocks CSC migration:

Here we employ wound healing assay, which tests the migration phenotype of CSCs. We make a scratch in growing cancer cell monolayer and measure the ability of CSCs to heal that wound in the presence or absence of compounds. Under normal conditions, CSCs can migrate to fill the gap formed after making the scratch while non-stem cancer cells migrate less. We treated the H1299 cells with

the same set of indicated compounds in the above paragraph. Again, the active hetero-bivalent ligand ERK5.1 inhibited the wound healing (at 10 μM), while the weaker hetero-bivalent ligand ERK5.3 and monomers (PP2 analogue and D-site peptide) did not, which is consistent with colony formation assay (Fig. 12.B). It indicates that ERK5.1 can inhibit CSC signaling in H1299 cells.

2.5.7. Hetero-bivalent ligand reduces CSC controlled cancer cell proliferation:

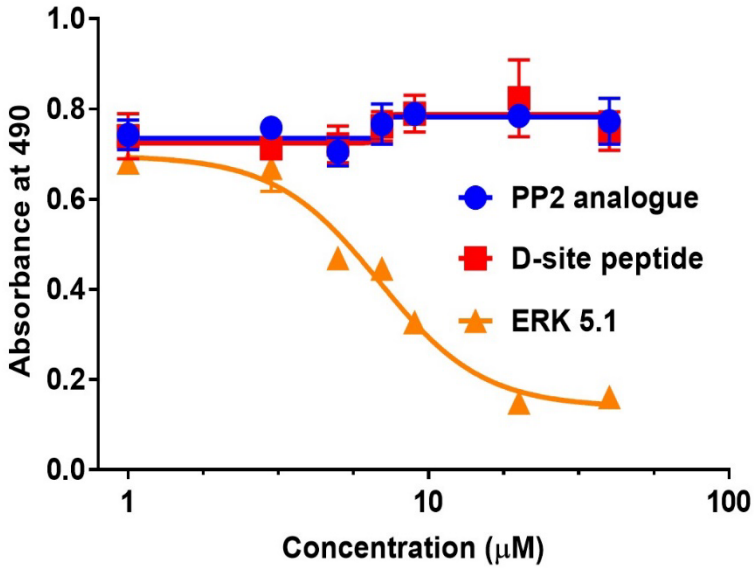

Figure 13. ERK5.1 inhibited the cell proliferation of H1299 cells. The standard MTS cell viability assay showed that only ERK5.1 (not PP2 analogue nor D-site peptide) inhibited cell proliferation (IC_{50} ~6.5 μM).

Finally, we measured the overall H1299 cancer cell proliferation using the standard cell viability MTS assay, as CSCs typically drive the overall cell survival, growth and proliferation. Briefly, H1299 cells were seeded and treated with different concentrations of PP2 analogue, D-site peptide, ERK5.1. Following with previous

results, only ERK5.1 inhibited total cell proliferation, as indicated by loss of cell growth with an IC_{50} 6.5 μM. Both monomers, PP2 analogue, and D-site peptide did not affect cancer cell growth (Fig. 13).

2.6. Conclusion:

We have developed the first CSC targeting hetero-bivalent ligand that inhibited CSC signaling in H1299 lung cancer cells. Using the hetero-bivalent ligand design concept, we exploited the D-site peptide, a critical peptide interaction that is necessary for MEK5 to interact and activate ERK5 kinase (MEK5 mediated ERK5 phosphorylation). D-site peptide alone is a very weak binder and requires additional MEK5 segment (either PB1 domain or Kinase domain) for proper binding to ERK5. So far, conventional ATP binding site inhibitors of ERK5 were unsuccessful in converting ERK5 inhibition to yield anti-CSC activity. Therefore, we targeted this D-site peptide that is known to activate ERK5 as a starting point of our design and connected that with the weak ATP binding site compound-PP2 analogue. Our hypothesis was to design a hetero-bivalent ligand that simultaneously inhibits MEK5 mediated ERK5 phosphorylation and ERK5 auto-phosphorylation to inhibit ERK5 signaling. Using two unique independent assay systems, MEK5 mediated ERK5 phosphorylation and ERK5 auto-phosphorylation inhibition were studied. Our approach is to simultaneously block D-site peptide interaction along with ATP binding pocket using a hetero-bivalent ligand design.

First, using a cell-based assay system, native MEK5 mediated ERK5 phosphorylation was studied. ERK5.1 inhibited this phosphorylation indicating that this hetero-bivalent ligand accesses the D-site peptide groove, which is critical for mediating MEK5: ERK5 interaction. Next, using FRET-based kinase inhibition assay, ERK5 auto-phosphorylation was studied. In this assay, ERK5.1 inhibited kinase activity, indicating it can access the ATP binding pocket of ERK5 kinase. Both of these results independently demonstrated that ERK5.1 can simultaneously inhibit D-site motif and ATP binding pocket of ERK5. Further, the inhibition of CSC signaling was studied using two gold standard CSC phenotypes: colony formation and wound healing. ERK5.1 inhibited the colony formation in clonogenicity assay and migration in wound healing assay. These results further confirm that inhibiting both ERK5 kinase activation and auto-phosphorylation using a single hetero-bivalent compound translates into anti-CSC activity.

2.7. Future directions:

Future ERK5 hetero-bivalent ligands will be designed to access a different linker path that connects the C-terminus of D-site peptide to the PP2 analogue (Fig. 14). We propose this design based on another docking pose of the PP2 analogue in which the alkyne group faces towards the alanine at the C-terminus of the D-site peptide (Fig. 14.B). Most importantly, we observed an additional binding pocket in

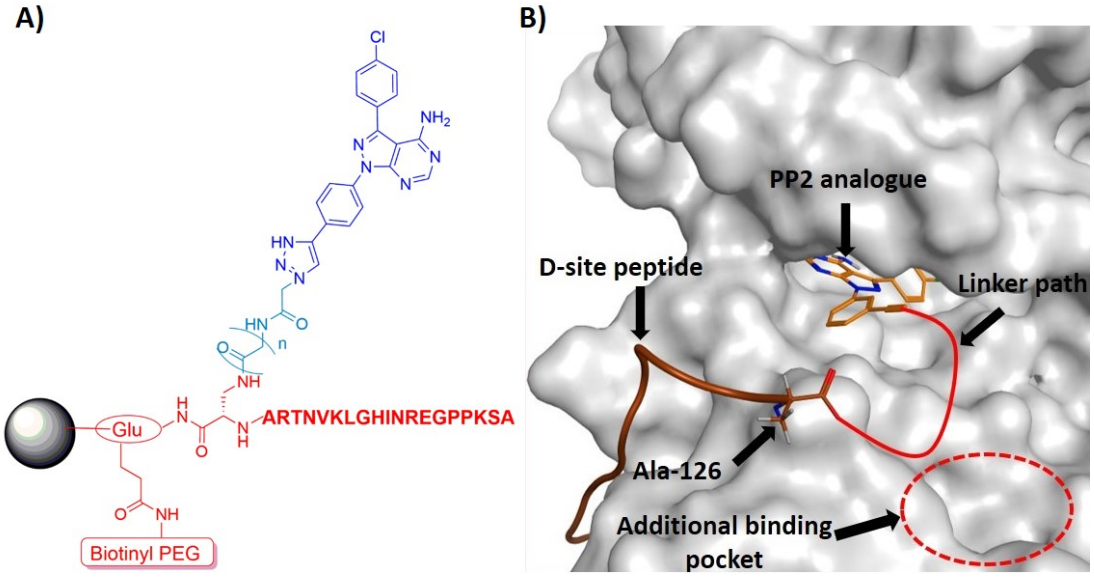

Figure 14. ERK5.2 series of hetero-bivalent ligand design. (A) Common structure (B) proposed hetero-bivalent ligand connecting the D-site peptide and PP2 analogue.

between the D-site peptide and PP2 analogue binding sites, as shown in Fig. 14(B). Therefore, we propose to develop a linker that can potentially occupy this area and access this additional binding pocket. Our idea is to design a single molecule that can bind to all three pockets simultaneously. In our design strategy, we will utilize Fmoc-Dap-IvDde-OH (Fmoc-N^{β}-(4,4-dimethyl-2,6-dioxocyclohex-1-ylidene)-3-methylbutyl-L-2,3-diaminopropionic acid) as a central linker to hold PP2 and D-site peptides. Both of these monomers will be connected using glycine linker and screen to find the optimum linker containing hetero-bivalent ligand. Next, we will use docking to find the best fitting small organic moiety that can fit into the additional pocket and then it will be incorporated into the optimized linker using

peptoid chemistry. We expect this approach to yield novel hetero-multivalent ligands with improved affinity and selectivity towards ERK5 kinase.

In addition, we can optimize the active hetero-bivalent ligand ERK5.1 in two different directions. First, we plan to identify unimportant residues of ERK5.1 that are not involved in forming any contacts with ERK5 and replace them with sarcosine residue to improve cell permeability of ERK5.1. So far, we identified four amino acids Asn-116, Ile-117, Asn-123, Thr-124 that do not interact with ERK5 kinase surface. Through introducing flexible sarcosine residue into peptide backbone imposes entropic penalty on the hetero-bivalent ligand, we still want to test the possibility of improved cell permeability, because the cell permeability achieved may surpass the entropic loss. In a second approach, we plan to shorten the linker length of ERK5.1 to check how it affects binding affinity and activity of the resultant hetero-bivalent ligand. We believe these changes will further improve cell permeability and activity of ERK5.1.

Moreover, we will work on obtaining co-crystals of ERK5.1 in complex with the ERK5 kinase domain, which will further support a dual-site (both ATP and D-site peptide) binding mode of the hetero-bivalent ligand. Besides, the co-crystal structure will help to identify critical interactions between ERK5.1 and the kinase domain that provide guidence for the development of potent bivalent analogues using further structure-based optimization studies in the future.

3. HETERO-BIVALENT LIGANDS TARGETING EPHRIN A3 (EPHA3) KINASE

3.1. Literature review:

Hetero-bivalent ligand design proved to be an effective strategy to develop potent and selective kinase inhibitors.[13, 23, 82] Much improved affinity and specificity towards the target kinase can be achieved by simultaneously targeting two heterogenous binding sites, namely; ATP and a peptide binding pocket. Since ATP binding pockets are conserved among the kinome, hetero-bivalent ligand design principles focus on targeting peptide binding pockets to gain selectivity.[13, 23]

The earlier hetero-bivalent designs primarily were based on attaching the ATP mimetic to a peptide, which is derived from an interacting protein known to bind to a binding pocket close to ATP binding site of the targeted kinase, using a suitable linker moiety.[28-29, 31, 33, 38-39, 83] The peptide sequence is usually obtained either from the crystal structures or previous known binding or activity studies of target kinases with their binding partners. For example, Tanya, et al. reported a selective bisubstrate inhibitor targeting protein kinase A (PKA).[28] Here, they have selected a peptide epitope from the PKA Inhibitor (PKI) that is known to the outside of the substrate peptide pocket and inhibit PKA catalytic activity. A miniature protein scaffold based avian pancreatic peptide (aPP) was utilized to display α helical PKI epitope and it was conjugated with K252a derivative, an indolocarbazole based natural product that is reported to inhibit several tyrosine and serine-threonine kinases. Interestingly, the bisubtrate inhibitor, 1-252A potently inhibited PKA with

IC_{50} of ~3.5 nM, which is thirty-fold greater compared to a miniature protein itself (IC_{50}~117 nM). However, the potency was decreased about 30 fold compared to K252a (IC_{50}~0.14 nM). Next, the specificity of these compounds was tested against the most closely related kinases, protein kinaseB (PKB), protein kinase C alpha (PKCα), protein kinaseG (PKG) and calcium/calmodulin-dependent protein kinase I (CamKI). The bisubstrate inhibitor only inhibited PKG with an IC_{50} of 680 nM, which is around 200 fold less potent than PKA, but did not inhibit any of the other kinases at concentration up to 1 μM. Interestingly, K252A was not selective towards PKA.

Later, Scott, et al. reported an interesting approach that does not require structural information of target kinase for designing hetero-bivalent inhibitor.[84] This design also knows as warhead guided phage display where a small molecule that targets the ATP binding pocket of a target kinase and phage displayed peptide library were attached to two ends of Fos: Jun heterodimer complex. Here, the staturosporine, a promiscuous kinase inhibitor, attached to Fos directs the heterodimeric complex towards the ATP binding pocket while peptide library displayed on Jun finds a secondary binding pocket in proximity to the ATP binding site of PKA. Using a few rounds of phage selection, they selected a hetero- bivalent inhibitor, consists of a cyclic peptide and staturosporine conjugate, which potently inhibited PKA (IC_{50} ~ 2.5 nM). The potency increment was about 93 and 21000 fold more compared with staturosporine (IC_{50}~243 nM) and the cyclic peptide (IC_{50}~57 μM) alone. Further

linker optimization yielded a more potent inhibitor that exhibited good selectivity among a panel of 80 kinases.[85]

3.2. Statement of problem:

Current hetero-bivalent ligand design strategies targeting protein kinases mostly focus on using already known peptide sequences derived from the binding partners or identified using combinatorial and phage display methods. These methods require either structural information of peptide complexes with the kinase or biochemical screening methods to identify and characterize the sequences, which require extensive time and effort. Moreover, almost all previously reports of kinase targeted hetero-bivalent ligand designs utilized shorter linkers to connect a peptide binding to a binding pocket much closer to the ATP binding site. Not much attention has been given to exploring additional pockets farther away from the ATP site. Therefore, new strategies are needed to further expand distance binding pockets, identify peptides for those binding pockets and developing longer linkers to bridge to ATP binding site analogues.

3.3. Hypothesis:

We hypothesize that already existing natural peptide sequences **"belongs to that same kinase"** can be used as the outside ATP binding moiety in hetero-bivalent ligand design. To the best of our knowledge, such an idea has not been explored before. We believe such hot spots and sequences may exist away from the ATP

binding site area and an optimized longer linker can be developed to connect such a peptide with an ATP binding site analogue. The long-term goal of this research is to demonstrate that linkers can be utilized in harnessing additional binding pockets on kinase surfaces as well. My contribution is to optimize the linker connecting the (i) ATP and distal peptide binding pockets and (ii) ATP and additional peptide pockets, that exist in path of linker connecting ATP and distal peptide pocket. In future, we will optimize the remaining linker between two peptide binding pockets to prove that linker explored additional peptide pocket can improve the overall affinity.

3.4. Materials and methods:

3.4.1. General:

As discussed in 2.4.1.

3.4.2. Chemical synthesis:

3.4.2.1. Synthesis of 6-(9H-purin-6-ylamino)hexanoic acid or purinehexanoic acid:

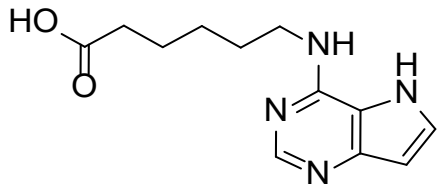

Compound was synthesized as previously described.[86]

^{1}H NMR (600 MHz, DMSO-d6, ppm): 8.13 – 8.03 (d, 2H), 7.61 (br s, 1H), 3.41 (br s, 2H), 2.16 (t, 2H, *J* = 7.2 Hz), 1.57-1.46 (m, 4H), 1.31-1.26 (m, 2H).

3.4.2.2. Synthesis of biotinylated purinehexanoic acid monomer:

Compounds were synthesized on Novasyn TGR resin (MilliporeSigma, with a 0.20-0.30 mmol/g loading, 90 μm diameter) using previously established solid phase peptide and peptoid synthesis protocols and by modifying our previously published solid phase synthesis of hetero-bivalent ligands. [77, 87-88]

The synthesis procedure involves following steps.

Step 1, step 2 and step 3 as discussed in 2.4.2.3.

Step 4: After Fmoc deprotection, Fmoc-Lys-Boc-OH (X 2 times) was coupled to the resin using coupling agents [HBTU (5*n* mol) and HOBT (5*n* mol)] and base [DIPEA (10*n* mol)] in DMF (2 ml) for 2 hrs to get compound A.

Step 5: Fmoc deprotection was achieved by following conditions described in *step 3* of 2.4.2.3.

Step 6: Fmoc-PEG-OH was added repeatedly to get the necessary linker length to get compound B.

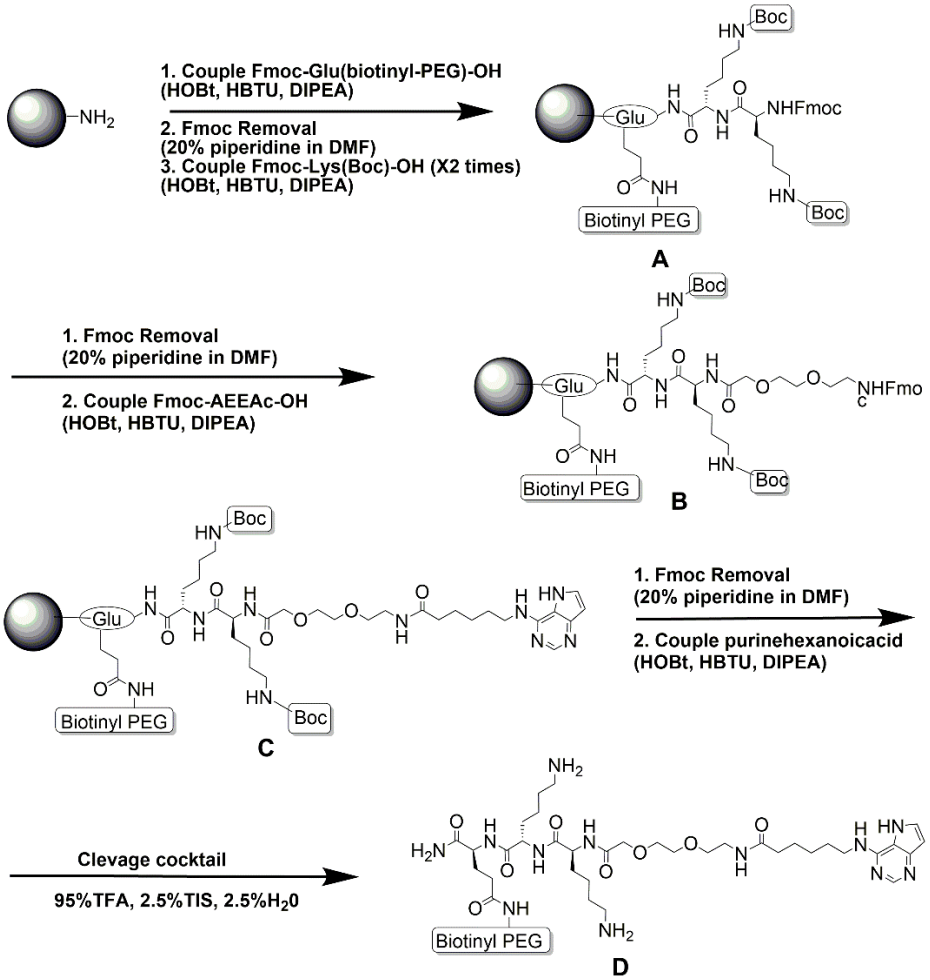

Scheme 4. Synthesis scheme of biotinylated purinehexanoicacid monomer.

Step 7: 6-aminopurinehexanoic acid (5*n* mol) was coupled to the resin using coupling reagents HBTU (5*n* mol) and HOBT (5*n* mol) and base DIPEA (10*n* mol) in DMSO (2 ml) for 2 hrs to get compound C. Then the resin was washed with DMF (10 x 2 ml).

Step 8: The compounds were cleaved using conditions described in *step 7* in 2.4.2.3. (compound D, yield~67%-20 mg) and analyzed using MALDI-TOF and HPLC.

3.4.2.3. Synthesis of biotinylated ESL peptide monomer:

The synthesis procedure involves following steps.

Step 1-3 were similar as discussed in 2.4.2.3 to get compound A and *step 4-6* was similar to 3.4.2.2. to yield compound B.

Step 7: The amino acids in ESL peptide (NLLLD) were coupled (Fmoc-Asp(OtBu)-OH, Fmoc-Leu-OH (x 3 times), Fmoc-Asn(Trt)-OH)

Step 8: N-terminal was capped using Boc-Gly-OH as discussed in *step 6* of 2.4.2.4 to get compound C.

Step 9: The compound was cleaved using conditions described in *step 7* in 2.4.2.3 (compound D, yield~55%-22 mg).

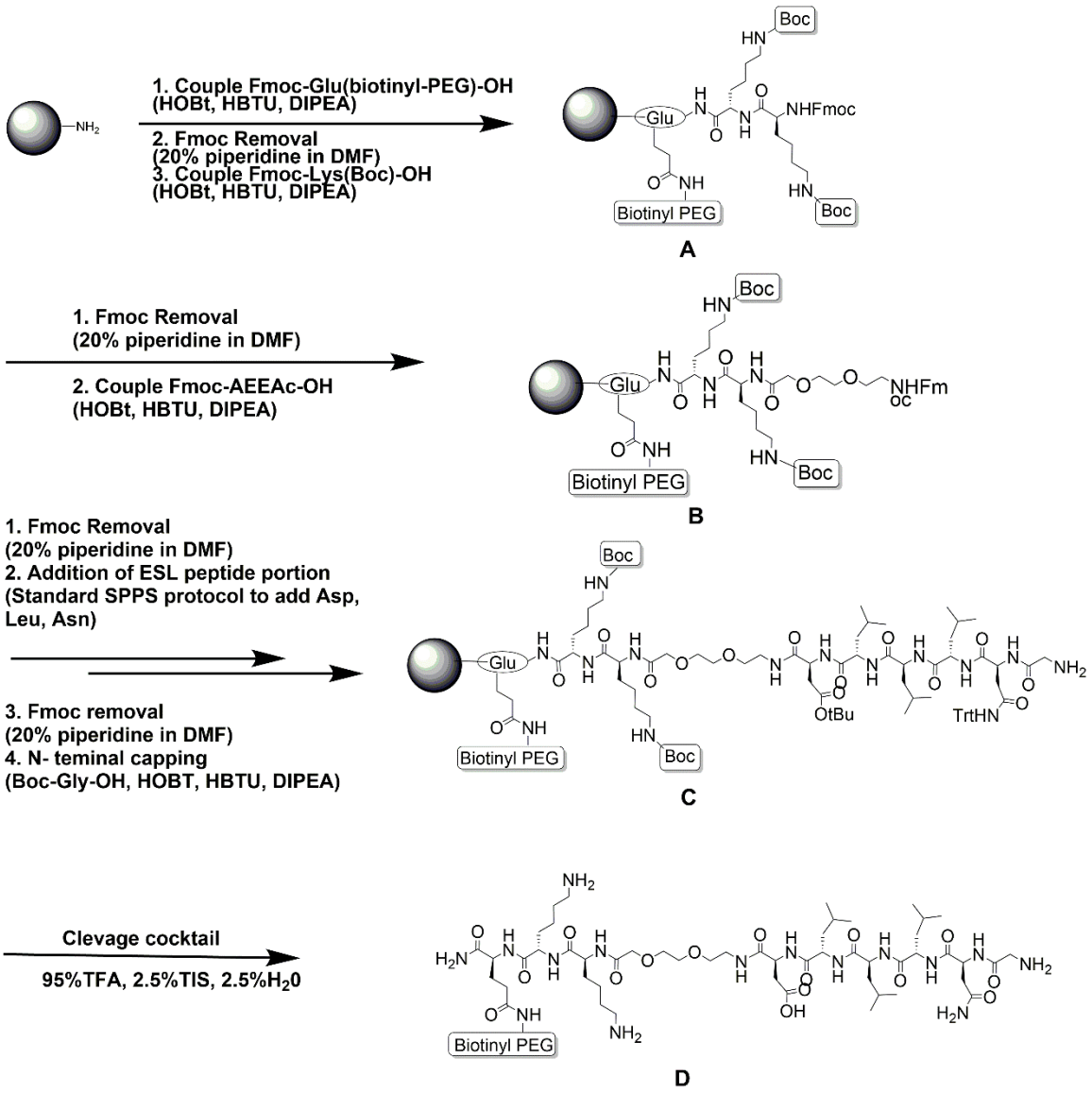

Scheme 5. Synthesis scheme of biotinylated ESL peptide.

3.4.2.4. Synthesis of PP2 analogue:

The compound was synthesized as described previously.[76]

3.4.2.5. Synthesis of Biotinylated PP2 monomer:

The compound was synthesized as discussed in 2.4.2.1.

3.4.2.6. Synthesis of EPHB1 & 2 series of hetero-bivalent ligands:

The synthesis procedure involves following steps.

Steps 1, 2 and 3 were followed as discussed in synthesis of 2.4.2.3.

Step 4: The resin was treated with Fmoc-Lys (ivDde)-OH (5*n* mol), HBTU (5*n* mol), HOBT (5*n* mol), and DIPEA (10*n* mol) in DMF (2 ml) at room temperature for 2 hrs and then washed with DMF (10 x 2 ml).

Step 5: Fmoc was deprotected and using the conditions described in *step 5* of 3.4.2.3. ESL peptide portion was added.

Step 6: N-terminal was capped using Boc-Gly-OH using the conditions used in *step 6* of 2.4.2.4.

Step 6: IvDde was deprotected using 5% hydrazine [3 x (2 ml x 10 min)]. The resin was again washed with DMF (10 x 2 ml).

Step 7: The linker portion was extended by coupling amino acids Fmoc-PEG-OH (x Y times), Fmoc-Gly-OH (x a times) following *step 2* and *step 3* of 2.4.2.3.

Step 8: 6-aminohexanoic acid was introduced into the sequence using the conditions described in *step 7* of 3.4.2.2. to yield EPHB1 series compounds.

EPHB2 series of compounds were synthesized by following *Step 9, 10* as described below.

Step 9: After washing the resin with DMF, 1M bromoacetic acid (1 ml), 1.5M diisopropylcarbodiimide (DIC) (1 ml) were coupled to resin using microwave at 10% power for 15 seconds. Next, the resin was washed with DMF (10 x 2 ml) and

coupled with 2M 3-azido-1-propylamine (2 ml) using microwave at 10% power for 15 seconds. The resin was washed with DMF after the reaction (10 x 2 ml).

Step 10: The reaction vessel was treated with Copper Iodide (3 *n*) and PP2 analogue (3 *n*) in n-methylpyrrolidine (NMP) for overnight at room temperature. The resin was drained and washed with with water (3 x 2 ml) and NMP (5 x 2 ml).[89]

Step 11: Compounds were cleaved from the resin using the conditions discussed in *step 7* of 2.4.2.3. [yields: EPHB1.1 (24.1%-13 mg), 1.2 (22.3%-12.5 mg), 1.3 (23.1%-13.1 mg), 1.4 (21.4%-12.5 mg), 1.5 (21.7%-13.1 mg), 1.6 (20.1%-12.5 mg),1.7 (19.7%-12.7 mg), 1.8 (17.9%-11.7 mg), 1.9 (17.1%-11.6 mg), 1.10 (16.5%-11.8 mg), 1.11 (16.1%-11.7 mg); EPHB2.1 (19.7%-11.8 mg), 2.2 (18.5%-11.3 mg), 2.3 (18.1%-10.8 mg), 2.4 (17.3%-11 mg), 2.5 (16.8%, 11 mg) and analyzed using MALDI-TOF and HPLC.

3.4.2.7.Synthesis of Fmoc-Phe(4-(n-azidoalkanoic)-OH:

Till Compound 3 was synthesized as discussed before.[90-91]

(i) Synthesis of compounds 4A and 4B:

Compound 3 (1.06 g, 2.31 mmol) was added to EDC (362.67 mg, 2.31mmol), HOBT (472 mg, 3.5 mmol), triethyl amine (467.5 mg, 4.62 mmol) in DCM (30 mL) and either 5-azidovalericacid (330 mg, 2.31 mmol) or 6-azidohexanoic acids (362 mg, 2.31 mmol) in two different RB flask allowed to react for overnight. Then, dil.HCl was added to reaction mixture and the organic layer was washed twice with

water, dried over $MgSO_4$ evaporated and separated using silica gel column to yield compound 4A (580 mg, 43%) or 4B (552 mg, 40%) as brown red color solid.

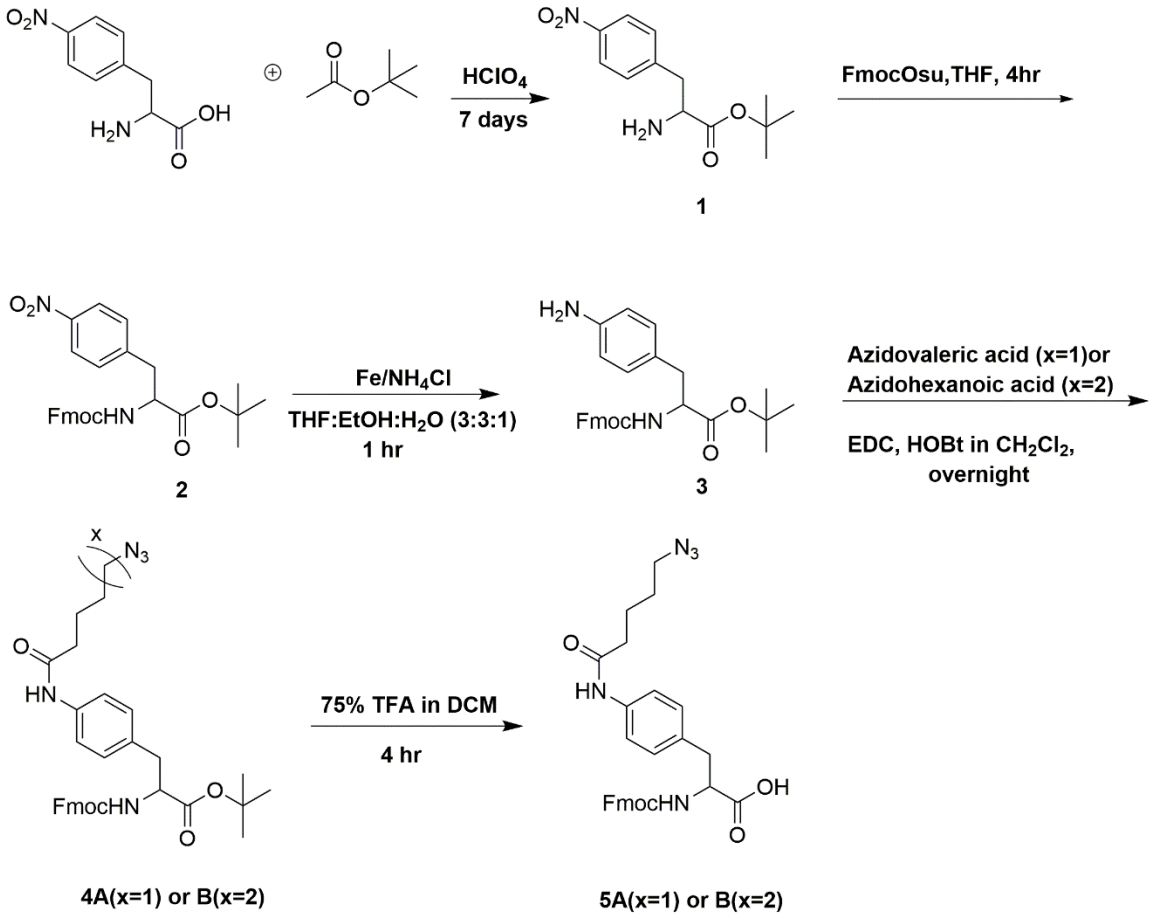

Scheme 6. Synthesis scheme of Fmoc-Phe(4-(n-azidoalkanoic)-OH.

4A or tert-butyl 2-(((9H-fluoren-9-yl)methoxy)carbonyl)-3-(4-(5-azidopetanamido)phenyl)propanoate:

^{1}H NMR (500 MHz, DMSO-d_6): δ 7.75-7.73 (d, 2 H, *J* = 7.8 Hz), 7.56-7.54 (t, 2 H, *J* = 8.4 Hz), 7.43-7.33 (m, 4 H), 7.31-7.27 (m, 2 H), 7.09-7.07 (d, 2 H, *J* = 8.1 Hz), 5.31-5.30 (d, 1 H, *J* = 7.8 Hz), 4.41-4.29 (m, 2 H), 4.19-4.17 (t, 1 H, *J* = 7.2 Hz),

3.31-3.29 (t, 2 H, *J* = 6.6 Hz), 3.06-3.02 (m, 2 H), 2.36-2.34 (t, 2 H, *J* = 6.6 Hz), 1.80-1.76 (m, 2 H), 1.67-1.63 (m, 2 H), 1.42 (s, 9H).

4B or tert-butyl 2-(((9H-fluoren-9-yl)methoxy)carbonyl)-3-(4-(6-azidohexanamido)phenyl)propanoate:

^{1}H NMR (500 MHz, DMSO-d_6): δ 7.75-7.73 (d, 2 H, *J* = 7.8 Hz), 7.56-7.54 (t, 2 H, *J* = 8.4 Hz), 7.43-7.33 (m, 4 H), 7.31-7.27 (m, 2 H), 7.09-7.07 (d, 2 H, *J* = 8.1 Hz), 5.31-5.30 (d, 1 H, *J* = 7.8 Hz), 4.41-4.29 (m, 2 H), 4.19-4.17 (t, 1 H, *J* = 7.2 Hz), 3.29-3.27 (t, 2 H, *J* = 6.6 Hz), 3.04-3.00 (m, 2 H), 2.33-2.31 (t, 2 H, *J* = 6.6 Hz), 1.76-1.72 (m, 2 H), 1.62-1.58 (m, 2 H), 1.42 (s, 9H), 1.18-1.21 (m, 2 H).

(ii) Synthesis of compound 5A and 5B:

Compound 4A (150 mg, 0.257 m mol) or 4B (150 mg, 0.251 m mol) was added to 1 mL TFA: DCM (3:1) and allowed to stir for 4 hrs. TFA was evaporated to yield either 5A as light yellow color solid (124 mg, 90%) or 5B as yellow color solid (115 mg, 85%).

5A or 2-(((9H-fluoren-9-yl)methoxy)carbonyl)-3-(4-(5-azidopetanamido)phenyl)propanoic acid:

^{1}H NMR (500 MHz, DMSO-d_6): δ 9.82 (s, 1 H), 7.85-7.83 (d, 2 H, *J* = 7.2 Hz), 7.70-7.57 (m, 2 H), 7.47-7.46 (d, 2 H, *J* = 6 Hz), 7.38-7.34 (m, 2 H), 7.29-7.23 (m, 2 H), 7.15-7.14 (d, 2 H, *J* = 7.8 Hz), 4.17-4.08 (m, 4H); 3.32-3.30 (t, 2 H, *J* = 6.6 Hz), 3.00-2.75 (m, 2 H), 2.29-2.27 (t, 2H, *J* = 6.9 Hz)1.61-1.51 (m, 2 H).

5B or 2-(((9H-fluoren-9-yl)methoxy)carbonyl)-3-(4-(6-azidohexanamido)phenyl)propanoic acid:

^{1}H NMR (500 MHz, DMSO-d_6): δ 9.82 (s, 1 H), 7.85-7.83 (d, 2 H, *J* = 7.2 Hz), 7.70-7.57 (m, 2 H), 7.47-7.46 (d, 2 H, *J* = 6 Hz), 7.38-7.34 (m, 2 H), 7.29-7.23 (m, 2 H), 7.15-7.14 (d, 2 H, *J* = 7.8 Hz), 4.17-4.08 (m, 4 H); 3.30-3.27 (t, 2 H, *J* = 6.6 Hz), 2.98-2.73 (m, 2 H), 2.26-2.24 (t, 2 H, *J* = 6.9 Hz), 1.57-1.44 (m, 4 H), 1.31-1.29 (m, 2 H).

3.4.2.8.Synthesis of EPHB peptide (biotinylated and non-biotinylated):

Step 1,2 and 3 were followed as discussed in 2.4.2.3. *Step 2* was avoided in case of non-biotinylated EPHB peptide.

Step 4: Fmoc group was deprotected, and the amino acids in EPHB peptide namely, Fmoc-Trp-OH, Fmoc-Ile-OH, Fmoc-Phe-OH, Fmoc-Glu(OtBu)-OH, Fmoc-(4-nitro)phe-OH, Fmoc-Asn(Trt)-OH, Fmoc-Asp-(OtBu)-OH, Fmoc-Trp-OH to get compound A.

Step 5: $SnCl_2.2H_2O$ in DMF (3n) was added to syringe to reduce the p-nitro group of Fmoc-(4-nitro)phe-OH (compound B).

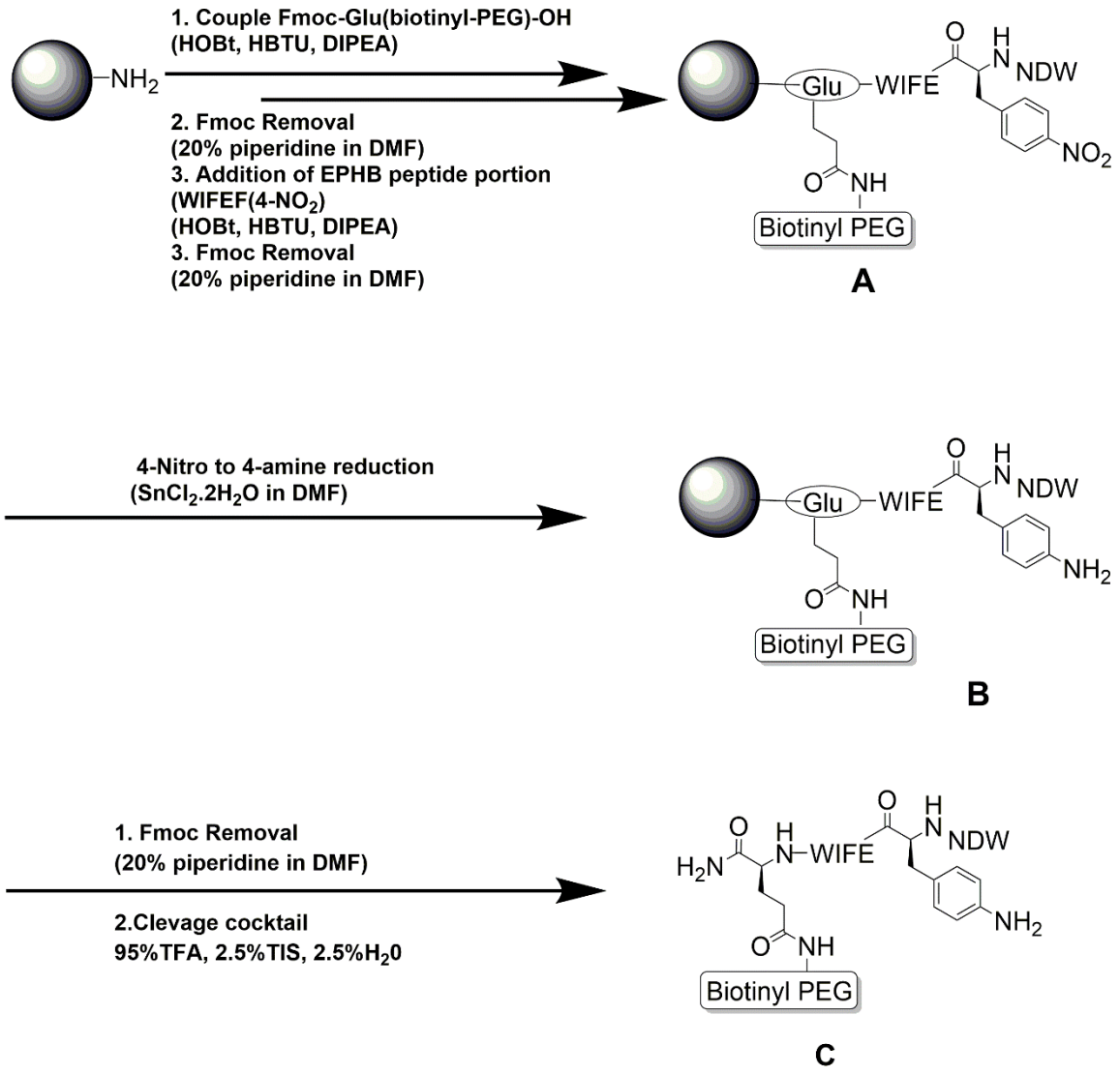

Scheme 7. Synthesis scheme of biotinylated EPHB peptide

Step 6: The Fmoc group was deprotected and the compounds were cleaved using the conditions discussed in *step 7* of 2.4.2.3. (compound C, yields~31% (13.4 mg) and 29% (8.5 mg) for non-bionylated and biotinylated EPHB peptide, respectively) and analyzed using MALDI-TOF and purified using HPLC.

3.4.2.9. Synthesis of EPHB3 series of hetero-bivalent ligands (biotinylated and non-biotinylated):

Step 1,2 followed as discussed in 2.4.2.3. to get compound A. *Step 2* was avoided in case of non-biotinylated EPHB peptide.

Step 3: Fmoc group was deprotected, and the amino acids in EPHB peptide namely, Fmoc-Trp-OH, Fmoc-Ile-OH, Fmoc-Phe-OH, Fmoc-Glu(OtBu)-OH, Fmoc-Phe(4-(n-azidoalkanoic)-OH were coupled using standard solid phase peptide synthesis protocol discussed in 2.4.2.3 to get compound B.

Step 4: The remaining amino acids (Fmoc-Asn(Trt)-OH, Fmoc-Asp-(OtBu)-OH, Fmoc-Trp-OH) were coupled and N-terminus was capped using Boc-Gly-OH to get compound C.

Step 5: Compounds were cleaved from the resin using conditions discussed in *step 7* of 2.4.2.3 [compound D, yields~Bt-EPHB3.1 (25%-14.1 mg), EPHB3.1 (22-12.5 mg%), Bt-EPHB3.2 (31%-13.1 mg), EPHB3.2 (28%- 12 mg)] and analyzed using MALDI and HPLC.

3.4.3. NMR spectra of compounds:

3.4.3.1. Purinehexanoic acid:

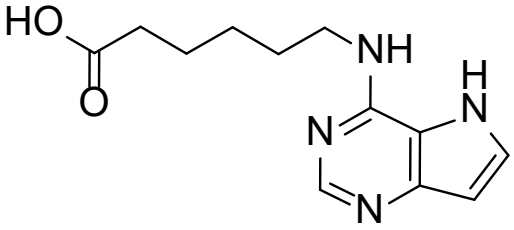

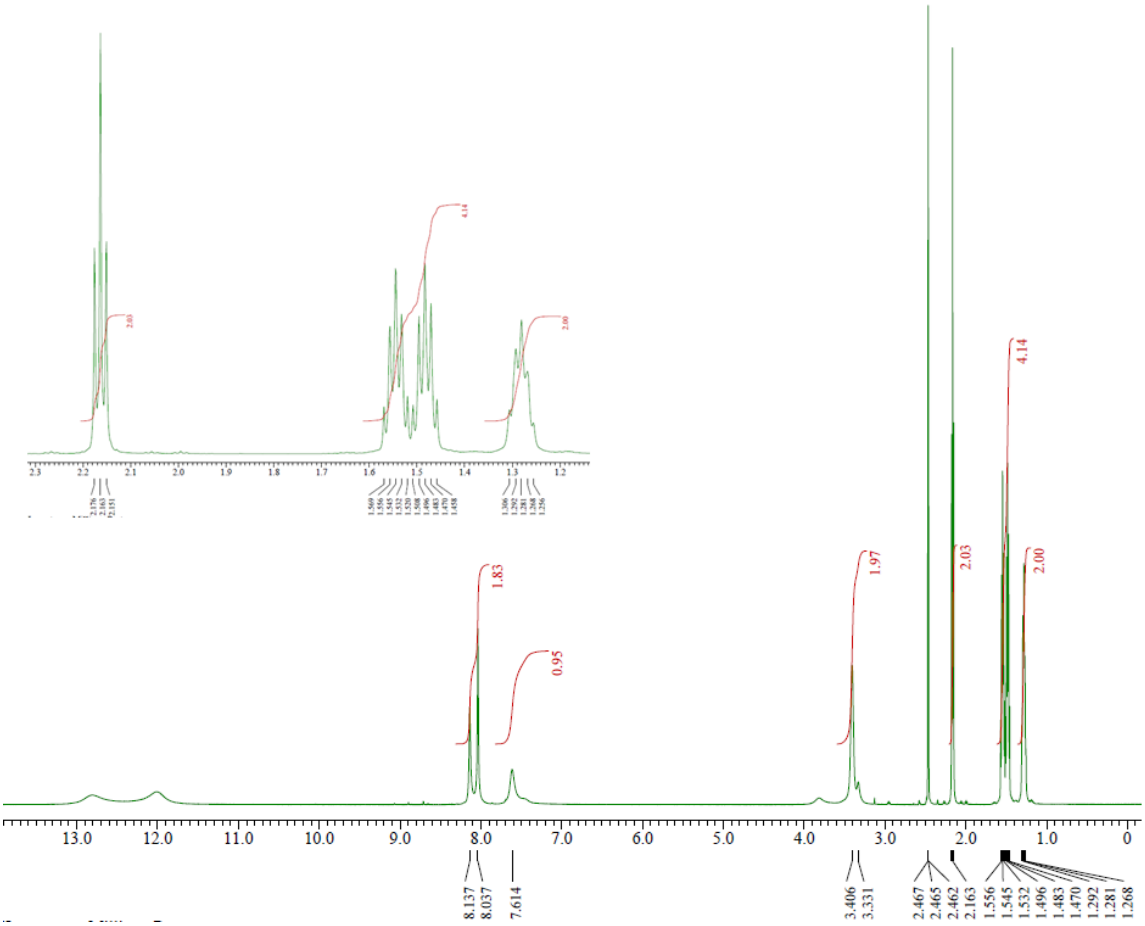

^{1}H NMR (600 MHz, $CDCl_3$)

3.4.3.2. Fmoc-Phe(4-(n-azidoalkanoic)-OH derivatives:

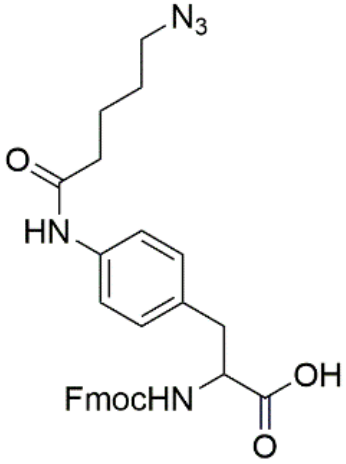

5A

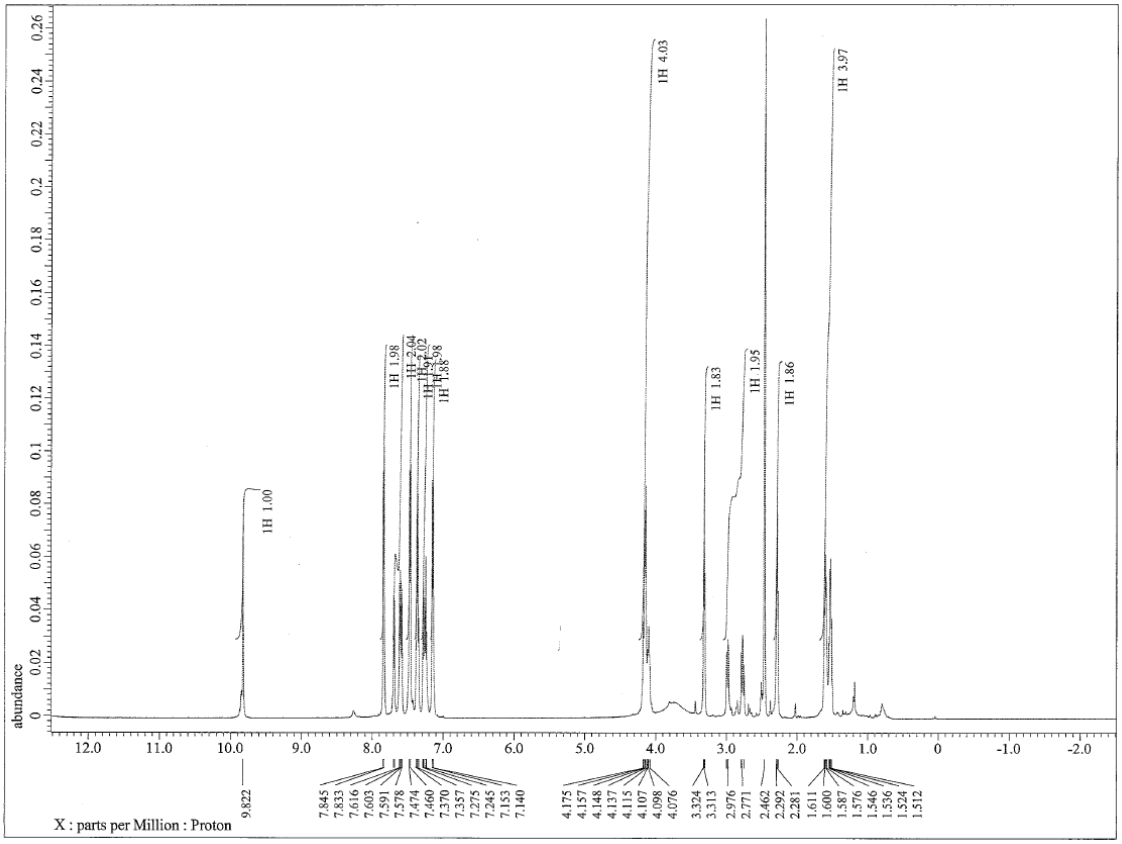

^{1}H NMR (600 MHz, $CDCl_3$)

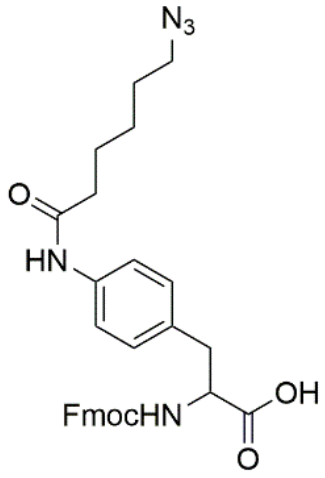

5B

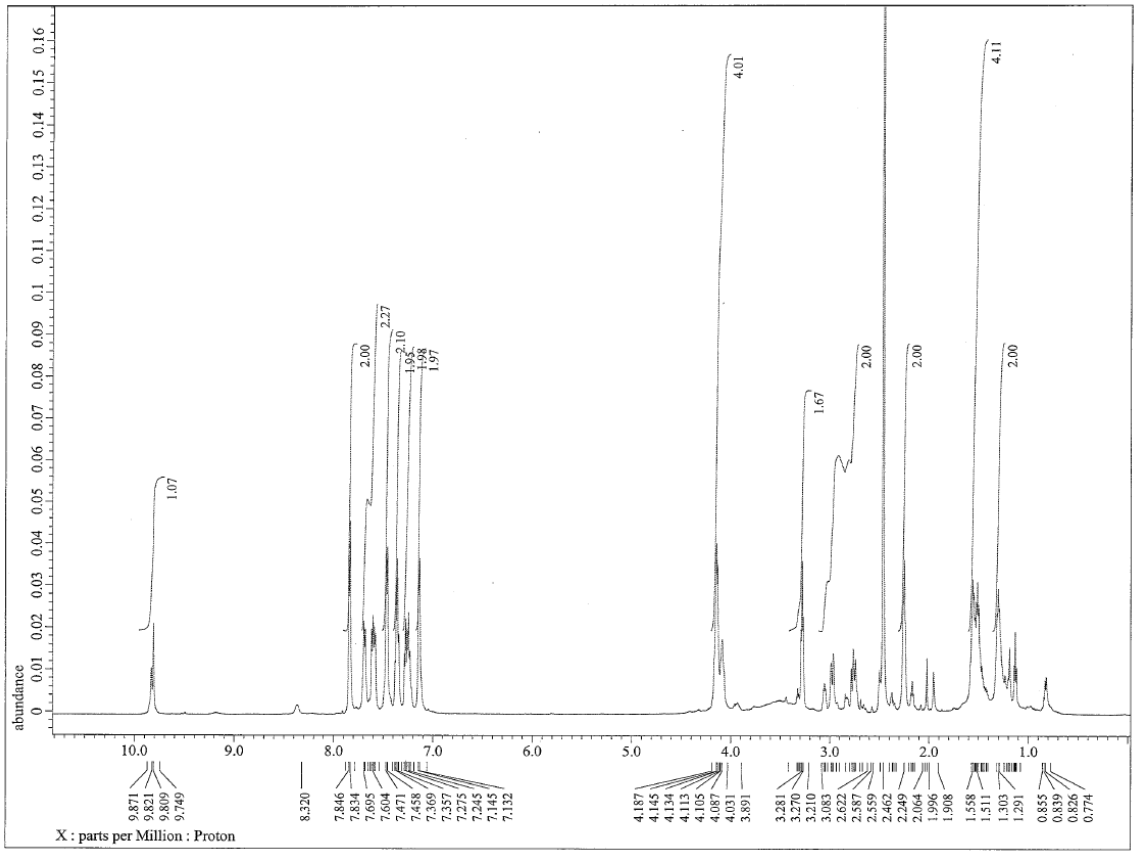

^{1}H NMR (600 MHz, $CDCl_3$)

3.4.4. Structure, Mass spectrum, and HPLC analysis of Compounds:

3.4.4.1. Structure, Mass spectrum, and HPLC analysis of biotinylated purinehexanoic acid:

(A)

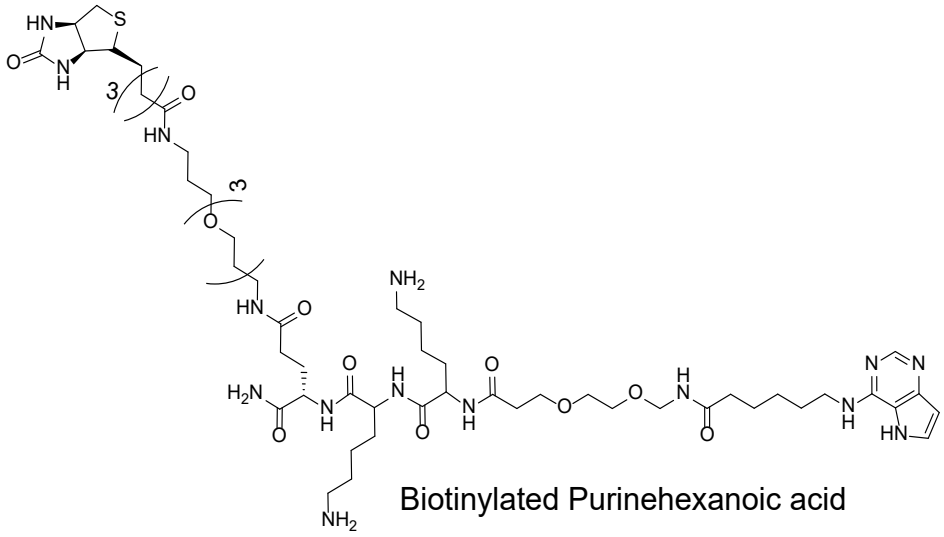

Biotinylated Purinehexanoic acid

Exact Mass – 1206.52

(B)

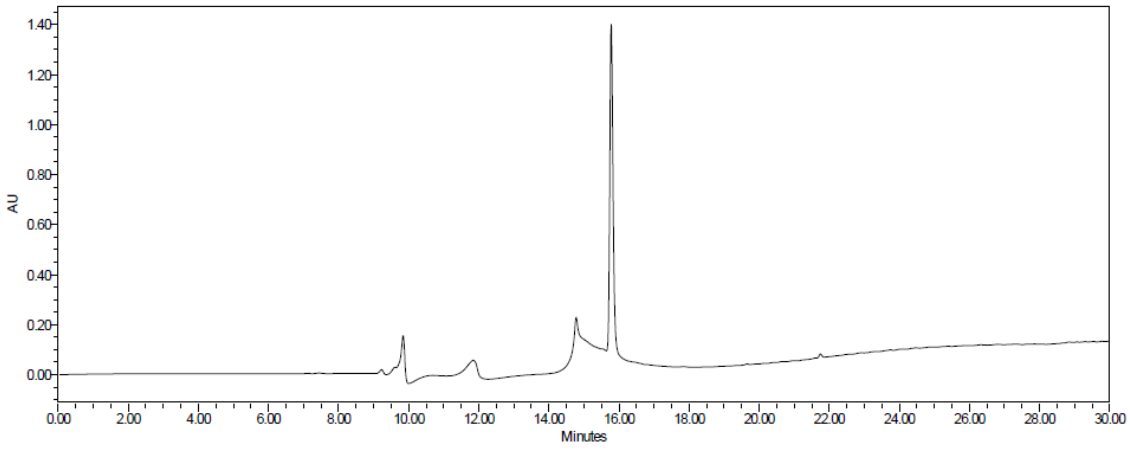

Note: We do not find any mass corresponding to the extra peaks in the beginning (10 and 12 mins), in crude sample. We believe these peaks are caused by the air bubbles. And, the tailed peak (13 mins) in front of compound peak also have the same mass, which indicates they both belongs to biotinylated purinehexanoic acid. This tailing has been observed for some compounds in EPHB1 series. We assume it might be due to PEG complexation with metals in mobile phase which interfered with the compound elution time to give two different peaks.

(C)

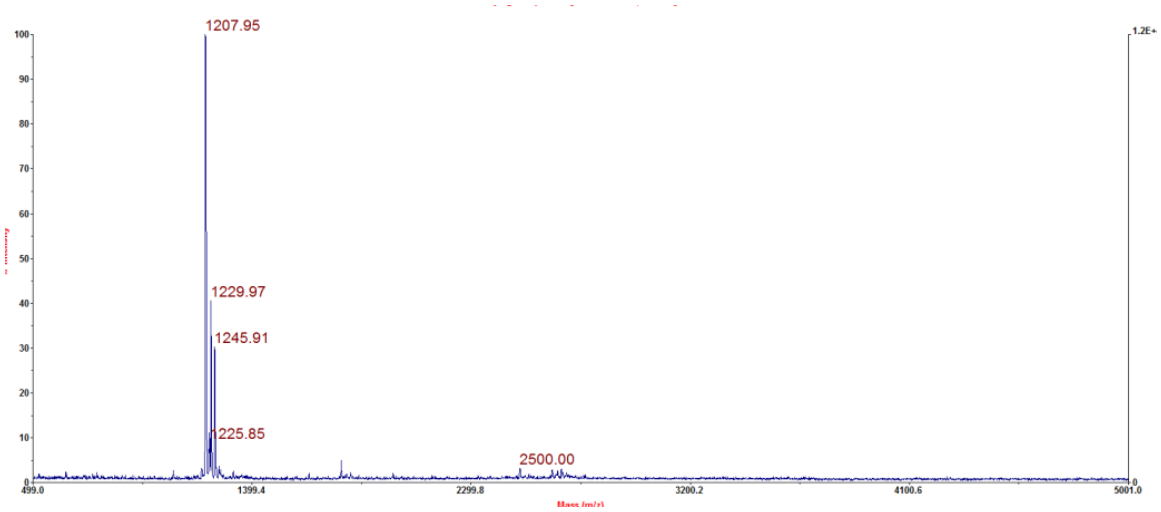

Characterization of biotinylated purinehexanoic acid: (A). Chemical structure. (B). Analytical HPLC. (C). MALDI-TOF spectrum.

(MALDI-TOF+) m/z = 1207.95 $[M+H]^+$, 1229.97$[M+Na]^+$, 1245.85$[M+K]^+$

3.4.4.2. Structure, Mass spectrum, and HPLC analysis of biotinylated ESL peptide:

(A)

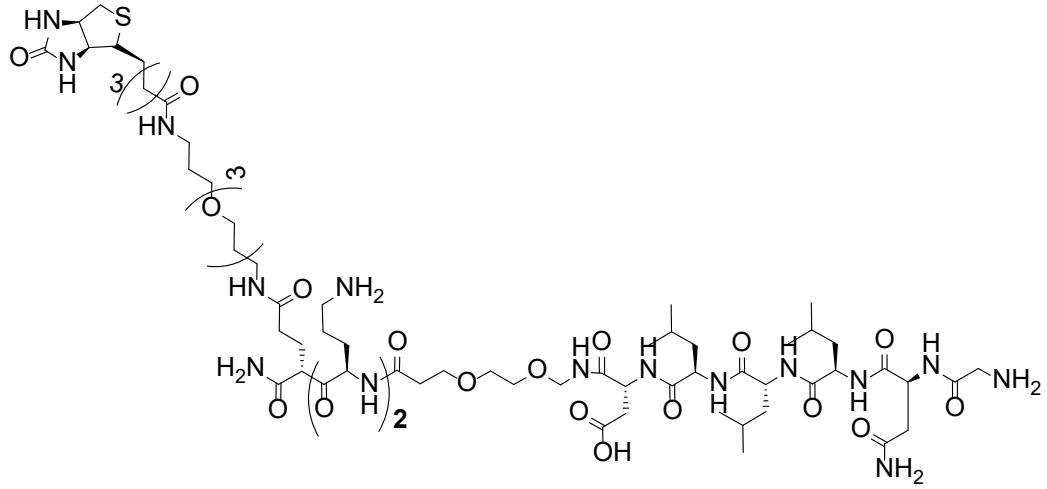

Biotinylated ESL peptide
Exact Mass-1599.96

(B)

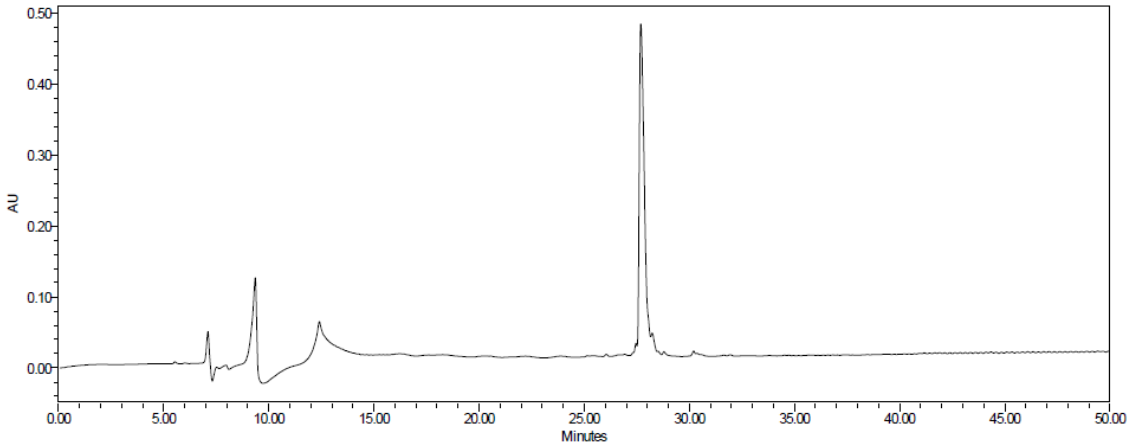

(C)

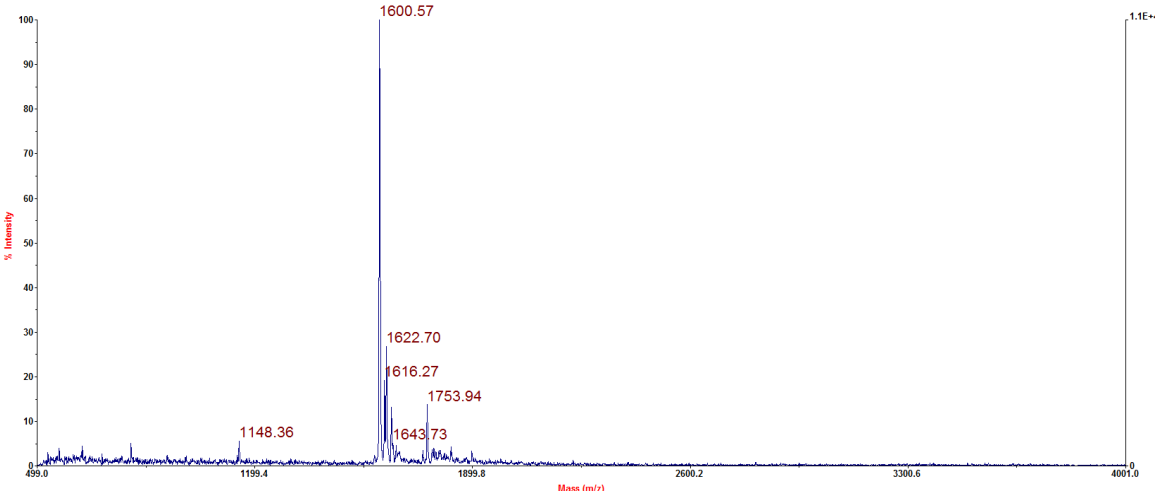

Characterization of biotinylated ESL peptide: (A). Chemical structure. (B). Analytical HPLC. (C). MALDI-TOF spectrum.

(MALDI-TOF+) m/z = 1600.57 $[M+H]^+$, 1622.70$[M+Na]^+$, 1643.73$[M+2Na]^+$

3.4.4.3. Structure, Mass spectrum, and HPLC analysis of EPHB1 series compounds

(A)

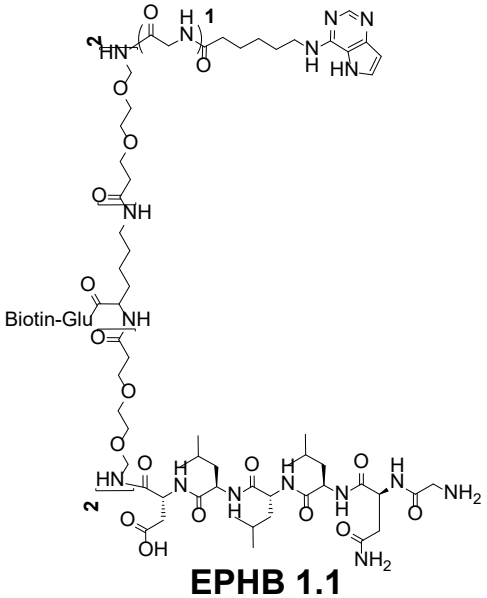

EPHB 1.1

Exact Mass 2196.19

(B)

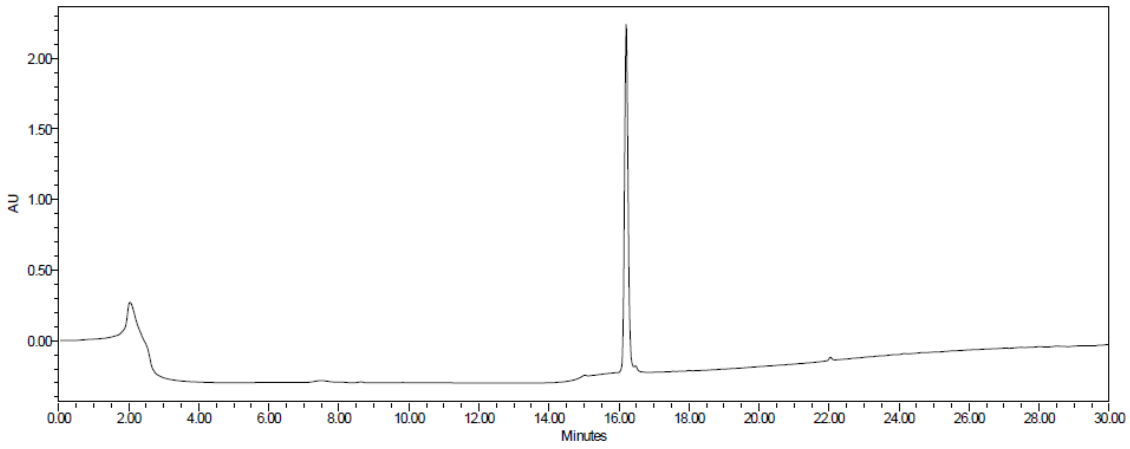

(C)

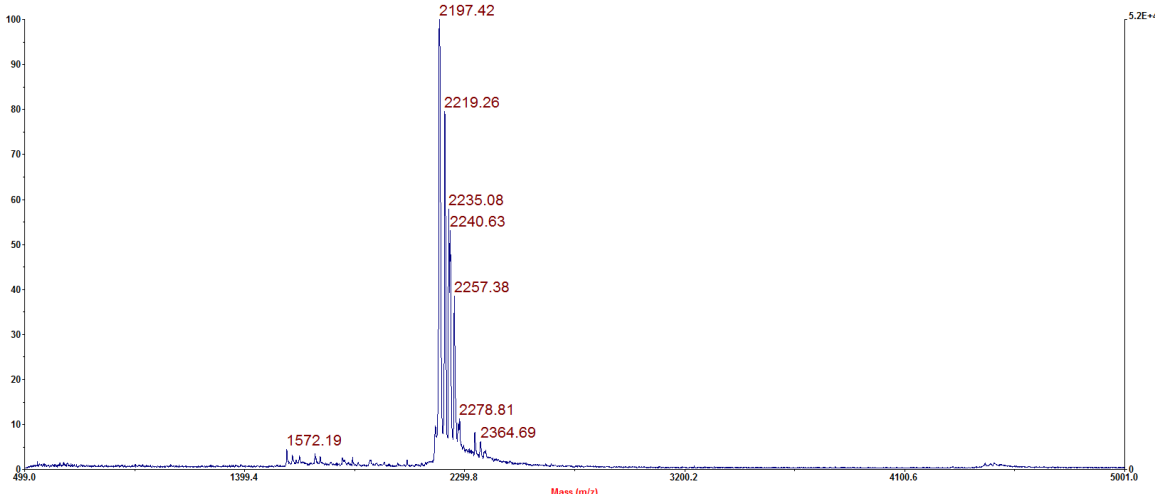

Characterization of EPHB1.1: (A). Chemical structure. (B). Analytical HPLC. (C). MALDI-TOF spectrum.

(MALDI-TOF+) m/z = 2197.42$[M+H]^+$, 2219.26$[M+Na]^+$, 2235.08$[M+K]^+$

(A)

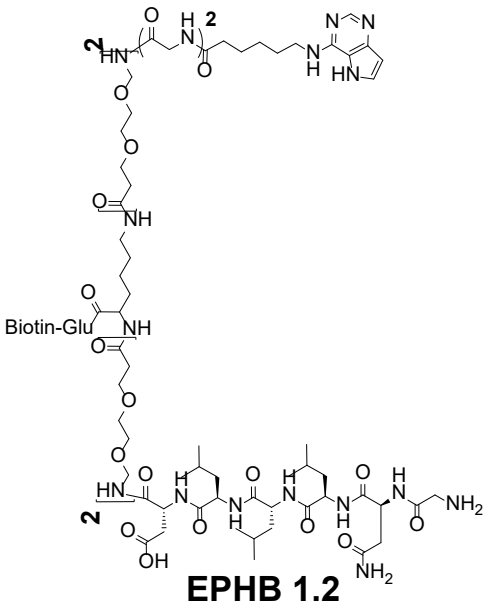

EPHB 1.2

Exact Mass 2253.21

(B)

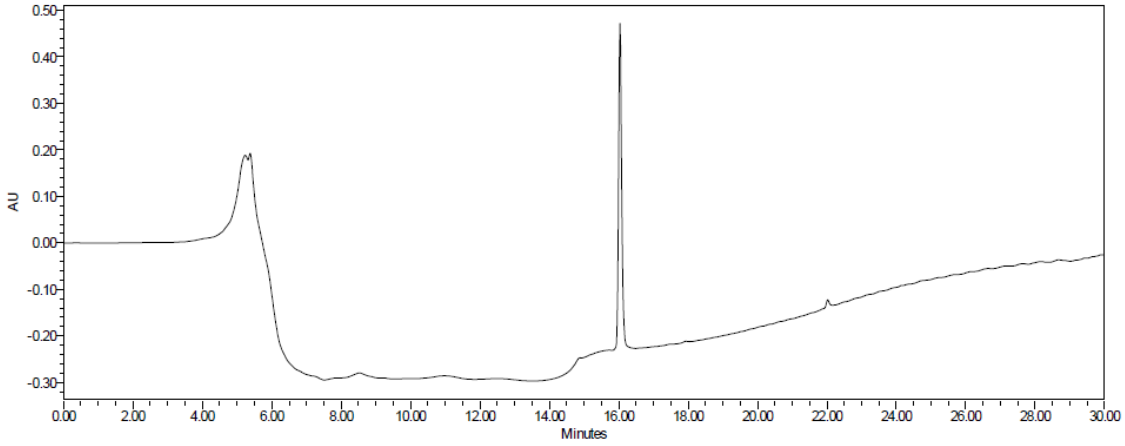

(C)

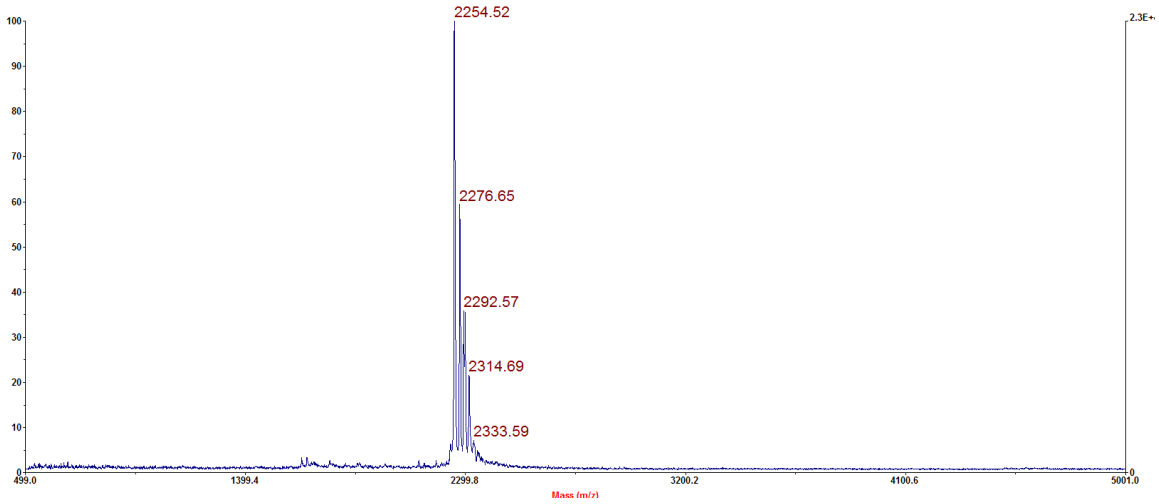

Characterization of EPHB1.2: (A). Chemical structure. (B). Analytical HPLC. (C). MALDI-TOF spectrum.

(MALDI-TOF+) m/z = 2254.52$[M+H]^+$, 2276.65$[M+Na]^+$, 2292.57$[M+K]^+$

(A)

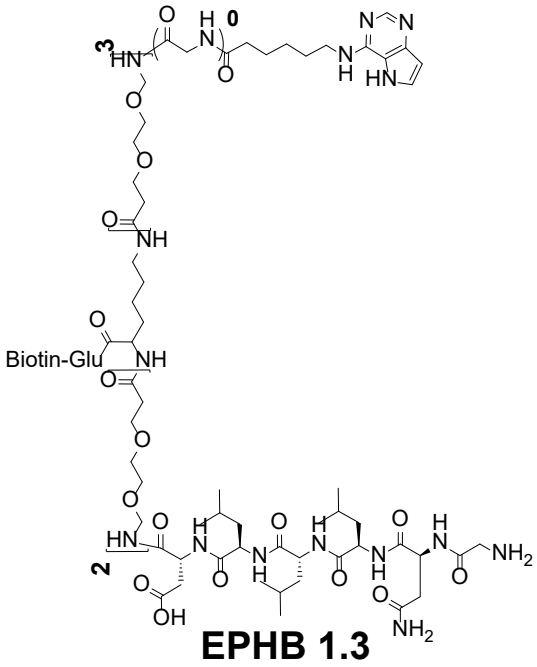

Exact Mass 2284.7

(B)

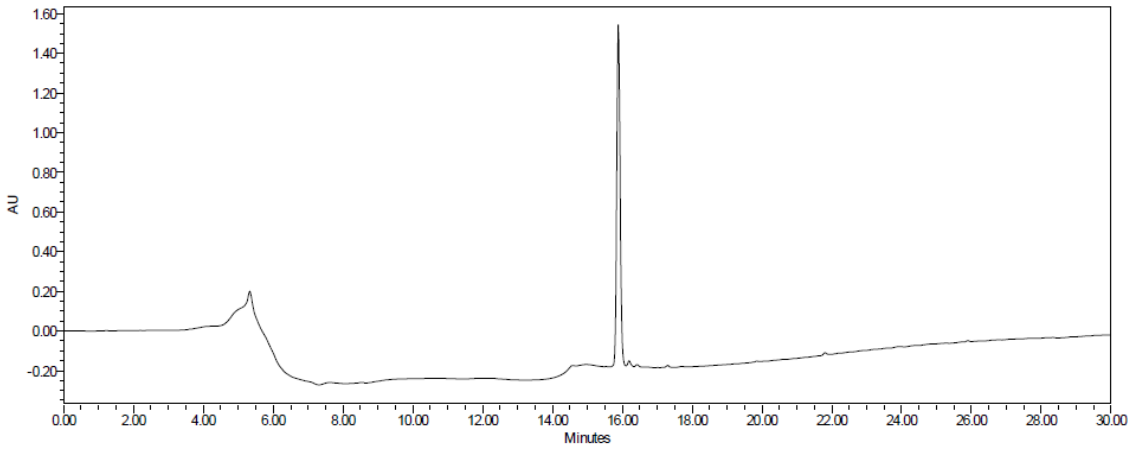

(C)

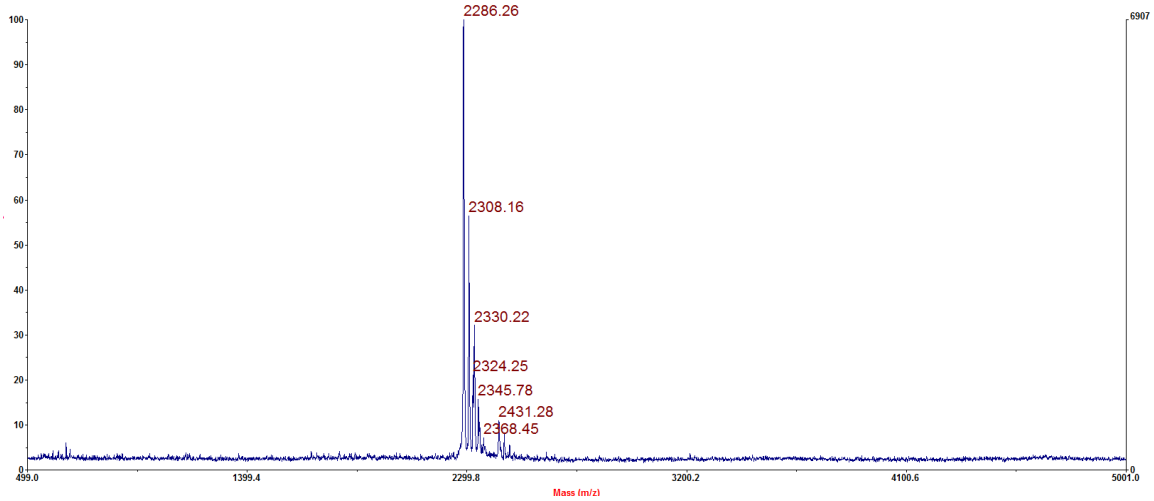

Characterization of EPHB1.3: (A). Chemical structure. (B). Analytical HPLC. (C). MALDI-TOF spectrum.

(MALDI-TOF+) m/z = 2286.26$[M+H]^+$, 2308.16$[M+Na]^+$, 2324.25$[M+K]^+$

(A)

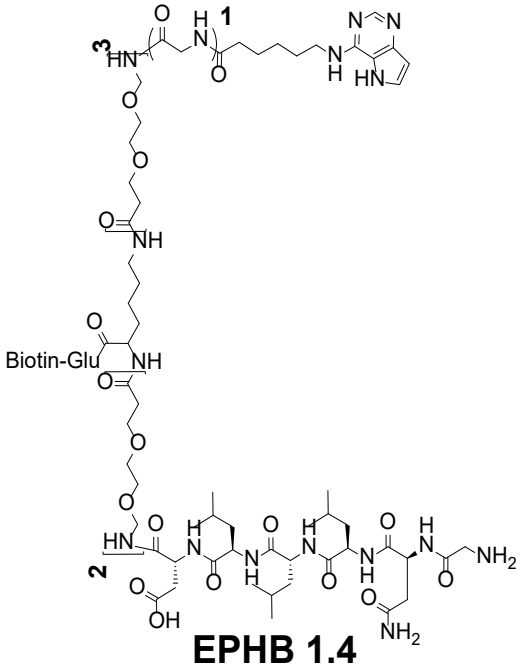

EPHB 1.4

Exact Mass 2341.26

(B)

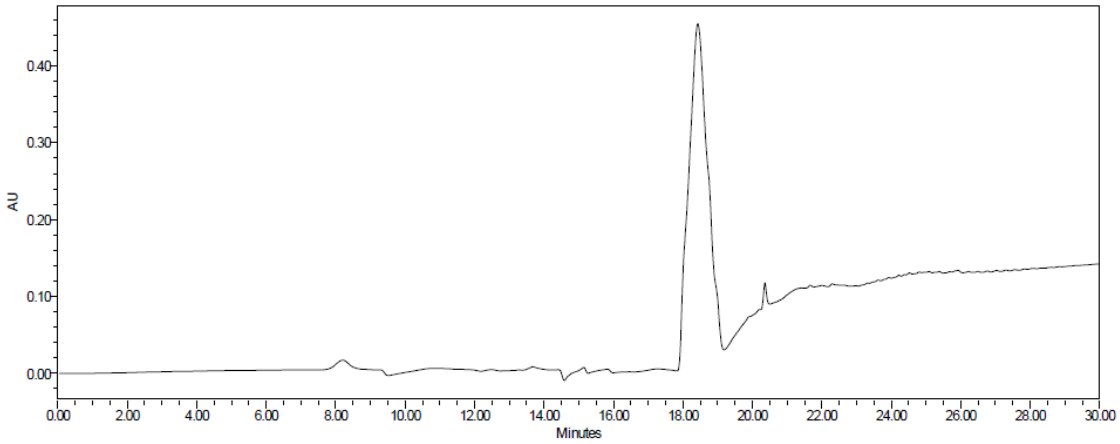

(C)

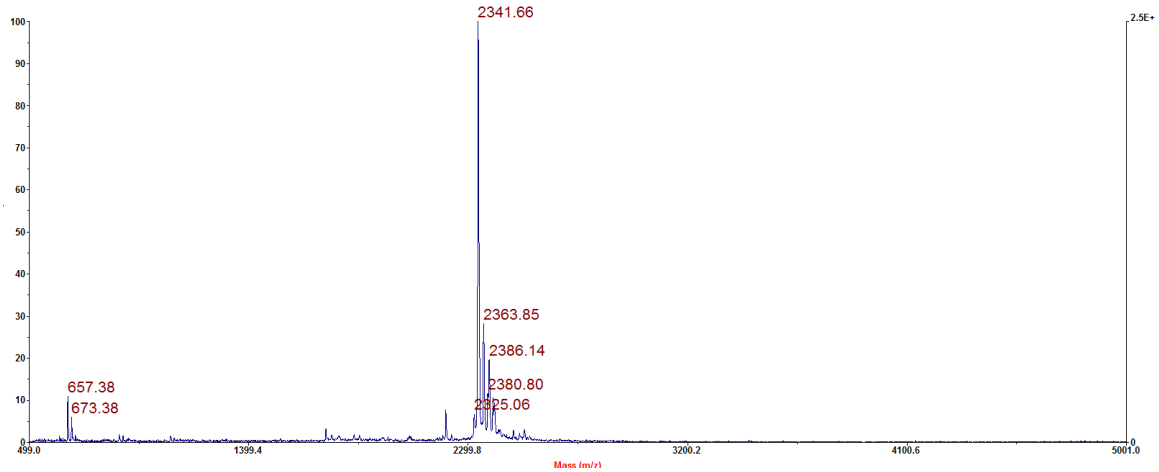

Characterization of EPHB1.4: (A). Chemical structure. (B). Analytical HPLC. (C). MALDI-TOF spectrum.

(MALDI-TOF+) m/z = 2341.66$[M+H]^+$, 2363.85$[M+Na]^+$, 2380.80$[M+K]^+$

(A)

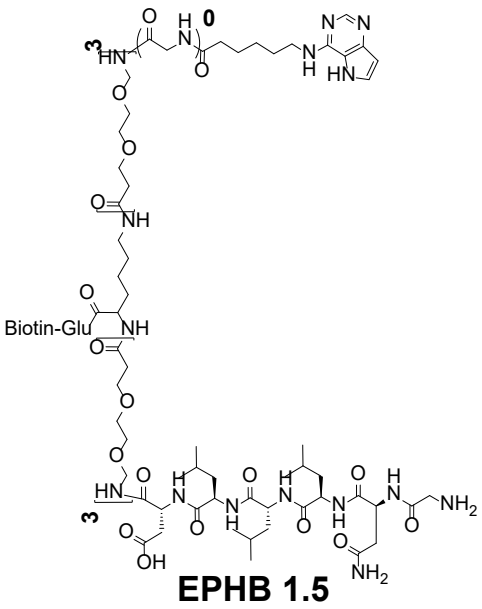

EPHB 1.5

Exact Mass 2429.32

(B)

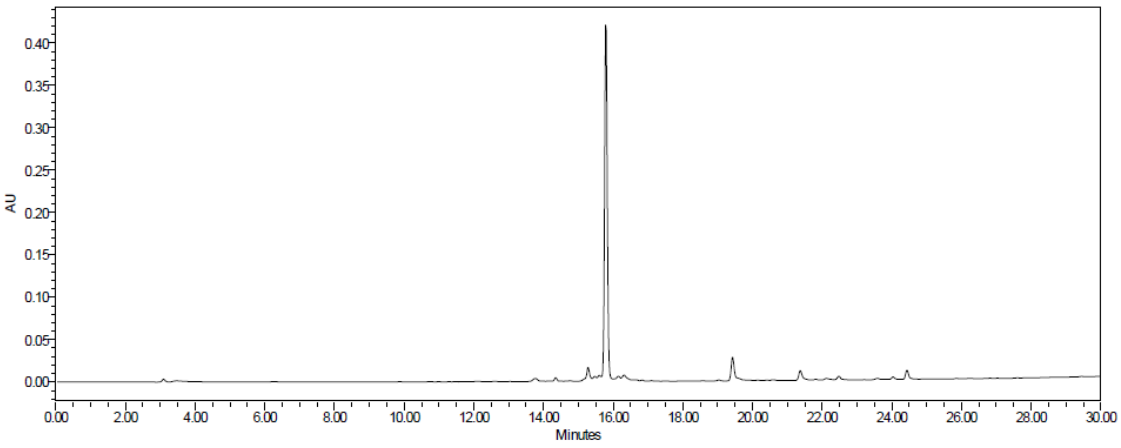

(C)

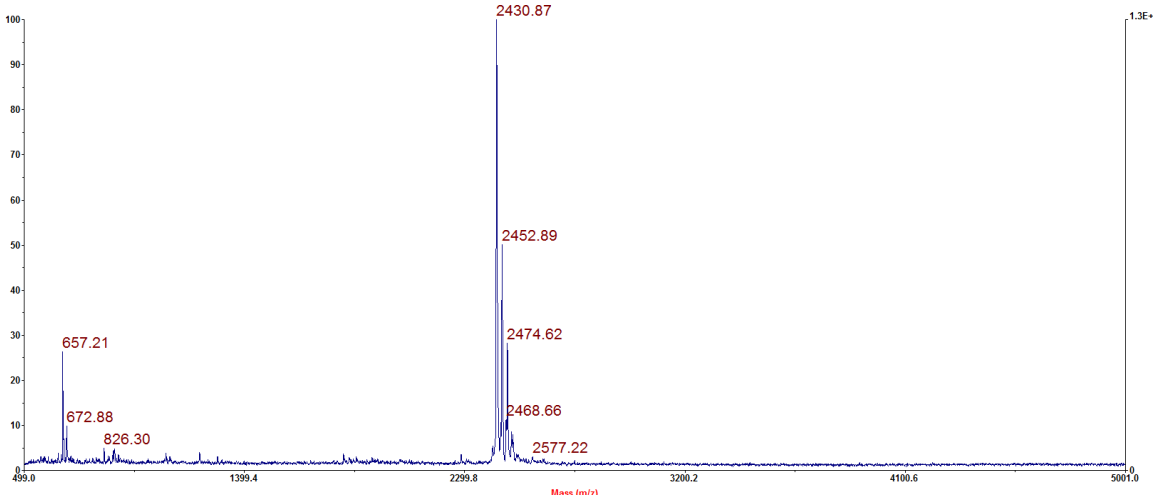

Characterization of EPHB1.5: (A). Chemical structure. (B). Analytical HPLC. (C). MALDI-TOF spectrum.

(MALDI-TOF+) m/z = 2430.87$[M+H]^+$, 2452.89$[M+Na]^+$, 2468.66$[M+K]^+$

(A)

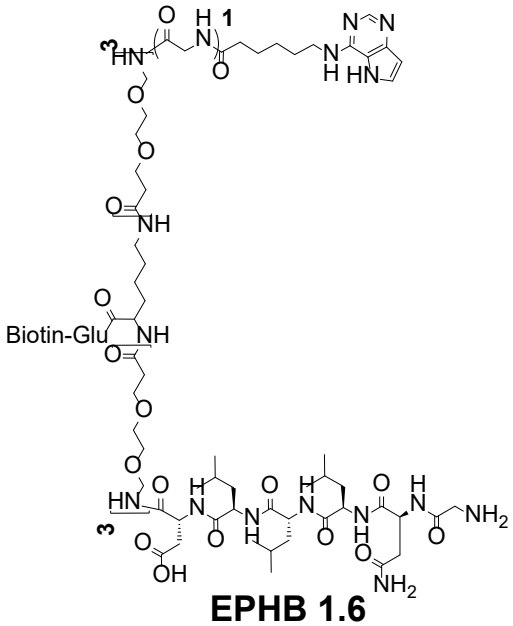

EPHB 1.6

Exact Mass 2486.54

(B)

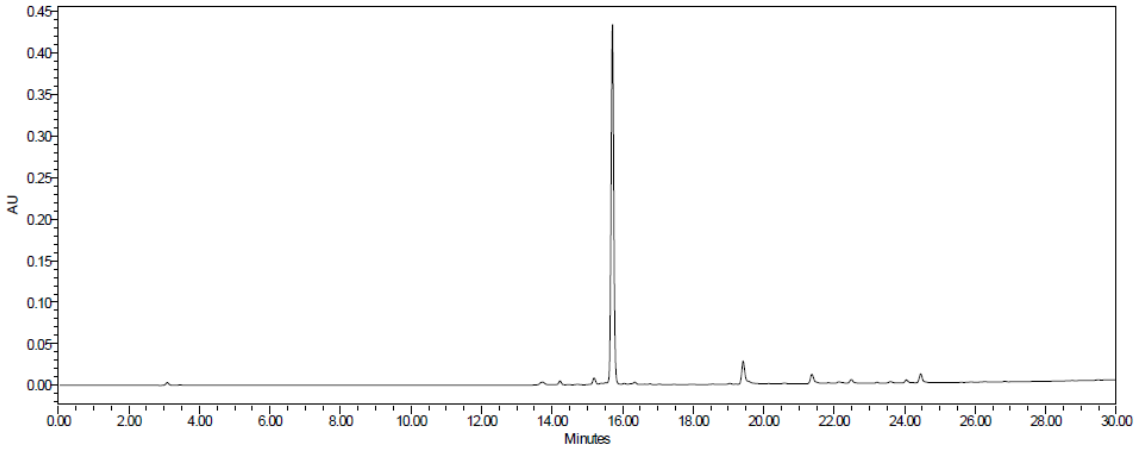

(C)

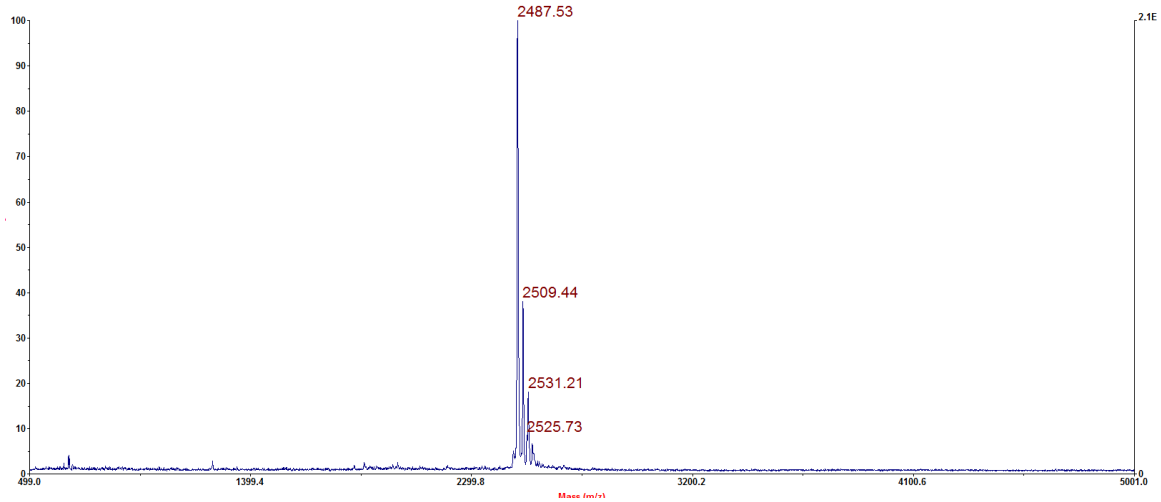

Characterization of EPHB1.6: (A). Chemical structure. (B). Analytical HPLC. (C). MALDI-TOF spectrum.

(MALDI-TOF+) m/z = 2487.53$[M+H]^+$, 2509.44$[M+Na]^+$, 2525.73$[M+K]^+$

(A)

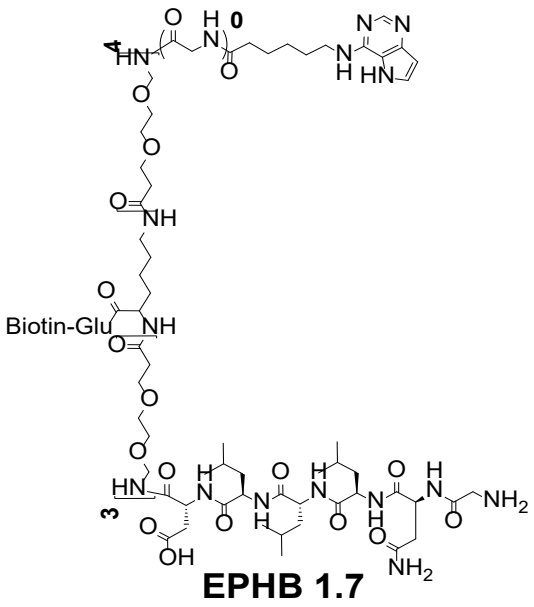

Exact Mass 2574.39

(B)

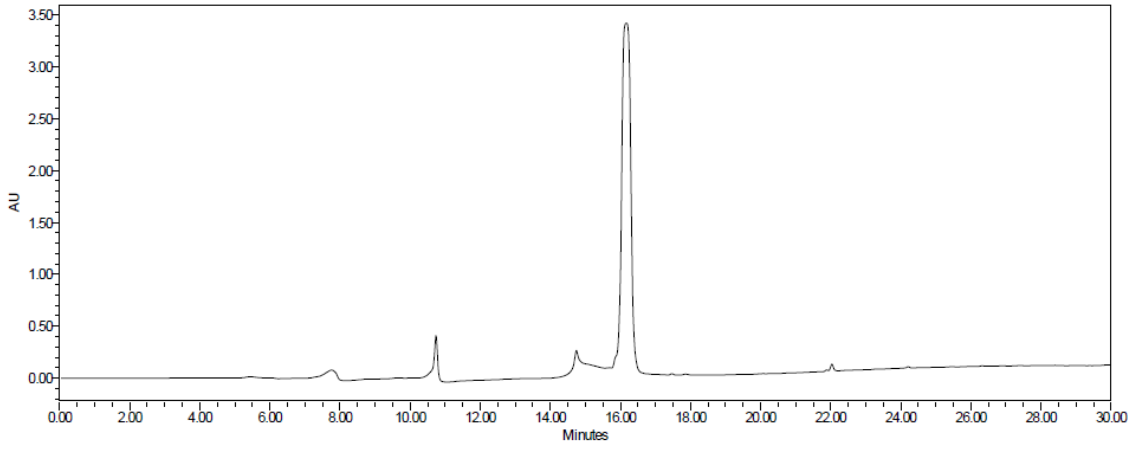

Note: We do not find any mass corresponding to the extra peak in the beginning (11 mins), in crude sample. We believe these peaks are caused by the air bubbles. And, the tailed peak (14.5 mins) in front of compound peak also have the same mass, which indicates they both belongs to EPHB1.7. We assume it might be due to PEG complexation with metals in mobile phase which interfered with the compound elution time to give two different peaks.

(C)

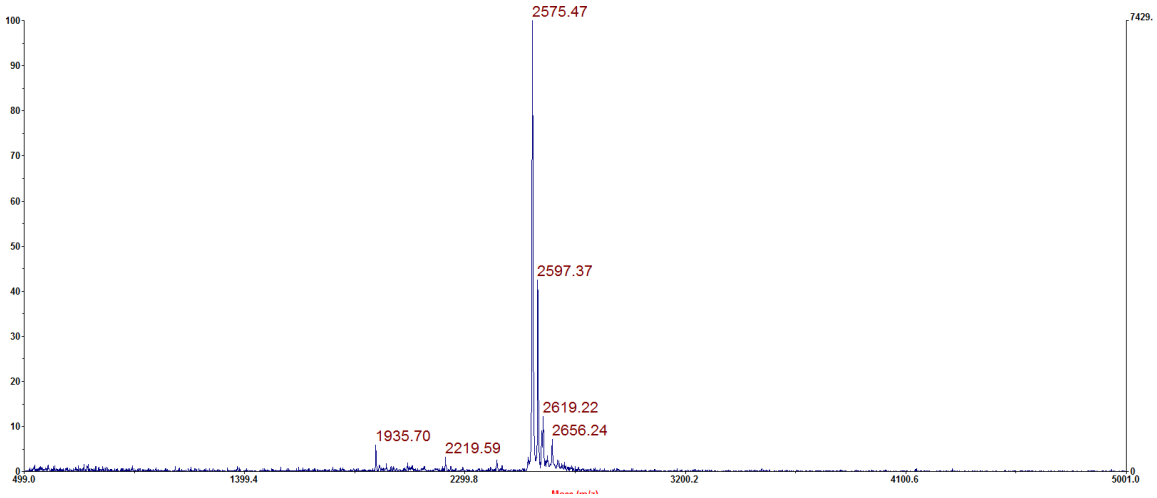

Characterization of EPHB1.7: (A). Chemical structure. (B). Analytical HPLC. (C). MALDI-TOF spectrum.

(MALDI-TOF+) m/z = 2575.47$[M+H]^+$, 2597.37$[M+Na]^+$, 2612.73$[M+K]^+$

(A)

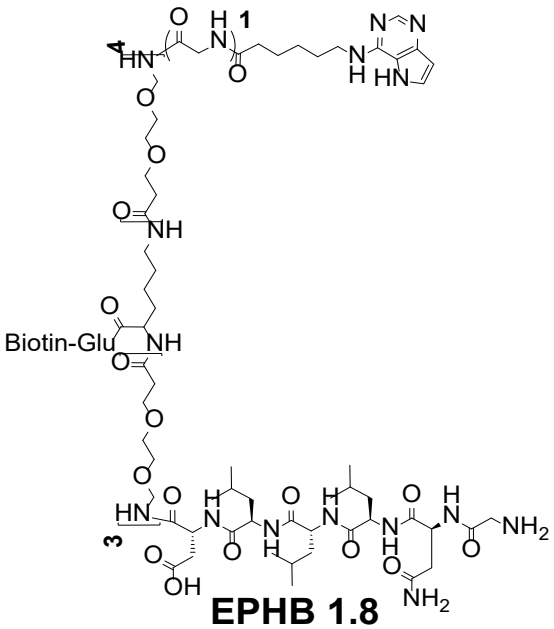

EPHB 1.8

Exact Mass 2631.4

(B)

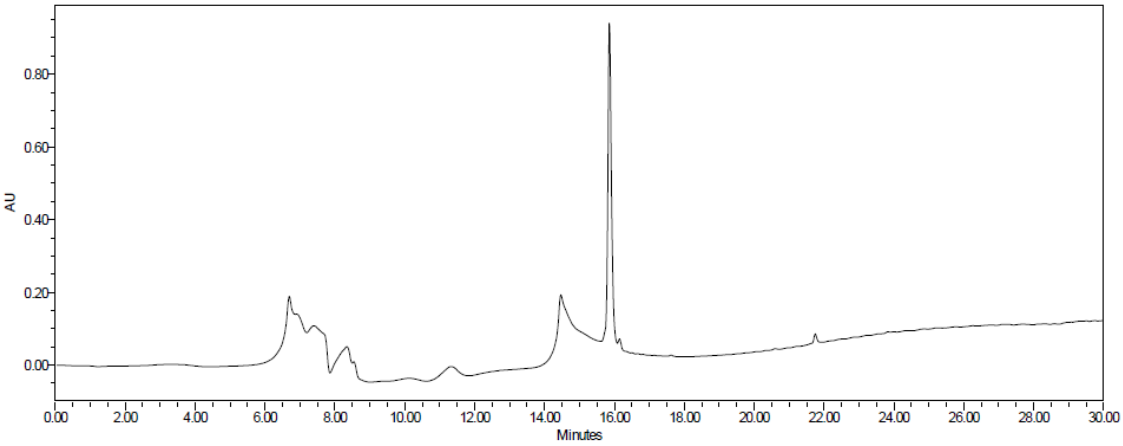

Note: We do not find any mass corresponding to the extra peaks in the beginning (6.5-11 mins), in crude sample. We believe these peaks are caused by the air bubbles. And, the tailed peak (14.5 mins) in front of compound peak also have the same mass, which indicates they both belongs to EPHB1.8. We assume it might be due to PEG complexation with metals in mobile phase which interfered with the compound elution time to give two different peaks.

(C)

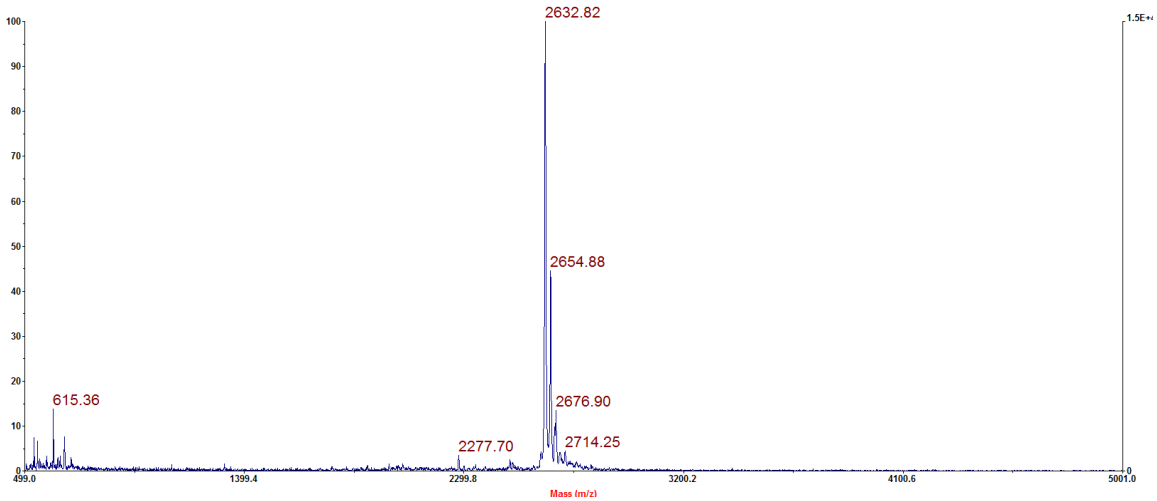

Characterization of EPHB1.8: (A). Chemical structure. (B). Analytical HPLC. (C). MALDI-TOF spectrum.

(MALDI-TOF+) m/z = 2632.42$[M+H]^+$, 2654.88$[M+Na]^+$, 2676.90$[M+2Na]^+$

(A)

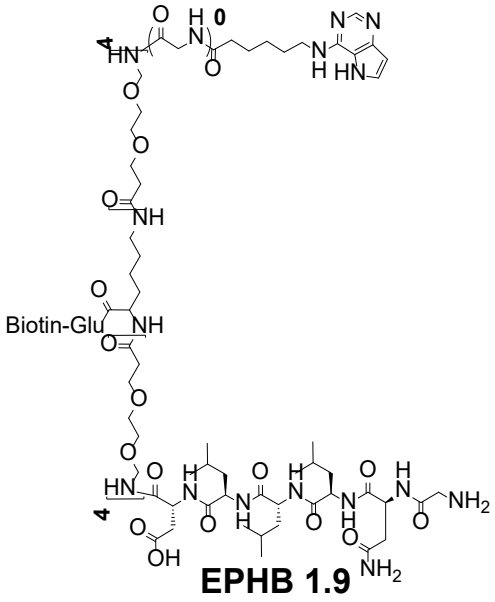

Exact Mass 2719.46

(B)

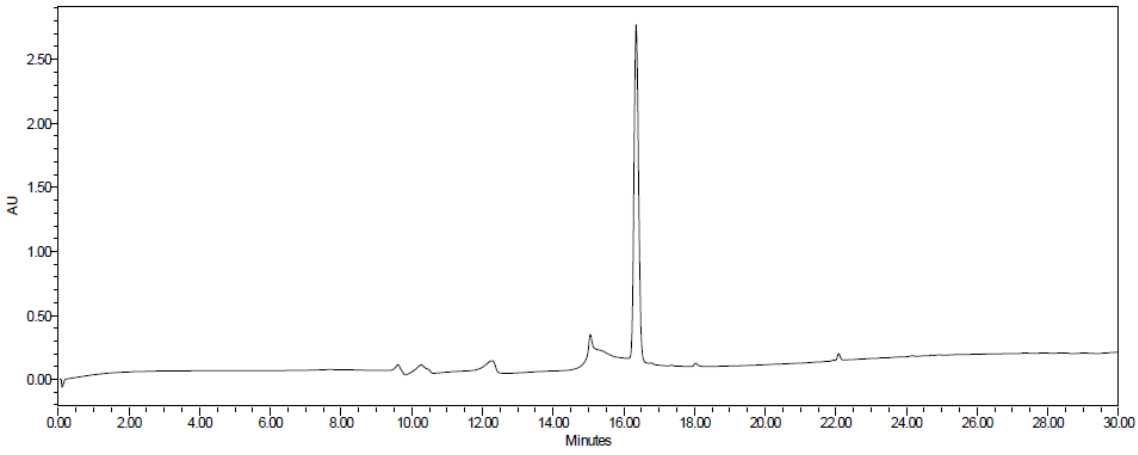

Note: We do not find any mass corresponding to the extra peak in the beginning (9.5-12 mins), in crude sample. We believe these peaks are caused by the air bubbles. And, the tailed peak (15 mins) in front of compound peak also have the same mass, which indicates they both belongs to EPHB1.9. We assume it might be due to PEG complexation with metals in mobile phase which interfered with the compound elution time to give two different peaks.

(C)

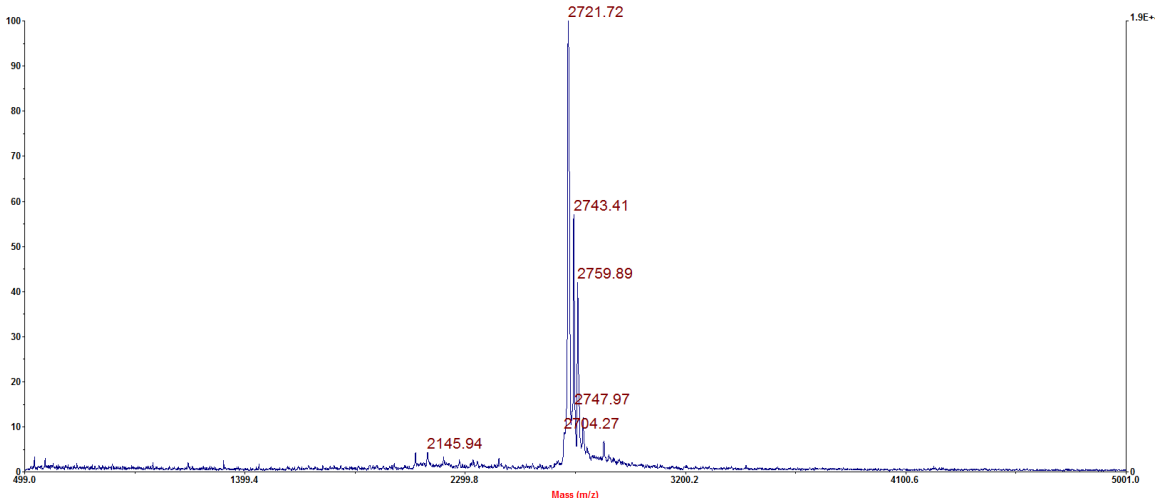

Characterization of EPHB1.9: (A). Chemical structure. (B). Analytical HPLC. (C). MALDI-TOF spectrum.

(MALDI-TOF+) m/z = 2721.72$[M+2H]^+$, 2743.41$[M+Na]^+$, 2759.89$[M+K]^+$

(A)

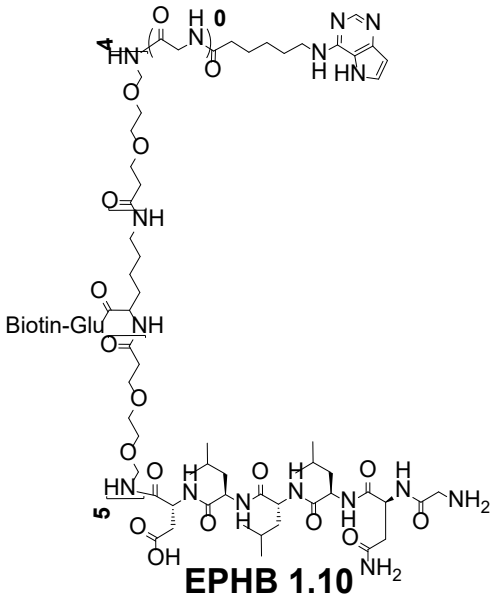

EPHB 1.10

Exact Mass 2864.54

(B)

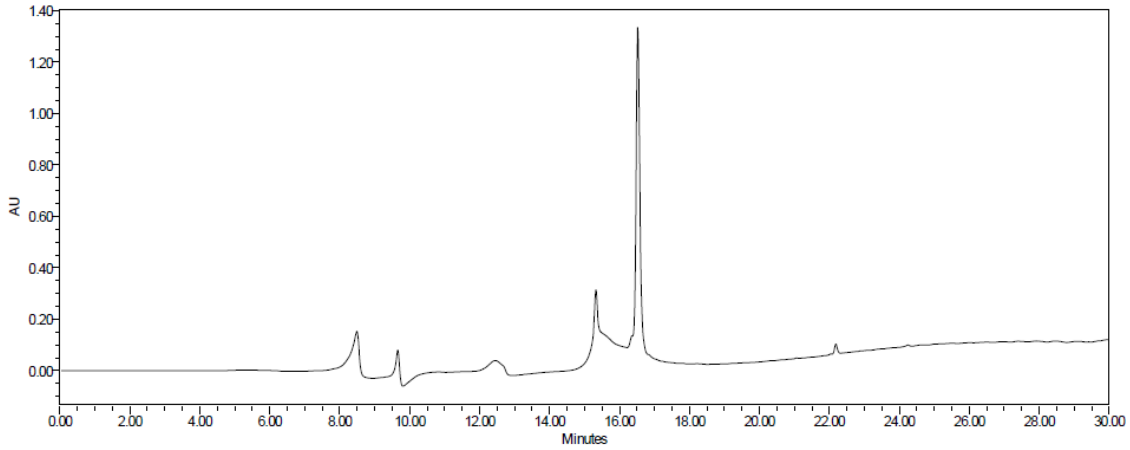

Note: We do not find any mass corresponding to the extra peak in the beginning (8.5-12.5 mins), in crude sample. We believe these peaks are caused by the air bubbles. And, the tailed peak (15.5 mins) in front of compound peak also have the same mass, which indicates they both belongs to EPHB1.10. We assume it might be due to PEG complexation with metals in mobile phase which interfered with the compound elution time to give two different peaks.

(C)

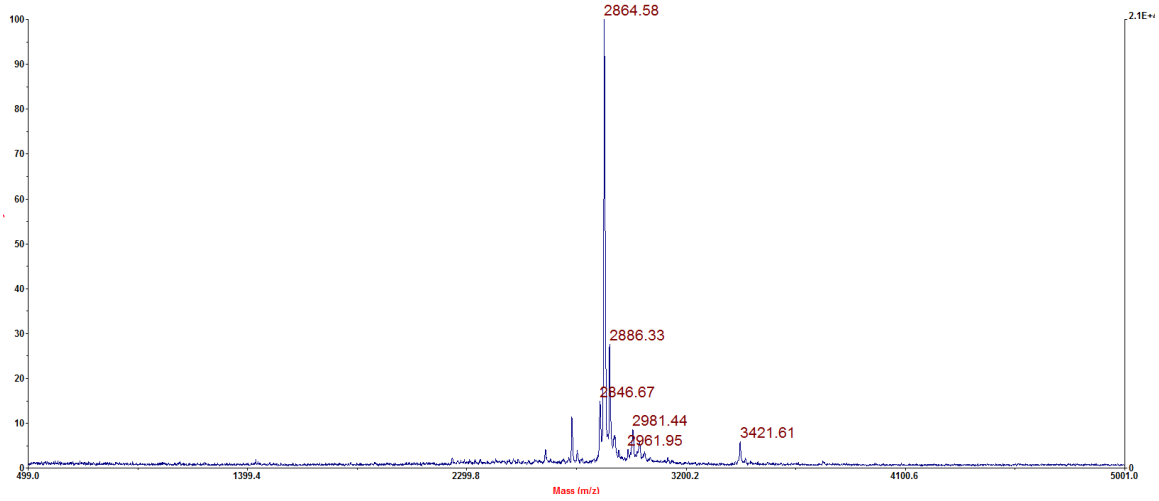

Characterization of EPHB1.10: (A). Chemical structure. (B). Analytical HPLC. (C). MALDI-TOF spectrum.

(MALDI-TOF+) m/z = 2864.58$[M+H]^+$, 2886.33$[M+Na]^+$, 2907.75$[M+2Na]^+$

(A)

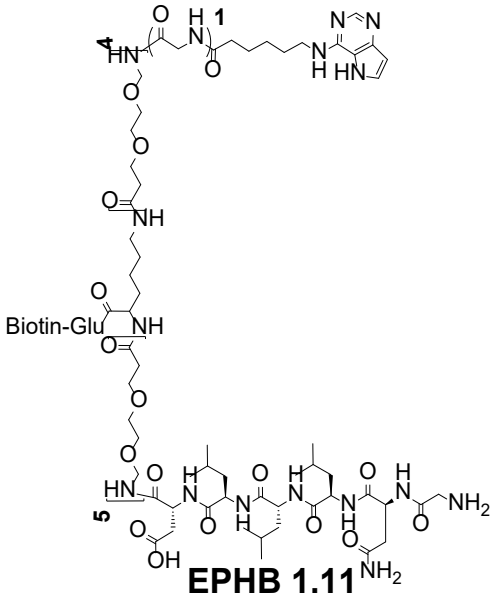

Exact Mass 2921.56

(B)

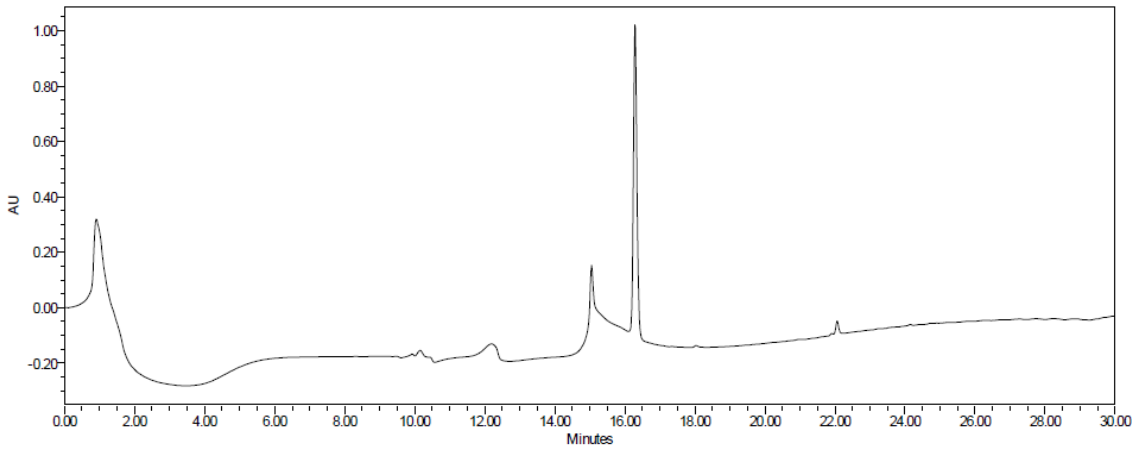

Note: We do not find any mass corresponding to the extra peak in the beginning (8.5 mins and 9.5 mins), in crude sample. We believe these peaks are caused by the air bubbles. And, the tailed peak (15.5 mins) in front of compound peak also have the same mass, which indicates they both belongs to EPHB1.10. We assume it might be due to PEG complexation with metals in mobile phase which interfered with the compound elution time to give two different peaks.

(C)

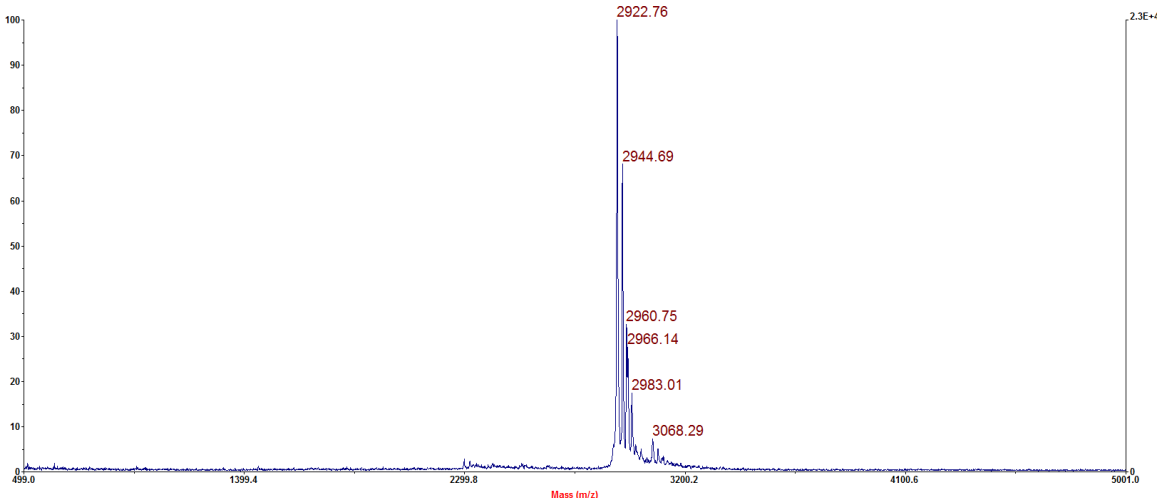

Characterization of EPHB1.11: (A). Chemical structure. (B). Analytical HPLC. (C). MALDI-TOF spectrum.

(MALDI-TOF+) m/z = 2922.76$[M+H]^+$, 2944.69$[M+Na]^+$, 2960.75$[M+K]^+$

3.4.4.4. Structure, Mass spectrum, and HPLC analysis of EPHB2 series compounds

(A)

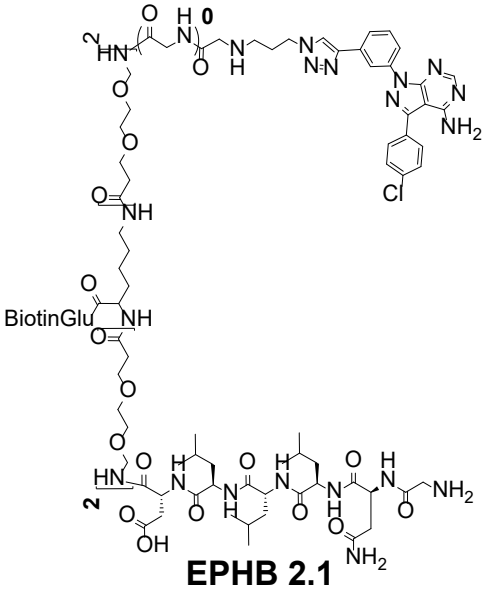

EPHB 2.1

Exact Mass 2394.20

(B)

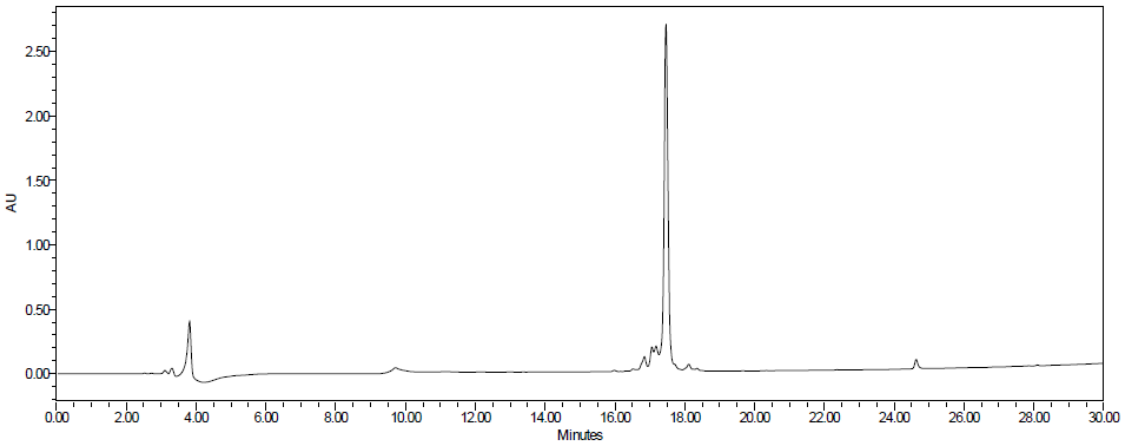

(C)

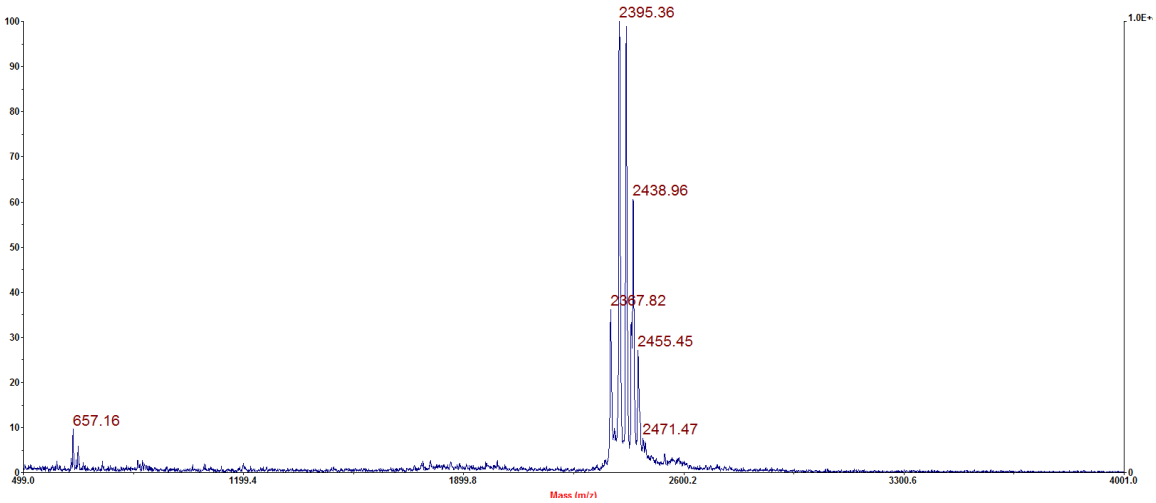

Characterization of EPHB2.1: (A). Chemical structure. (B). Analytical HPLC. (C). MALDI-TOF spectrum.

(MALDI-TOF+) m/z = 2395.36$[M+H]^+$, 2417.23$[M+Na]^+$, 2433.09$[M+K]^+$

(A)

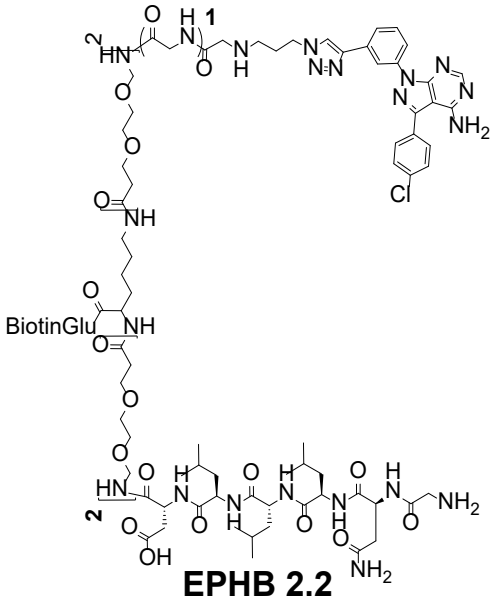

EPHB 2.2

Exact Mass 2451.22

(B)

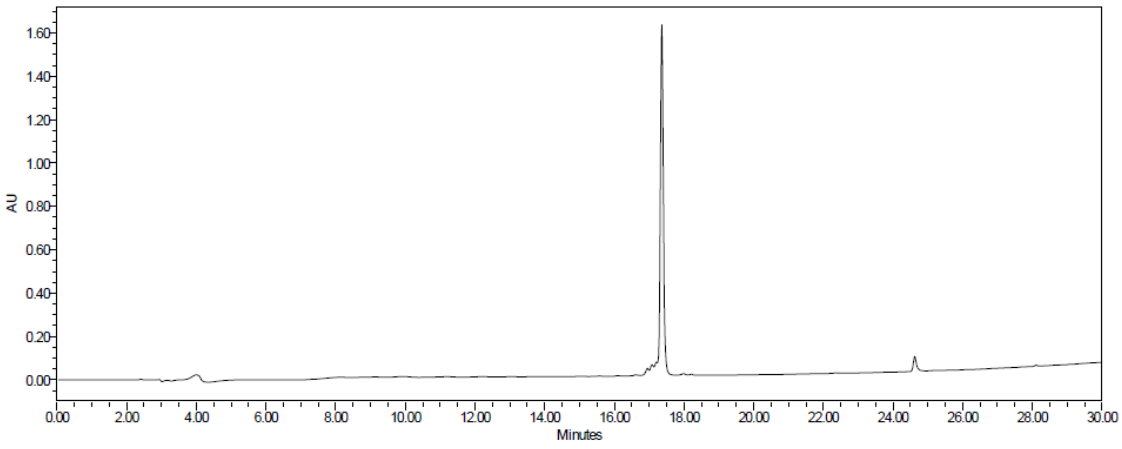

(C)

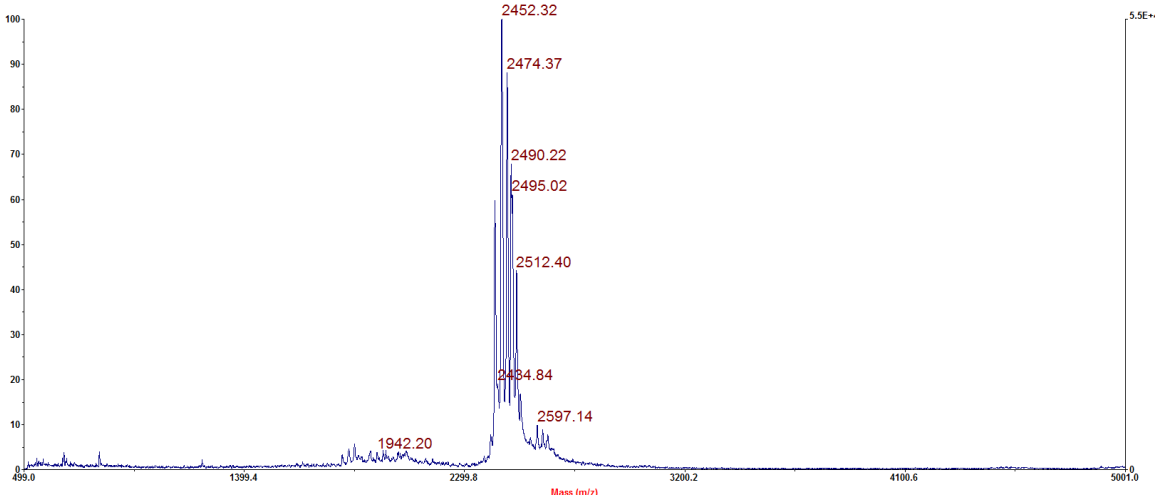

Characterization of EPHB2.2: (A). Chemical structure. (B). Analytical HPLC. (C). MALDI-TOF spectrum.

(MALDI-TOF+) m/z = 2452.32$[M+H]^+$, 2474.37$[M+Na]^+$, 2490.22$[M+K]^+$

(A)

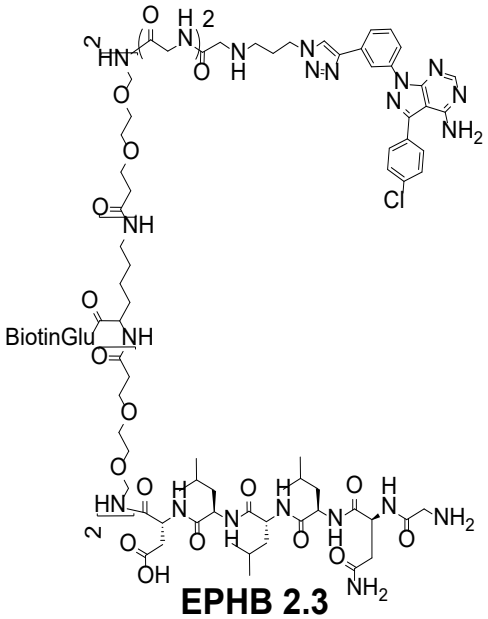

EPHB 2.3

Exact Mass 2508.24

(B)

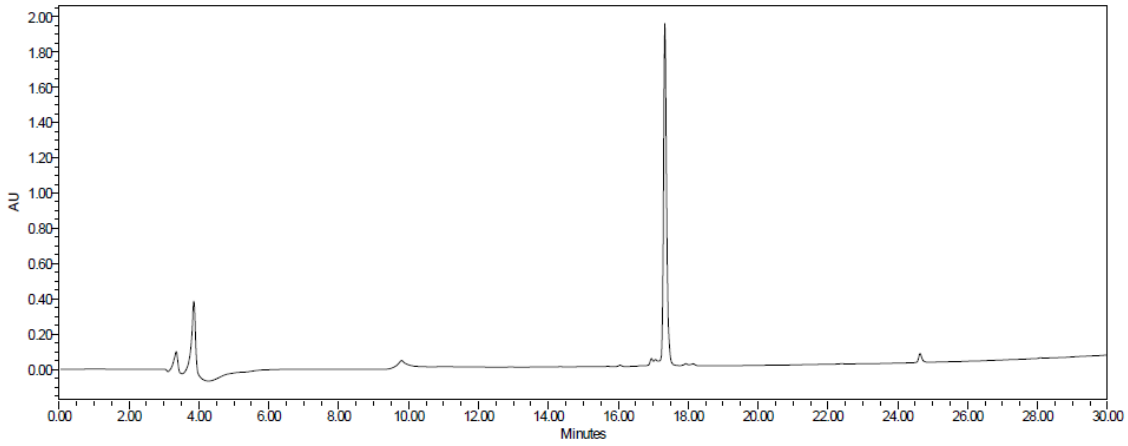

(C)

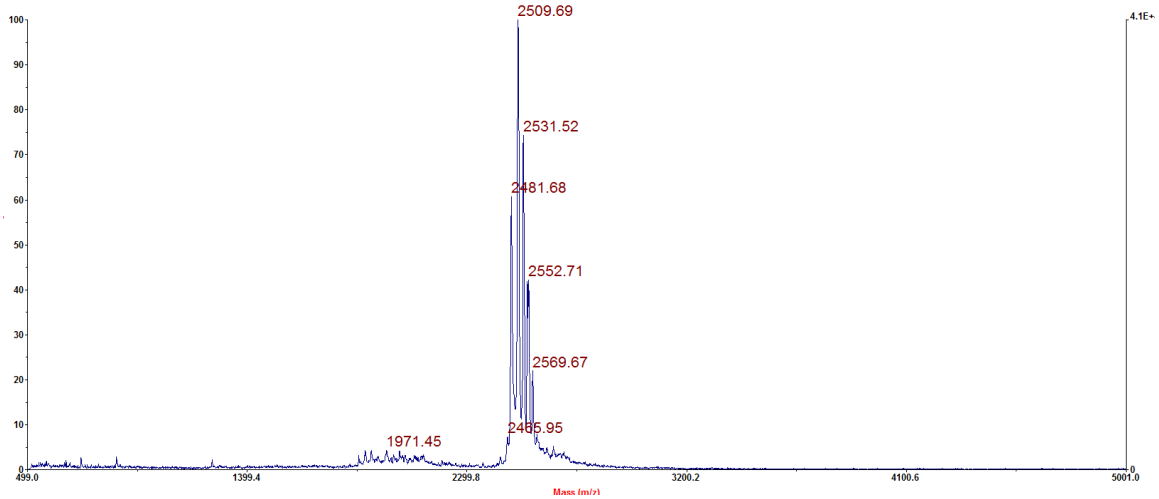

Characterization of EPHB2.3: (A). Chemical structure. (B). Analytical HPLC. (C). MALDI-TOF spectrum.

(MALDI-TOF+) m/z = 2509.69$[M+H]^+$, 2531.52$[M+Na]^+$, 2547.45$[M+K]^+$

(A)

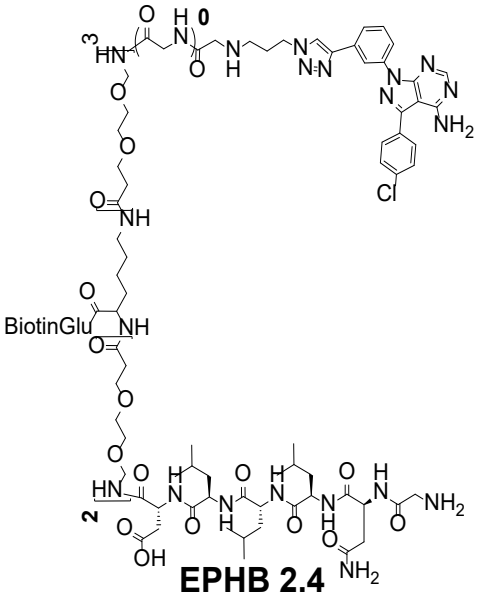

Exact Mass 2539.27

(B)

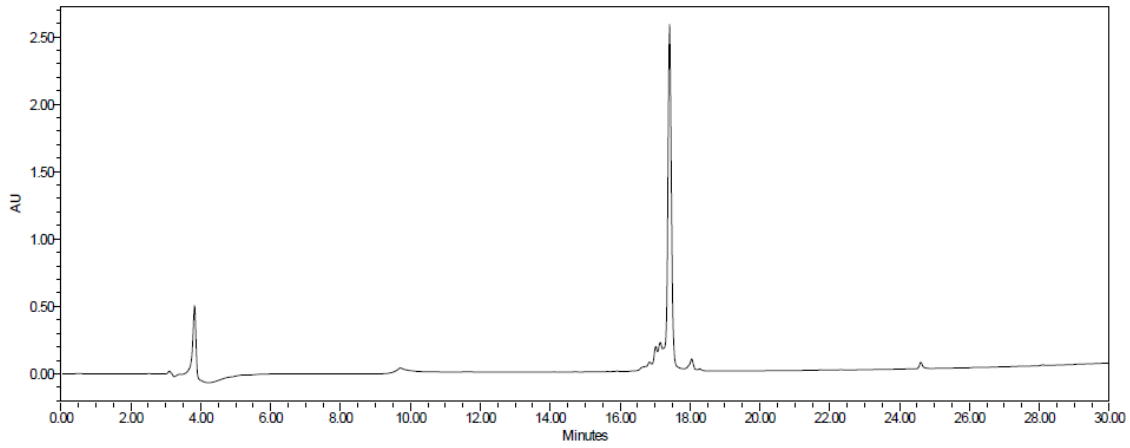

(C)

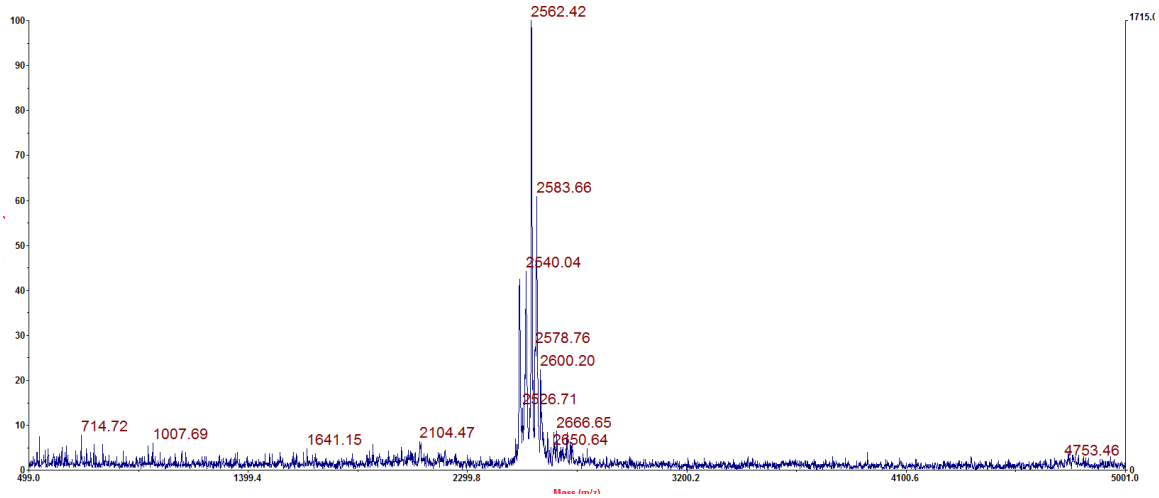

Characterization of EPHB2.4: (A). Chemical structure. (B). Analytical HPLC. (C). MALDI-TOF spectrum.

(MALDI-TOF+) m/z = 2540.04$[M+H]^+$, 2562.42$[M+Na]^+$, 2578.76$[M+K]^+$

(A)

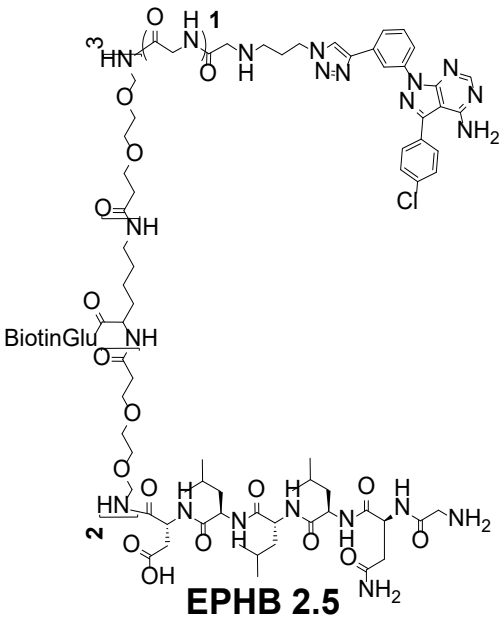

EPHB 2.5

Exact Mass 2596.3

(B)

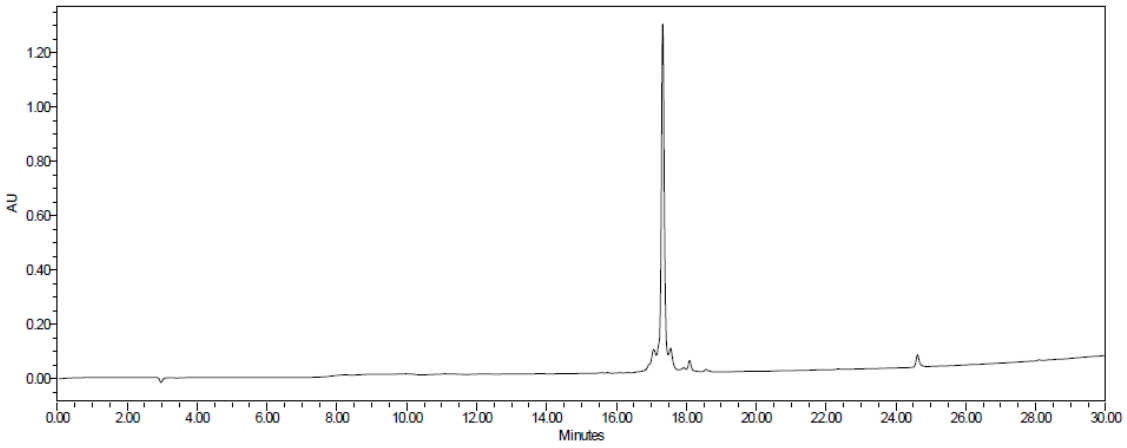

(C)

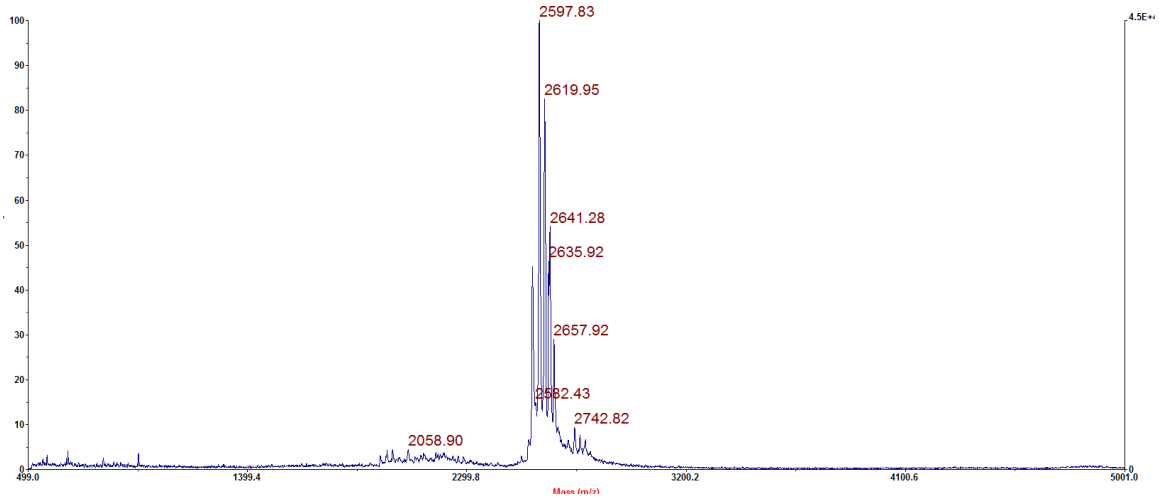

Characterization of EPHB2.5: (A). Chemical structure. (B). Analytical HPLC. (C). MALDI-TOF spectrum.

(MALDI-TOF+) m/z = 2597.83$[M+H]^+$, 2619.95$[M+Na]^+$, 2635.92$[M+K]^+$

3.4.4.5. Structure, Mass spectrum, and HPLC analysis of biotinylated EPHB peptide monomer

(A)

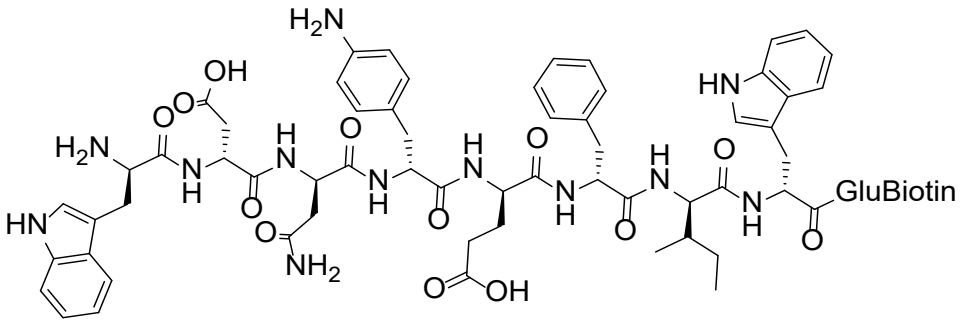

EPHB peptide monomer

Exact Mass 1727.00

(B)

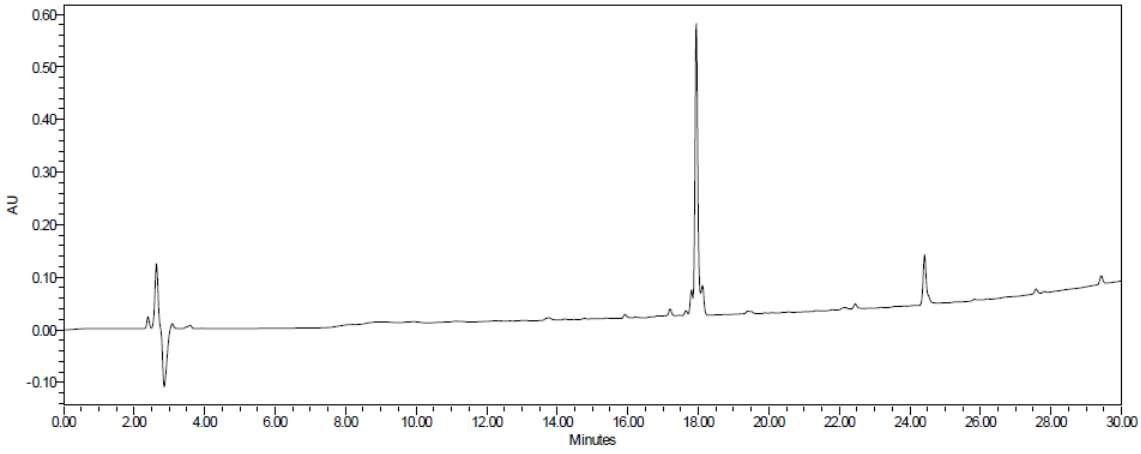

(C)

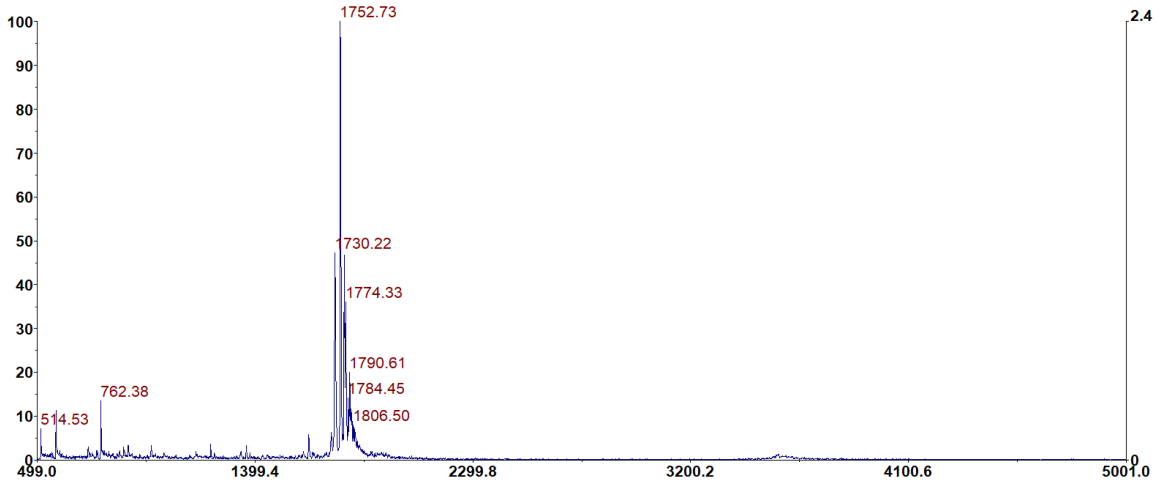

Characterization of EPHB peptide monomer: (A). Chemical structure. (B). Analytical HPLC. (C). MALDI-TOF spectrum.

(MALDI-TOF+) m/z = 1730.22$[M+H]^+$, 1752.73$[M+Na]^+$, 1774.33[M+K]

3.4.4.6. Structure, Mass spectrum, and HPLC analysis of non-biotinylated EPHB peptide:

(A)

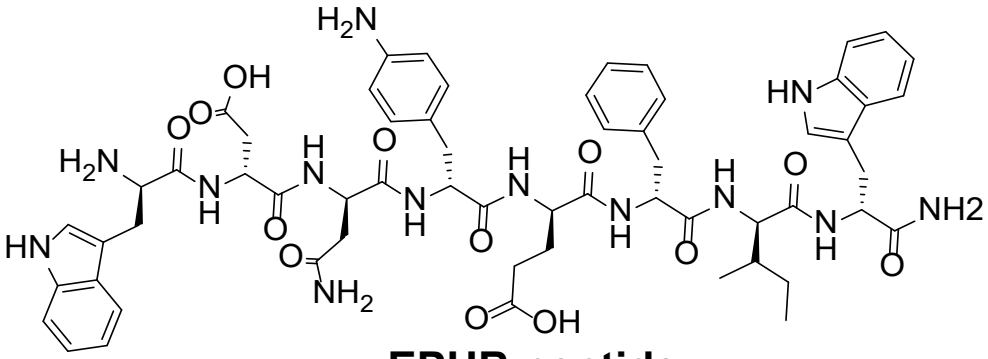

EPHB peptide

Exact Mass 1168.00

(B)

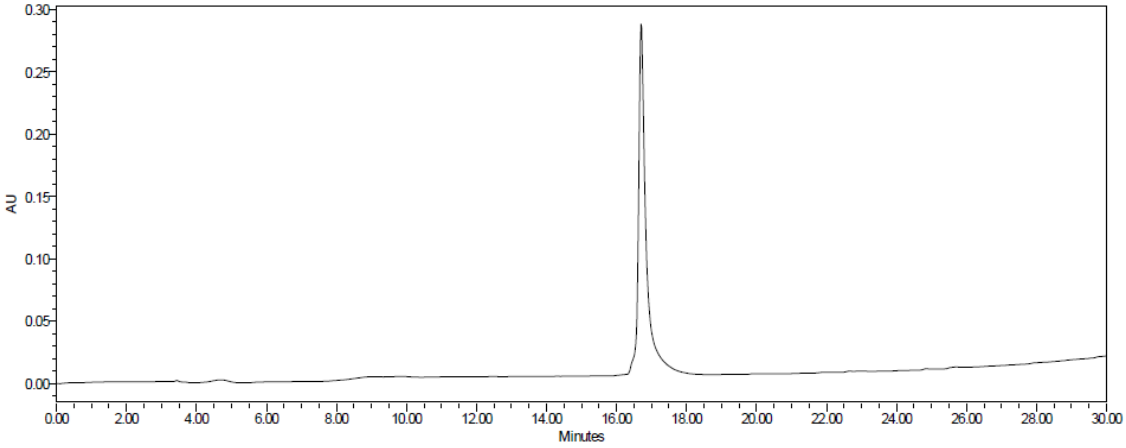

(C)

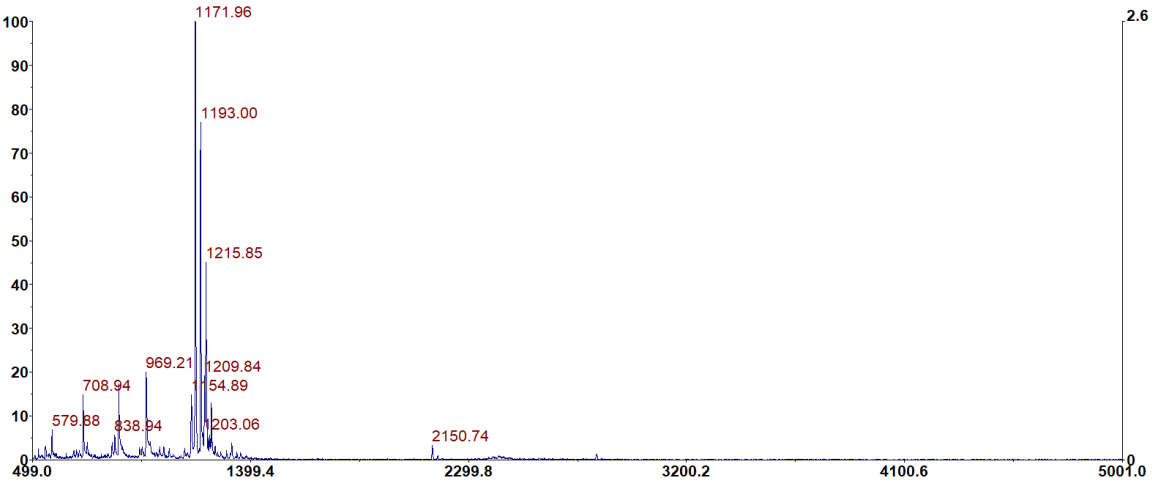

Characterization of EPHB peptide: (A). Chemical structure. (B). Analytical HPLC. (C). MALDI-TOF spectrum.

(MALDI-TOF+) m/z = 1171.96.81$[M+H]^+$, 1193.00$[M+Na]^+$, 1209.84$[M+K]^+$

3.4.4.7. Structure, Mass spectrum, and HPLC analysis of biotinylated EPHB3 series compounds

(A)

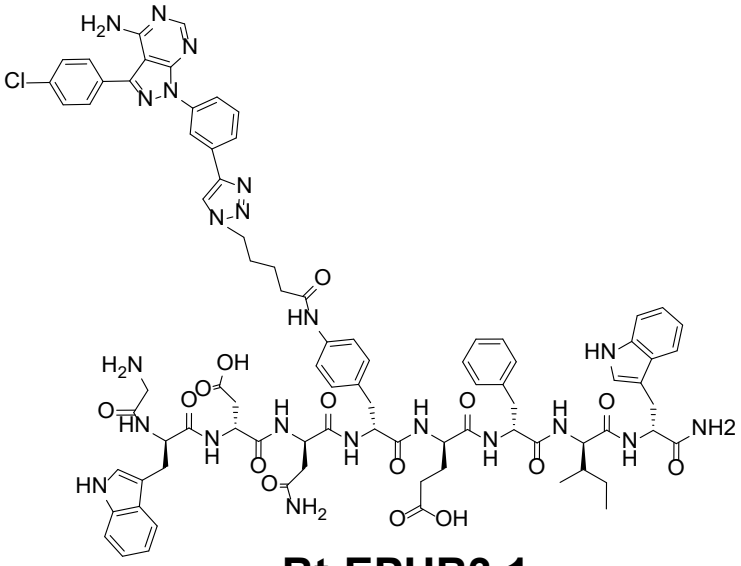

Bt-EPHB3.1

Exact Mass 2254.00

(B)

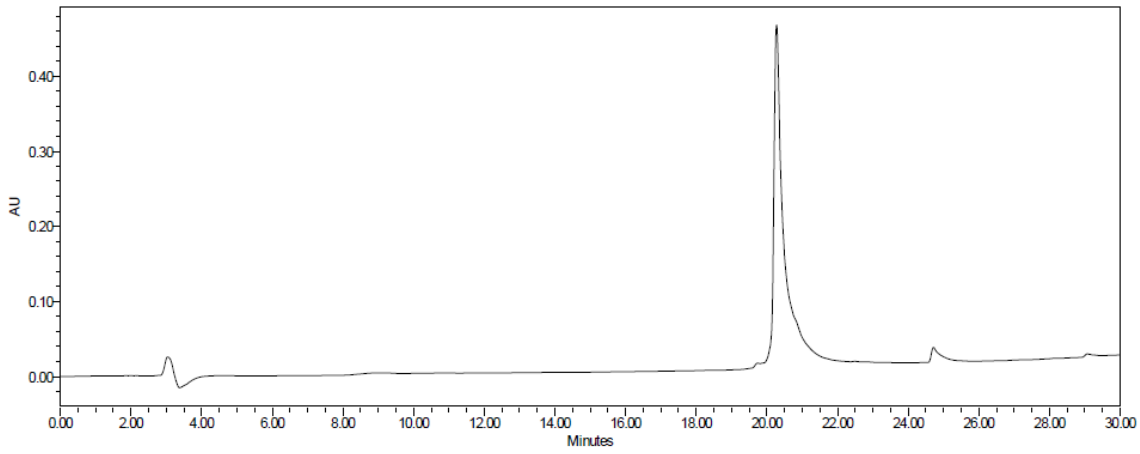

(C)

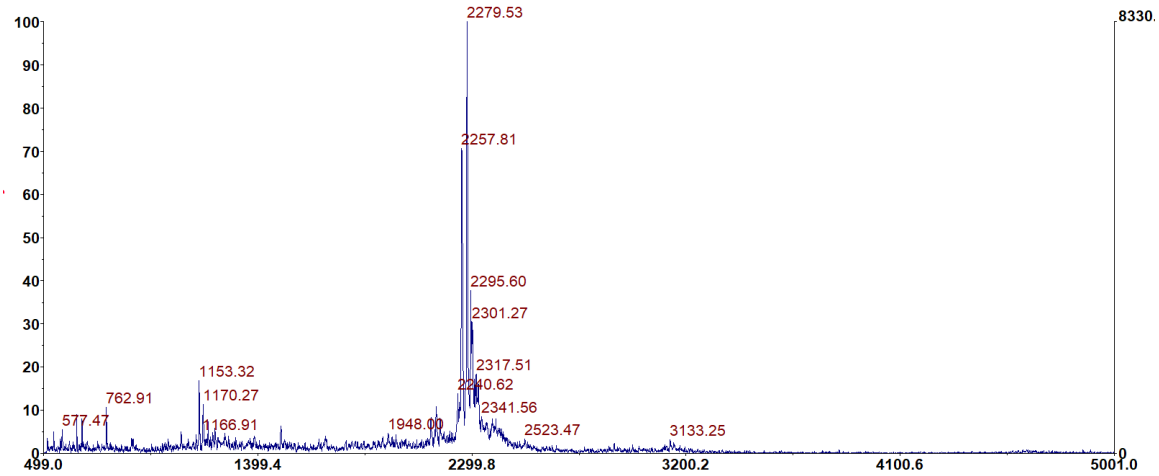

Characterization of Bt-EPHB3.1: (A). Chemical structure. (B). Analytical HPLC. (C). MALDI-TOF spectrum.

(MALDI-TOF+) m/z = 2257.81$[M+H]^+$, 2279.53$[M+Na]^+$, 2295.60$[M+K]^+$

(A)

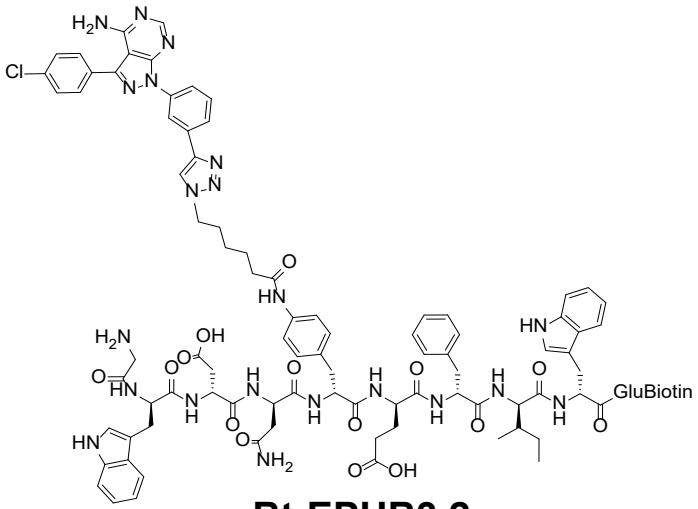

Bt-EPHB3.2

Exact Mass 2268.00

(B)

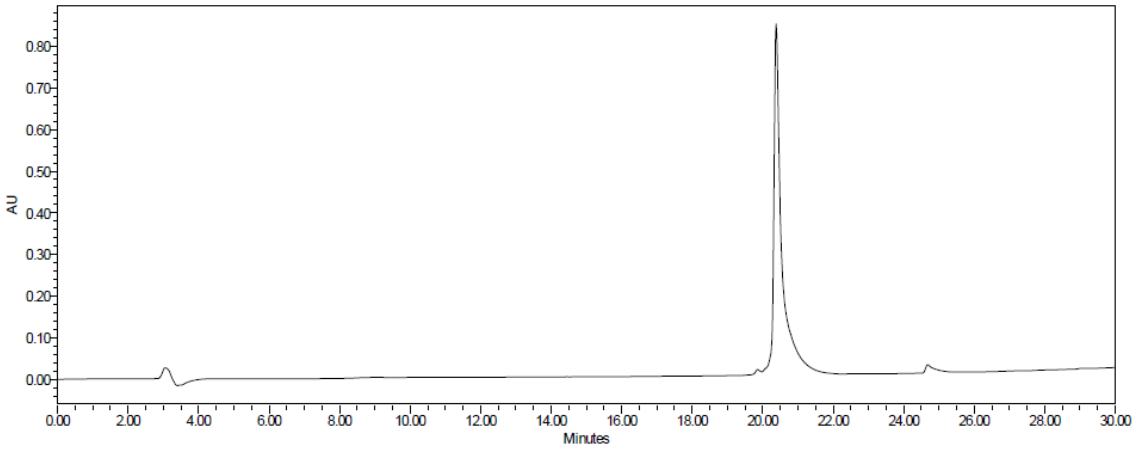

(C)

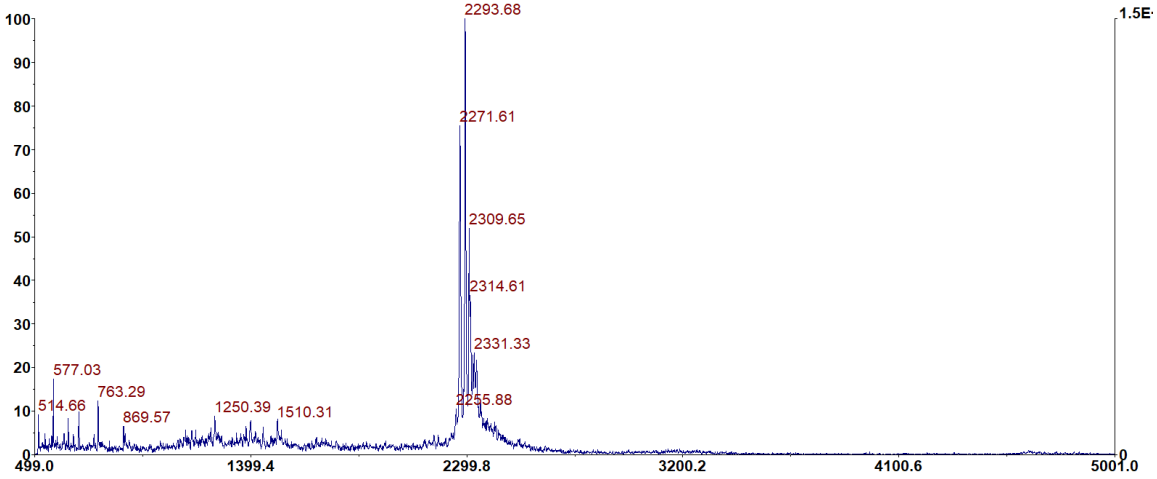

Characterization of Bt-EPHB3.2 (A). Chemical structure. (B). Analytical HPLC. (C). MALDI-TOF spectrum.

(MALDI-TOF+) m/z = 2271.61$[M+H]^+$, 2293.61$[M+Na]^+$, 2309.65$[M+K]^+$

3.4.4.8. Structure, Mass spectrum, and HPLC analysis of non-biotinylated EPHB3 series compounds:

(A)

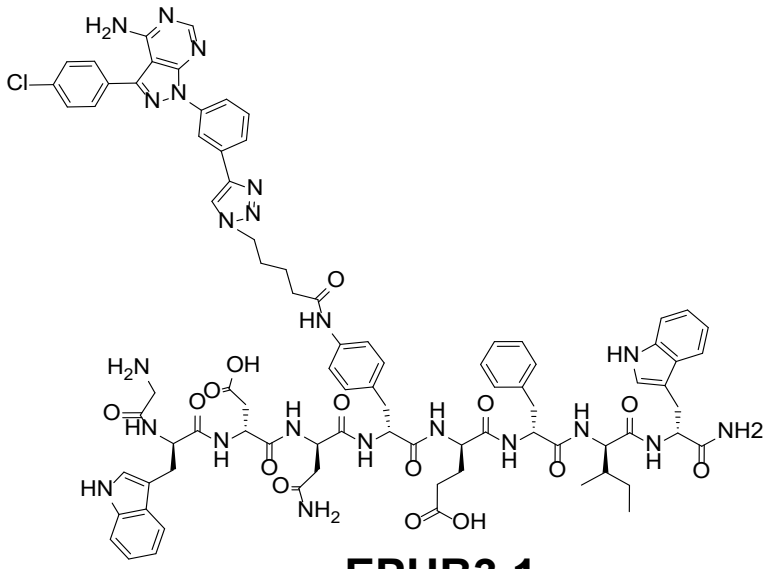

EPHB3.1

Exact Mass 1696.69

(B)

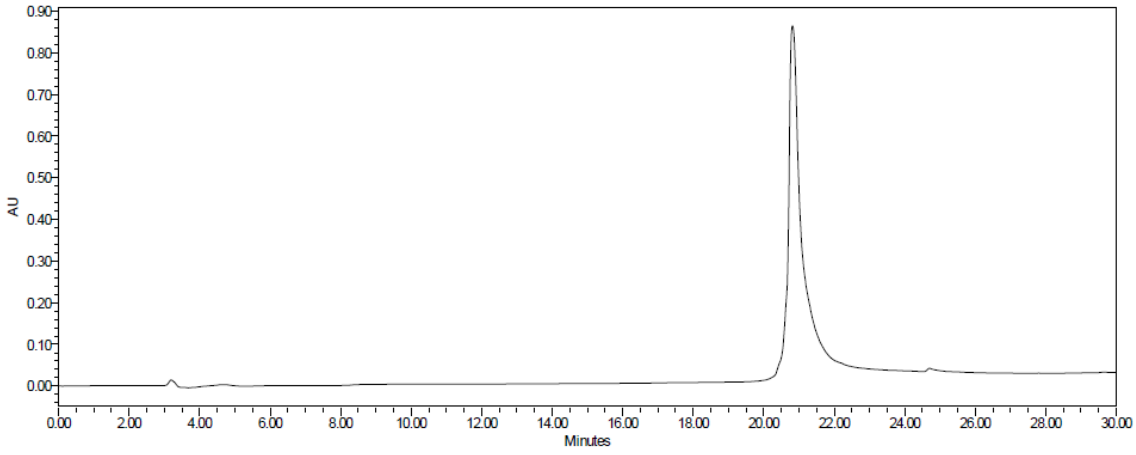

(C)

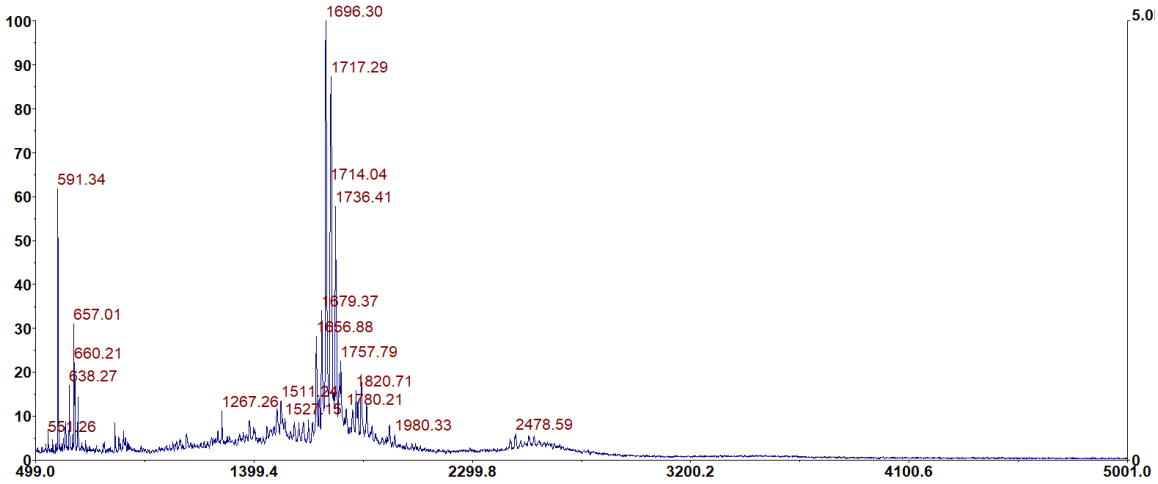

Characterization of EPHB3.1: A). Chemical structure. B). Analytical HPLC. C). MALDI-TOF spectrum.

(MALDI-TOF+) m/z = 1696.30$[M+H]^+$, 1717.29[M+Na]

(A)

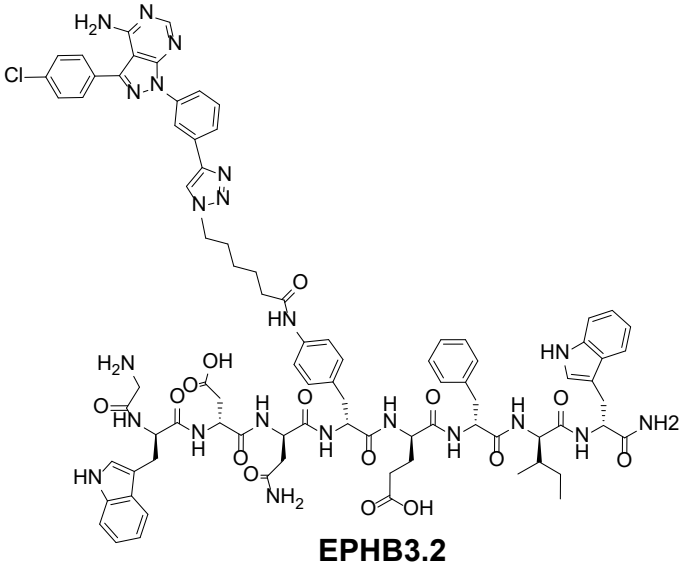

EPHB3.2

Exact Mass 1710.70

(B)

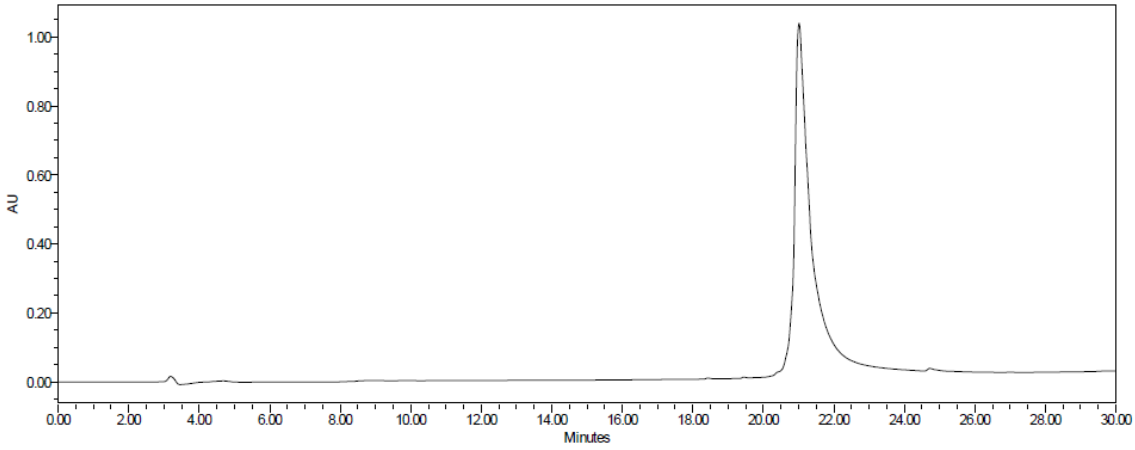

(C)

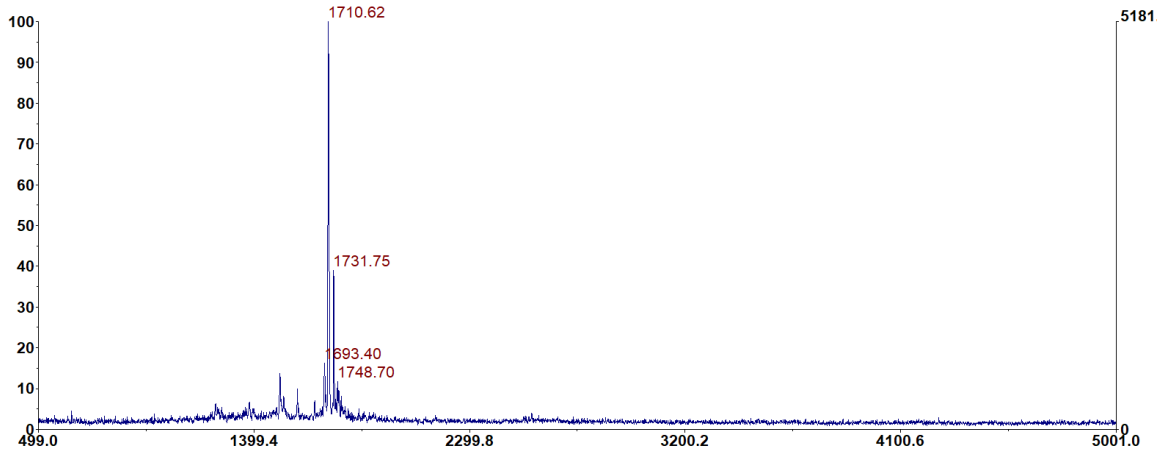

Characterization of EPHB3.2 (A). Chemical structure. (B). Analytical HPLC. (C). MALDI-TOF spectrum.

(MALDI-TOF+) m/z = 1710.62$[M+H]^+$, 1731.75$[M+Na]^+$, 1748.70$[M+K]^+$

3.4.5. Molecular modelling and docking studies:

MOE (Molecular Operating Environment, chemical computing group) software used for docking studies.[79] The crystal structure of EphA3 kinase in complex with ANP (PDB: 2GSF) was used for docking PP2 analogue. First, the receptor (EphA3 kinase) was prepared by (i). removing the co-crystallized ligand (ANP) (ii). correcting the structural issues in crystal structure using “structure preparation tool” (iii). adding and optimizing the H-bond network in kinase using protonate 3D tool. In a separate window, ligand (PP2 analogue) was prepared for docking by (i). drawing the structure using “build” tool (ii). assigning atom type and charges using MMFF94x force field (iii) minimizing ligand energy. Next, PP2 analogue was docked with EphA3 kinase and visualized.

Molecular modelling and docking results were visualized using either MOE or Discovery Studio (BIOVIA).

3.4.6. Biochemical Characterization:

3.4.6.1. ELISA-like binding assay:

White, 96 well nickel coated plates (Pierce™) were coated with 50 µL of His tagged recombinant EphA3 (Thermo Fisher Scientific, Waltham, MA) at a concentration of 1 µg/mL (diluted with Tris buffered Saline or TBS) for 1 hr at room temperature. All wells were washed with 3 X 100 µL of TBS and blocked with starting block buffer (Thermo Fisher Scientific, Waltham, MA). Fifty microliters of biotinylated

compounds in starting block buffer were added to each well and incubated for 1 hr. All wells were again washed with TBS (3 x 100 µL). Fifty microliters of streptavidin-horse radish peroxidase (HRP) (Novus biologicals, Littleton, CO) at 1:800 dilution in starting block buffer was added to each well and allowed to incubate for 1 hr. Finally, all wells were washed as discussed before and 50 µL of SuperSignal ELISA Pico Chemiluminescent Substrate (Thermo Fisher Scientific, Waltham, MA) was added to each well. The resulting luminescence signal was detected at all wavelengths using a Spectramax i3 microplate reader (Molecular Devices, San Jose, CA).

3.4.6.2. ADP-Glo kinase assay:

White, 384 well nickel coated plates (Pierce™) were coated with 5 µL of kinase reaction mixture (consists of 2 µL of EphA3 kinase (SignalChem, Richmond, CA) in kinase dilution buffer, 1 µL of ATP (Promega, WI) at 10 µM, 1 µL of poly E: Y peptide (SignalChem, Richmond, CA) at 200 µM and 1 µL of compound (in kinase dilution buffer) was incubated for 1 hr. Then reaction was then stopped by adding ADP-Glo reagent (Promega, WI). After 40 min of incubation, kinase detection reagent (Promega, WI) was added. The resulting luminescence signal was measured after 20 minutes at all wavelengths using a Spectramax i3 microplate reader (Molecular Devices, San Jose, CA).

3.5. Results and discussion:

3.5.1. Design of hetero-bivalent ligands targeting EphA3 kinase:

Here, we chose EphA3 kinase as a target kinase because of readily available crystal structures of two peptide ligands: (i). one unique peptide that is a part of the linker connecting EphA3 Sterile Alpha Motif (SAM) domain (also known as ESL peptide) and kinase domain appeared to bind to a true binding pocket much more distal to ATP binding site (Fig. 15).[92] (ii). another peptide binding to substrate peptide pocket in between the ATP and ESL peptide binding sites.[93] Therefore, we envisioned to design two hetero-bivalent ligands by connecting an ATP binding site moiety with (i). unique ESL peptide, and (ii). substrate peptide binding pocket using linker to yield two different hetero-bivalent ligands. Our future studies include finding the optimum linker that connects substrate and ESL peptide. Then, substituting a part of the linker with substrate peptide to yield hetero-bivalent ligand with enhanced affinity and selectivity towards EphA3 kinase.

3.5.1.1. Hetero-bivalent ligands targeting ATP and ESL peptide:

As discussed in the Chapter 1, the design strategy for a hetero-bivalent ligand involves selecting (i). an ATP binding site moiety, and (ii). a peptide sequence that interacts with the EphA3 kinase surface. When we carefully study the crystal structure of EphA3 kinase domain, we observed that the linker peptide connects the kinase domain with the SAM domain appeared to turn back and interact with

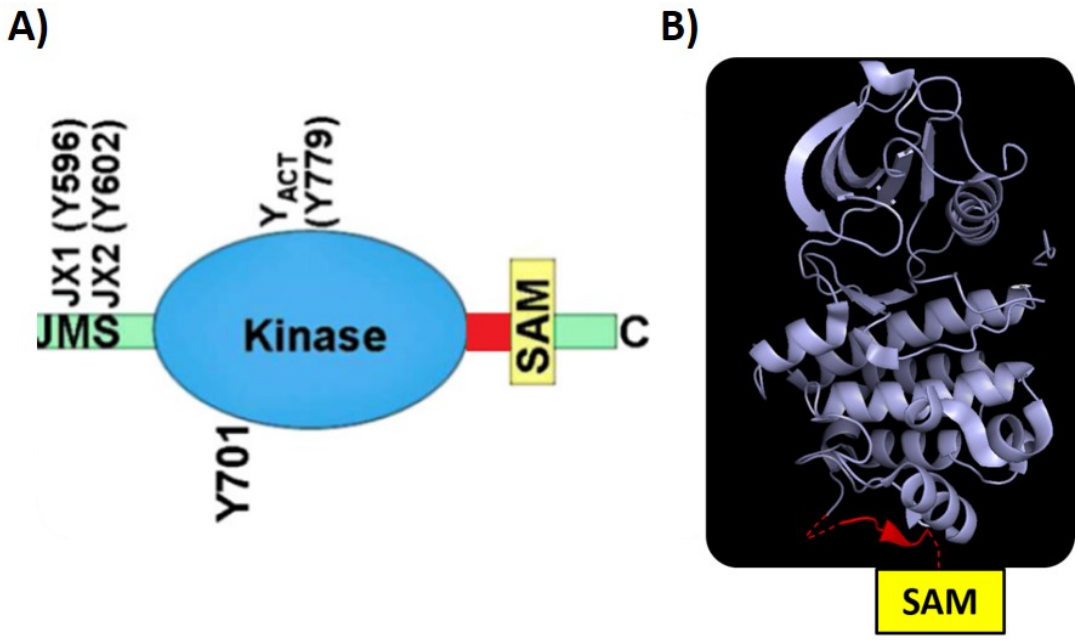

Figure 15. Structure of EphA3 kinase. (A). Schematic diagram showing the intracellular region of EphA3 receptor tyrosine kinase. (B). Crystal structure of EphA3 kinase domain. ESL peptide bound at the bottom of kinase.

the bottom of the kinase domain (Fig. 15.B).[92] This pentameric ESL peptide sequence (NLLLD) has a true binding pocket away from the ATP binding site (Fig. 16.C). The ESL peptide forms tight backbone hydrogen bond interactions with amino acids the αG loop (Tyr-841 to Pro-846), which projects the side chains of Leu-901, and Leu-903 firmly fits in complementary pockets formed by αG and αH loops at the bottom of the kinase. Therefore, we proposed to use this ESL peptide sequence outside the ATP binding moiety that can be connected to ATP binding site ligand using an optimized linker (Fig. 16A & B). Our main intention is not to design a drug here since EPHA3 kinase contribution of cancer progression is still an ambiguous area of research.[94-96]

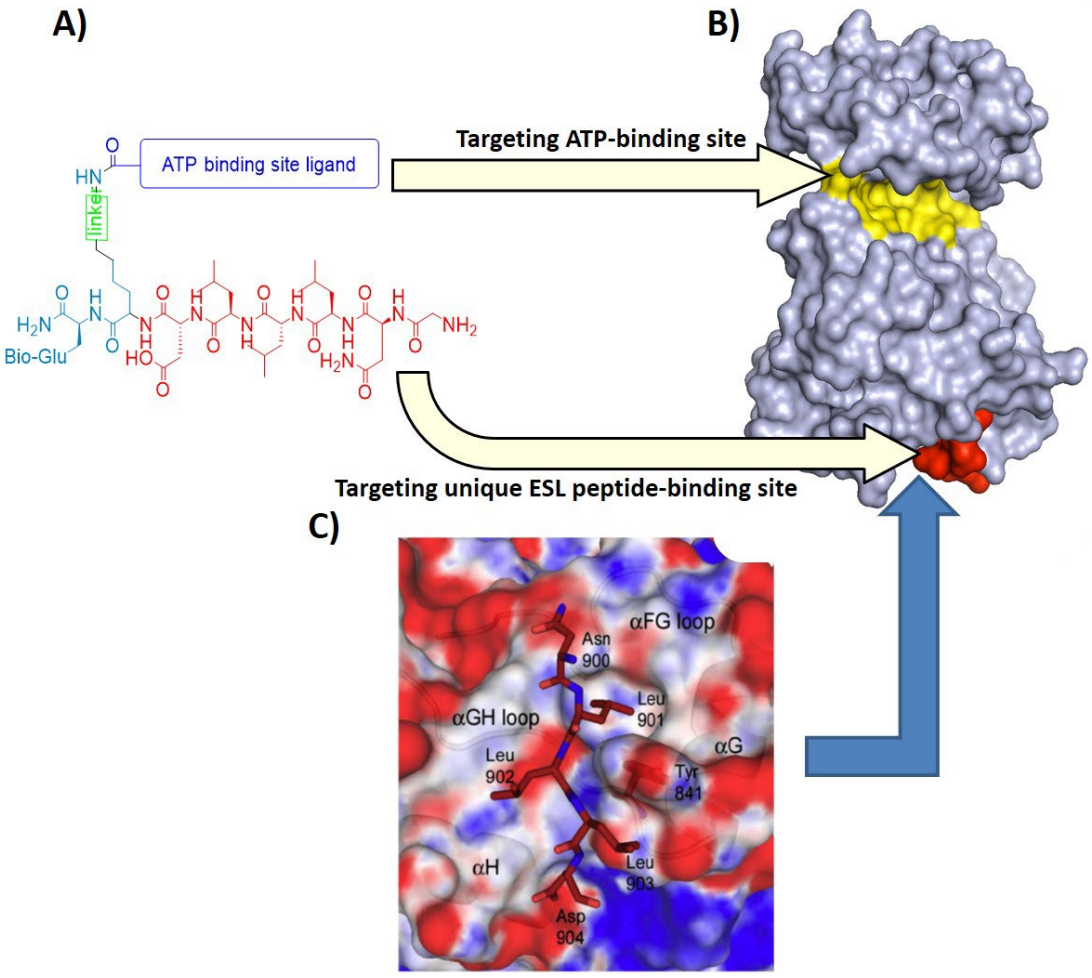

Figure 16. Crystal structure EphA3 kinase domain and unique hetero-bivalent ligand design. (A). Components of hetero-bivalent ligand that target binding sites. (B). ATP binding site and unique EphA3 SAM linker (ESL) peptide binding site located at the bottom of the kinase domain. (C). Crystal structure showing ESL peptide segment binding to a unique binding site on the bottom of the kinase domain.

To find an optimal linker that fits the longer distance between ATP binding pocket and ESL peptide, we crafted a two-step strategy, carefully looking for linker types that we can be used in our design. We first chose flexible linkers in our design even though they impose high entropic penalty upon binding. Our hypothesis was to give full freedom to the linker to achieve the most appropriate path on the kinase

domain while connecting these two distance binding monomeric units. Once we identify the optimal linker, we reasoned that we could rigidify it to reduce the entropic penalty associated with the binding event.

As mentioned earlier, we employed a two-step strategy to find optimum linkers covering the distance between ATP and ESL peptide binding pockets. First, the approximated distance was determined using a combinatorial approach. Next, the length identified in the first step was further fine-tuned using structural features of the ATP binding pocket of the kinase.

3.5.1.1.1. Combinatorial approach:

In this approach, we first selected a purine analogue as the ATP binding moiety as it is (i). known to interact with the ATP binding pocket, and (ii). easy to synthesize and rapidly couple onto solid phase. The next task was to select the linkers connecting the purine analogue and ESL peptide. As we opted to go with flexible linkers in our design, we chose two types of flexible linkers, namely, (i) AEEAc [polyethylene glycol (PEG)-based amino-ethoxy-ethoxy-acetyl moieties] and (ii) glycines to cover the entire distance. The PEG-based AEEAc linkers provide water-soluble characteristics to the linker while glycines provides slight hydrophobicity. The AEEAc consists of nine atoms length per residue, which can cover longer distance while glycine residue covers the small distance. According to the crystal structure shown in Fig. 15(B), the approximate distance between ATP

and ESL binding pockets is around 60 Å. Therefore, we decided to develop 11 hetero-bivalent ligands that only defers in linker lengths, which overall covers a distance around 54-106 Å. Moreover, the commercial availability of Fmoc analogues of AEEAc and glycine makes them more attractive for the hetero-bivalent ligand design. We carefully modified our previously published Fmoc based

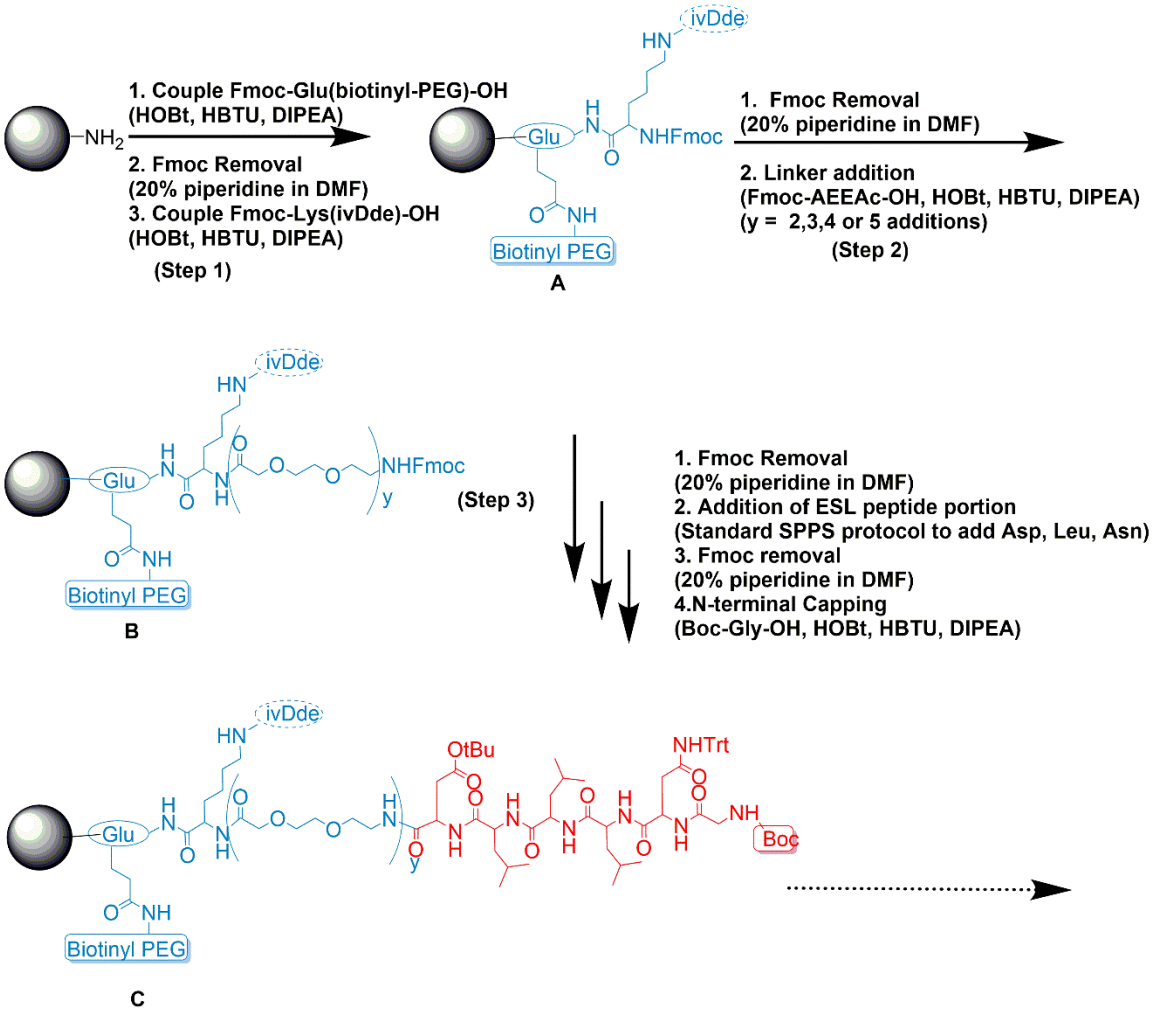

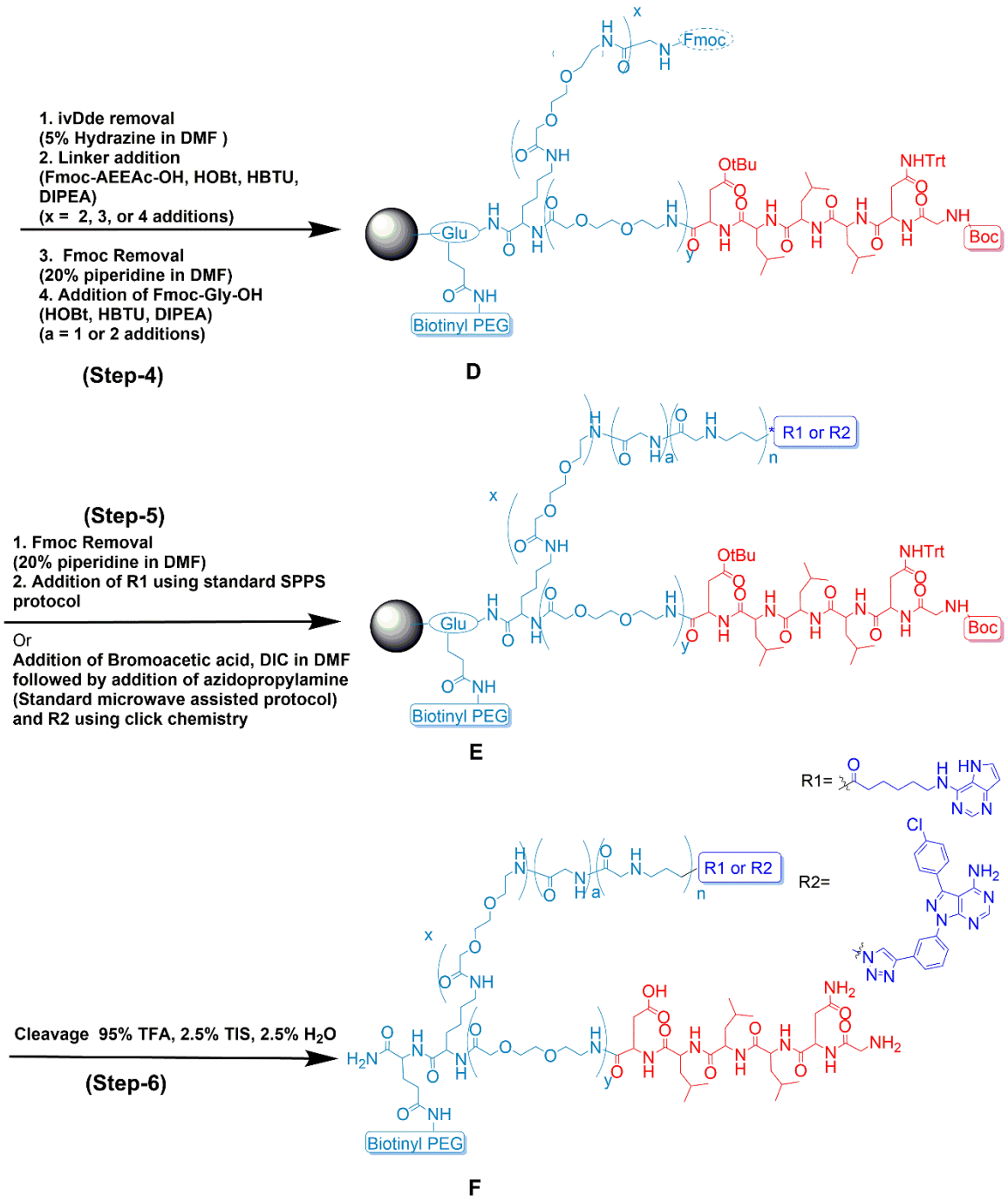

Scheme 8. Synthesis scheme of biotinylated EPHB1 and 2 series of ligands. R1 and R2 represents two different ATP binding site ligands (dark blue) ESL peptide sequence is showed in red and the linker region is highlighted in light blue.

solid-phase peptide synthesis protocol.[77] Here, we first coupled Fmoc-Glu(biotinyl-PEG)-OH that detects the binding event in ELISA-like binding assay. Next, using 20% piperidine, we removed Fmoc and coupled Fmoc-Lys(ivDde)-OH to obtain compound A**.** Lysine acts as a central linker in compound A, with two orthogonal protecting groups (*i.e.*, Fmoc and ivDde) on two braches (Scheme 8, step 1). First, we deprotect the Fmoc protecting group using 20% piperidine in DMF and built the ESL peptide containing arm by (i). growing the linker using Fmoc-AEEAc-OH moieties (y = 2, 3, 4, and 5) to obtain intermediate compound B (Scheme 8, step 2) (ii). the amino acids Fmoc-Asp-OH, Fmoc-Leu-OH (3 times), and Fmoc-Asn(Trt)-OH were coupled sequentially and N-terminus was subsequently capped using Boc-Gly-OH to obtain compound C (Scheme 8, step 3). Next, we deprotect the ivDde protecting group using 5% hydrazine in DMF and built the ATP binding moiety-containing arm by (i). elongating the linker using Fmoc-AEEAc-OH (x= 2, 3, and 4) and Fmoc-Gly-OH moieties (n= 0, 1, and 2) to yield compound D (Scheme 8, step 4) (ii). 6-aminopurine hexanoic acid was coupled at the N-terminal to obtain compound E (Scheme 8, step 5). Finally, the compounds were cleaved from the resin using cleaving cocktail [95% trifluoroacetic acid (TFA), 2.5% triisopropylsilane (TIS), and 2.5% H_2O] that deprotects all protecting groups in the hetero-bivalent ligand (compound F) (Scheme 8, step 6). The biotinylated purine analogue was synthesized in large scale following the published protocol.[37] The biotinylated ESL peptide was synthesized using standard Fmoc chemistry.

a) ELISA-like binding studies:

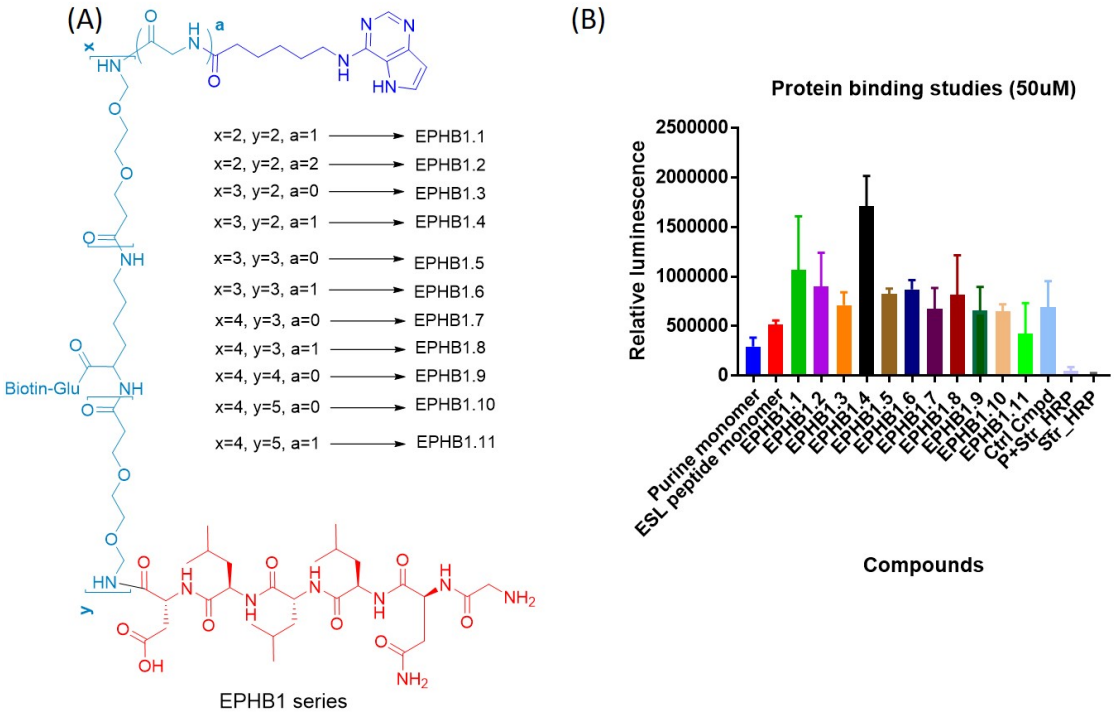

Figure 17. The first round of hetero-bivalent ligand design. (A). Outline of the hetero-bivalent ligands design. (B). ELISA-like binding assay results of 11 hetero-bivalent ligands binding to the EphA3 kinase domain at 50 μM. EPHB1.4 showed the best binding.

Next, ELISA-like binding assay was employed to select the hetero-bivalent ligands having optimum linker length.[37] All synthesized hetero-bivalent ligands (EPHB1.1-1.11) were screened using this assay at 50 μM concentration. As shown in Fig. 17(B), only EPHB1.4, having linker length around 64 Å, showed greater binding affinity towards the EphA3 kinase domain when compared with remaining hetero-bivalent ligands (except EPHB1.1 which also have slightly strong binding affinity than others). Both monomers, 6-aminopurine hexanoic acid and ESL peptide, showed weak binding affinity towards the EphA3 kinase domain. These results

indicated that an approximate linker length of 64 Å, corresponding to EPHB1.4, proved to be optimum, indicating this length provides a good scaffold to hold both 6-aminopurine hexanoic acid and ESL peptide into their binding pockets.

3.5.1.1.2. Structural based approach:

Here, we plan to further fine-tune the linker length that was identified in the first step. Once again, we decided to synthesize six compounds that only differs at the linker that were estimated to cover around 51-65 Å linker lengths. We also wanted to replace the 6-aminopurine hexanoic acid with a molecule known to target the ATP binding pocket of EphA3 kinase. Here, we chose the same PP2 analogue used in the ERK5 targeted project (Chapter 2) because it was known to interact with the ATP binding site of EphA3 kinase as well.[76] We used the same synthesis route as described earlier (for the EPHB1 series) except replacing azidopropylamine at R1 after deprotecting Fmoc at the N-terminus in step 5. Using the standard microwave-assisted peptoid protocol, 3-azido-1-propylamine was introduced into peptide sequence after coupling the free N-terminus with bromoacetic acid and diisopropyl carbodiimide (DIC).[97-98] Finally, the PP2 analogue (R2) was incorporated using CuAAC with *N*-methyl-2-pyrrolidone (NMP) as solvent. The resin was then treated with the cleaving cocktail (95% TFA, 2.5% TIS, and 2.5% H_2O) to release the hetero-bivalent ligand from the resin. Using this

synthesis strategy, six compounds were synthesized that were estimated to cover around 51-65 Å linker length.

a) ELISA-like binding studies:

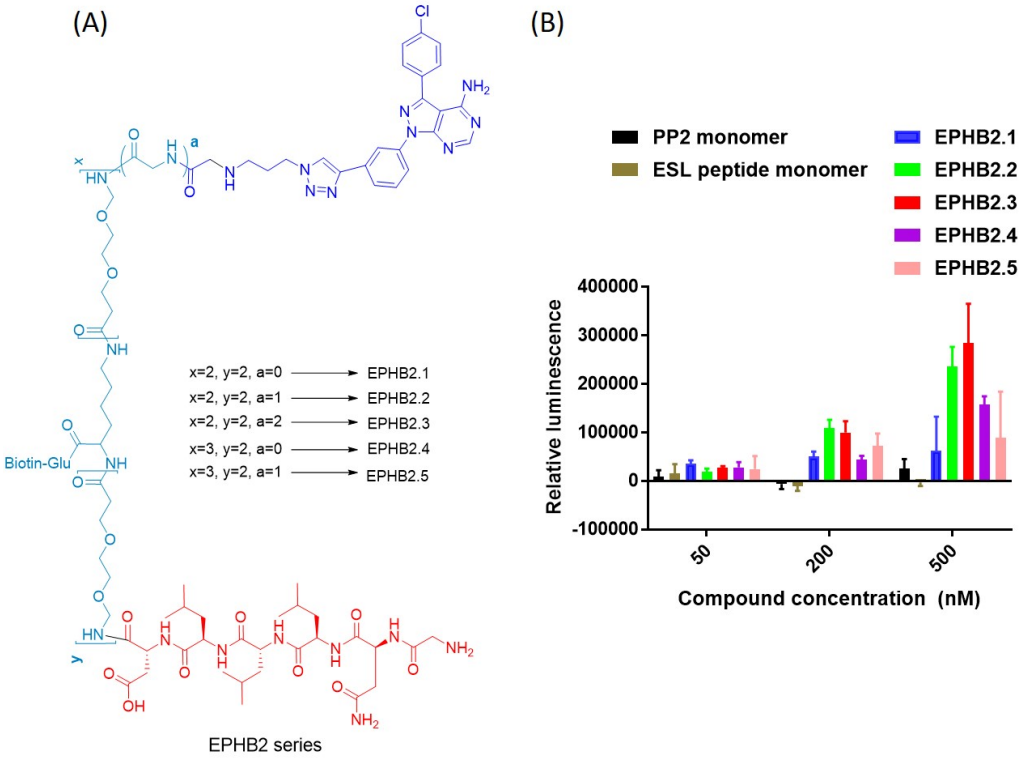

Figure 18. The second round of fine-tuned hetero-bivalent ligand design. (A). Outline of the fine-tuned hetero-bivalent ligand design. (B). ELISA-like binding assay results of five focused hetero-bivalent ligands binding to the EphA3 kinase domain at 50, 200, and 500 nM. EPHB2.3 showed the best binding.

All hetero-bivalent ligands in this series (EPHB2.1-2.5) were screened using the same ELISA-like binding assay at three different concentrations 50, 200, and 500 nM along with monomers: PP2 and ESL peptide. Among all of the compounds, only EPHB2.3, having a linker length around 57 Å, showed greater binding affinity towards the EphA3 kinase domain (Fig. 18.B). Also, the other two hetero-bivalent

ligands, EPHB2.2 (shorter linker length-54 Å) and EPHB2.4 (the longer linker length-61 Å) showed less binding affinity compared with EPHB2.3, indicating that EPHB2.3 was the optimum linker containing derivative. These studies finally indicated that 57 Å linker length correctly place the PP2 and ESL peptide simultaneously into their binding pockets, thus contributing to synergistic binding behavior observed in the ELISA-like binding assay.

b) Full concentration gradient ELISA-like binding studies:

Next, the same ELISA-like binding assay was employed to find the dissociation constant (K_d) of the stronger binding hetero-bivalent ligand EPHB2.3 and weaker binding hetero-bivalent ligand EPHB2.5, and monomers (PP2 and ESL peptide). As shown in Fig. 19, the two hetero-bivalent ligands, EPHB2.3 and EPHB2.5, exhibited full sigmoidal binding curve, with estimated K_d ~ 250-300 nM. However, the monomers exhibited poor solubility, which limited the highest concentrations to be used in the ELISA-like binding assay. The monomers did not yield full binding curves up to the measured concentrations (>50 μM), indicating their weak binding behavior. Though our assay could not measure the K_d of the PP2 analogue, we considered a previous report of PP2 analogue interaction with ATP binding pocket

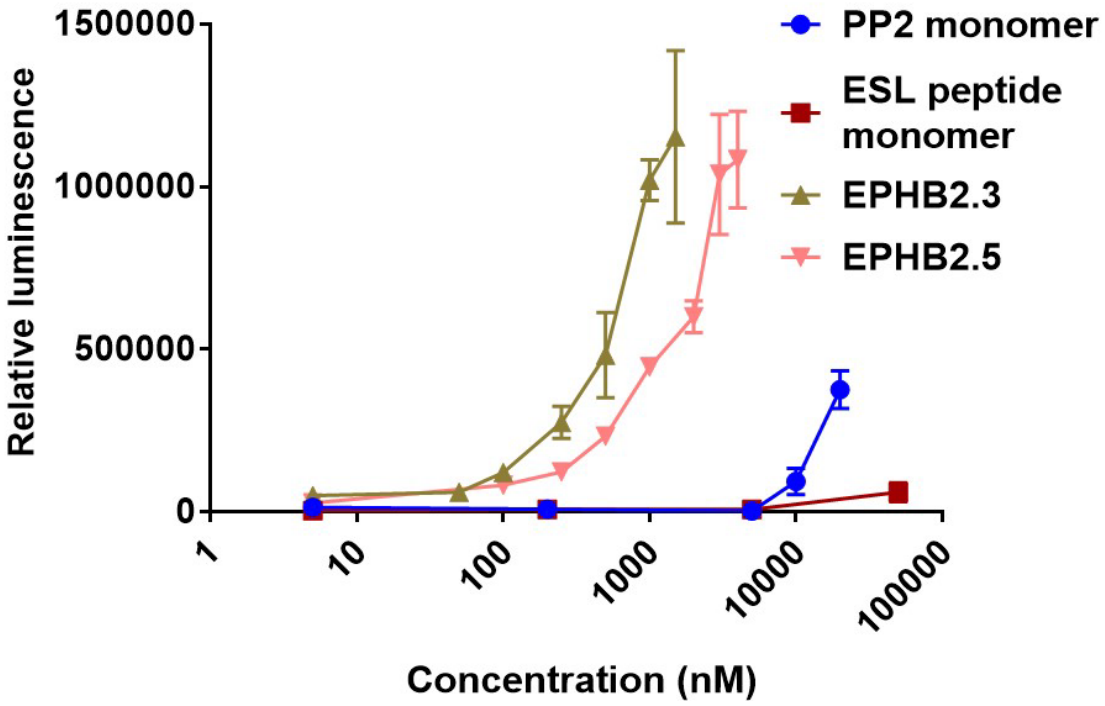

Figure 19. Results of concentration gradient ELISA-like binding assay using EphA3 kinase domain. Full binding curves of EPHB2.3, EPHB2.5, PP2, and ESL peptide.

of EphA3 kinase and estimated the K_d value to be around 200-300 μM.[31] Also, our assay could not quantitate the binding of ESL peptide (due to solubility problem). However, the presence of this unique peptide binding site in multiple crystal structures indicates that ESL peptide indeed a ligand for EphA3 kinase.[93, 99-100] We interpret that it might have very weaker binding characteristics (even at millimolar range K_d). Considering all this information, we estimate that our optimized hetero-bivalent ligands display >1000-fold binding affinity compared to either the PP2 analogue and the ESL peptide towards EphA3 kinase.

c) Competitive ELISA-like binding assay to confirm hetero-bivalents ligands indeed binding to EphA3:

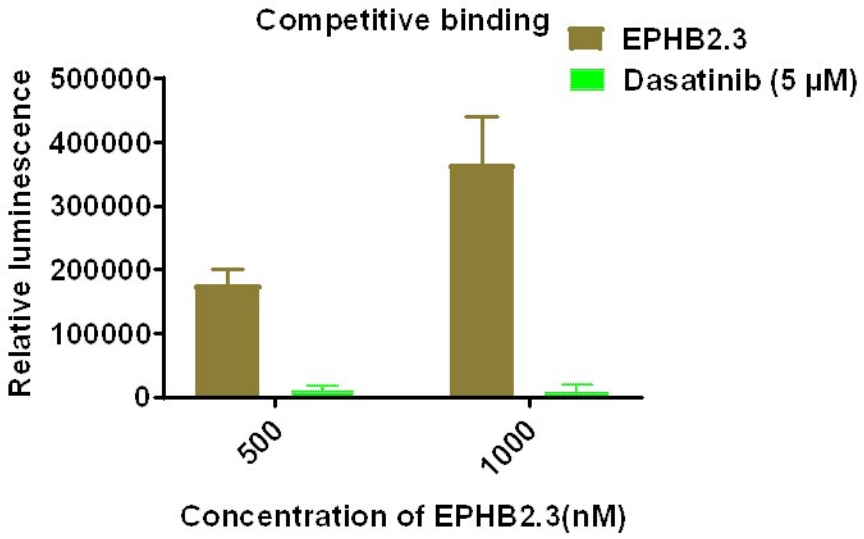

Figure 20. Binding competition of biotinylated EPHB2.3 with dasatinib against EphA3 kinase using ELISA-like assay. Dasatinib readily competed with EPHB2.3 to bind to EphA3 kinase domain at 500 and 1000 nM.

We performed the same ELISA-like binding assay in the presence of dasatinib, a potent EphA3 kinase inhibitor.[101] Briefly, the EphA3 kinase coated plates were first saturated with dasatinib (5 µM) and then competed with biotinylated EPHB2.3 at 0.5 and 1 µM. Unbound compound was washed away, and the bound EPHB2.3 was probed using the same streptavidin-HRP system that described above. The luminescent signal would be detected only when EPHB2.3 is bound. Dasatinib clearly inhibited the binding of EPHB2.3, indicating EPHB2.3 also binds to the ATP binding site (using the PP2 moiety) (Fig. 20). This study rules out the possibility of non-specific binding (common in typical plate based assay systems like ELISA-like

binding assays) exists due to non-specific interactions of compounds or proteins with the plate.

3.5.1.2. Hetero-bivalent ligands targeting ATP and substrate peptide:

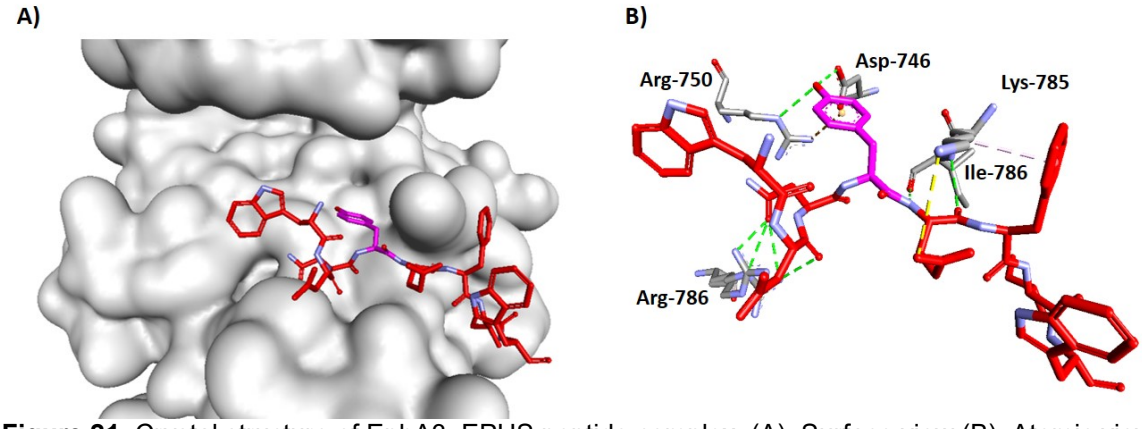

Figure 21. Crystal structure of EphA3: EPHS peptide complex. (A). Surface view (B). Atomic view of non-covalent interactions between EPHS peptide and EphA3 kinase (light grey-blue color: EphA3 kinase and red-blue color: EPHS peptide). Hydrophobic, ionic, Cation-π and hydrogen bond interactions were highlighted in light pink, yellow, red and green color, respectively.

In this hetero-bivalent ligand design approach, we chose the EphA3 substrate peptide as the secondary sequence to be attached to the ATP binding ligand. This is also known as EPHS peptide, an octameric sequence (WDNYEFIW) that is previously reported to interact with the EphA3 kinase domain.[93] Most importantly, the crystal structure of this EPHS peptide with the EphA3 kinase domain demonstrated that this peptide binding pocket is located in between PP2 and ESL peptide binding pockets. It provides an unique opportunity to use this EPHS peptide as a replacement for the highly flexible and non-optimized linker portion of our EPHB2.3 hetero-bivalent ligand developed in the studies described above. We first began by attaching this EPHS peptide to PP2 analogue. To find the most

appropriate linker to connect the EPHS peptide with PP2 analogue, we first examined the crystal structure of EphA3 kinase in complex with EPHS peptide. In this structure, the EPHS peptide makes several non-covalent interactions with EphA3 kinase (Fig. 21.B). Typical interactions involve (i). H-bond interaction between (a). carboxylate of Asp-746 in EphA3 and 4-OH group of Tyr-4 (b). ε-amine of Arg-750 in EphA3 and 4-OH group of Tyr-4 (c) guanidine group of Arg-786 from EphA3 and carbonyl groups of Asp-2 & Asn-3 (ii). backbone H-bond interactions between the amine and carbonyl groups of Ile-786 in EphA3 kinase with carbonyl and amine groups of Glu-5, respectively (iii). salt bridge between amine of Lys-785 in EphA3 kinase and the carboxylate of Glu-5 (iv) cation). Cation-π interaction between guanidine group of Arg-750 in EphA3 and phenyl group of Tyr-4 (v). hydrophobic interaction between carbon side chain of Lys-785 in EphA3 and Phe-6. The first task was to decide which amino acid can be used to attach the linker. As per the crystal structure, both N-terminus amine of Trp-1 and 4-OH group of Tyr-4 face towards the ATP binding pocket. Here, we chose 4-OH group of Tyr-4 to attach the linker because: (i). Tyr-4 has naturally existing linker path that kinases use for phosphate transfer, and (ii). attaching a linker at this position was previously reported to be most favorable as it mimics transition state of kinase

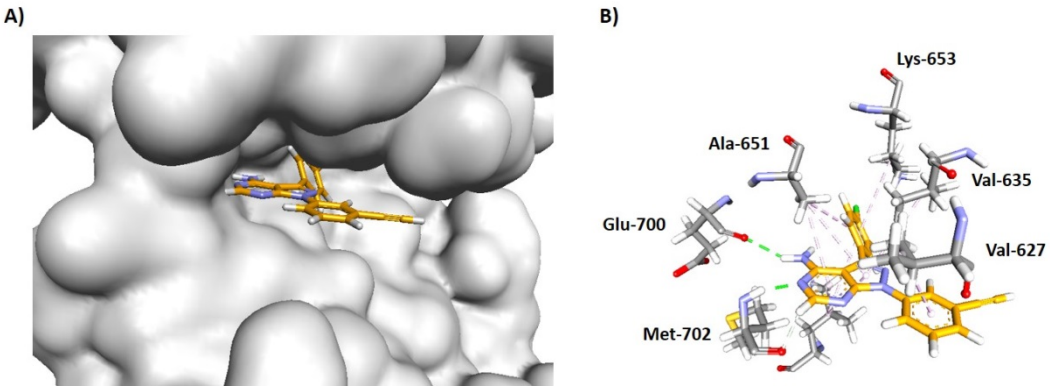

Figure 22. Docking result of PP2 analogue in the ATP binding pocket of EphA3 kinase. (A). Surface view (B). Atomic view. Non-covalent interactions between PP2 analogue and highlighted amino acid residues (light grey-blue color: EphA3 kinase and orange blue color: PP2 analogue). H-bond interactions and hydrophobic interactions are highlighted in green and light pink color, respectively.

mediated phosphate transfer where the substrate peptide makes maximum contacts with its binding pocket.[13, 30]

We next docked PP2-analogue with the ATP binding pocket of the EphA3 kinase domain. Typical contacts include: (i). hydrogen bond interaction between, (a). carbonyl group of Glu-700 in EphA3 and the 6-amino group of adenine, (b). carbonyl group of Met-702 in EphA3 and N1 of adenine, and ii). hydrophobic interaction between, (a). Val-627, Val-635, Ala-651, Lys-653 in EphA3 and the adenine ring (b). Val-627 in EPHA3 and N9-phenyl of the adenine ring (Fig. 22.B). These contacts are similar to a typical type-I inhibitor which projects aryl alkyne group towards Tyr-4 in substrate peptide. The distance between 4-OH group of Tyr-4 and aryl alkyne group of PP2 analogue found to be approximately 12 Å, which is analogous to previously reported distance between ATP and substrate peptide binding pockets of transition state complexes of other kinases (Fig. 23).[30-

[31] Most importantly, the 4-OH group of Tyr-4 make a H-bond interaction with carboxylate group of Asp-746 that was previously reported to be critical as removal of hydroxyl group or substituting acidic proton with other substituents, yielded a very weak bisubstrate inhibitors.[82, 102] So, we envisioned to use an amine at this position, which is also an H-bond acceptor, previously reported to be well tolerated at this position. To cover the 12 Å distance between PP2 and EPHS peptide binding pockets, we chose azidoalkanoic acids as linkers to cover 10-12 Å lengths.The amine group of 4-amihophenylalanine is a weak nucleophile. It require harsh conditions to couple with azidoalkanoic acids that is not compatible with solid-phase synthesis. So, we synthesized the corresponding azidoalkanoic acid

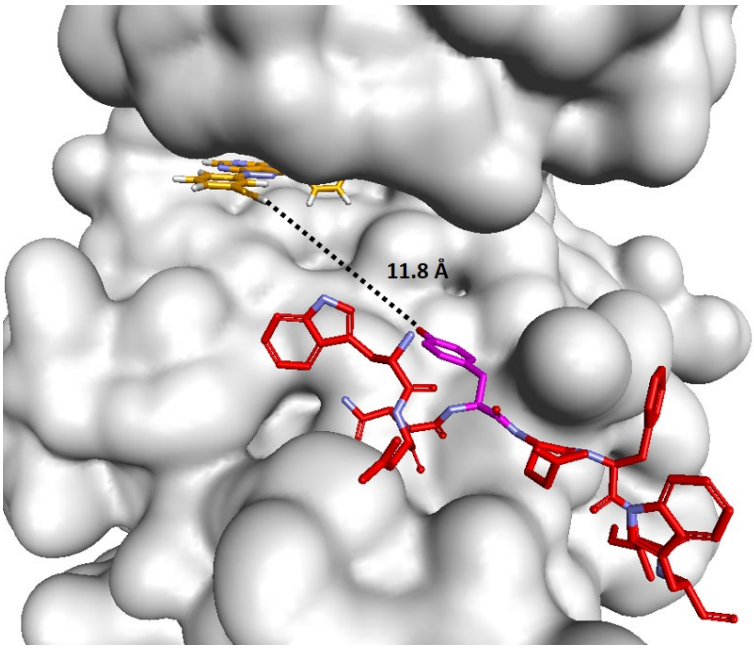

Figure 23. Estimated distance between PP2 analogue and EPHS peptide. The pose obtained from the docking result of PP2 analogue (Figure. 20) was superimposed with crystal structure of EphA3: EPHS peptide complex. EPHS peptide highlighted in red color whereas Tyr4 and PP2 analogue were highlighted pink-blue and orange-blue color, respectively

analogues of 4-aminophenylalanine or Fmoc-Phe(4-(n-azidoalkanoic)-OH using a solution phase synthesis (scheme 6 discussed in Chapter 3.4.2.7) and envisioned using these analogues in the solid-phase synthesis.

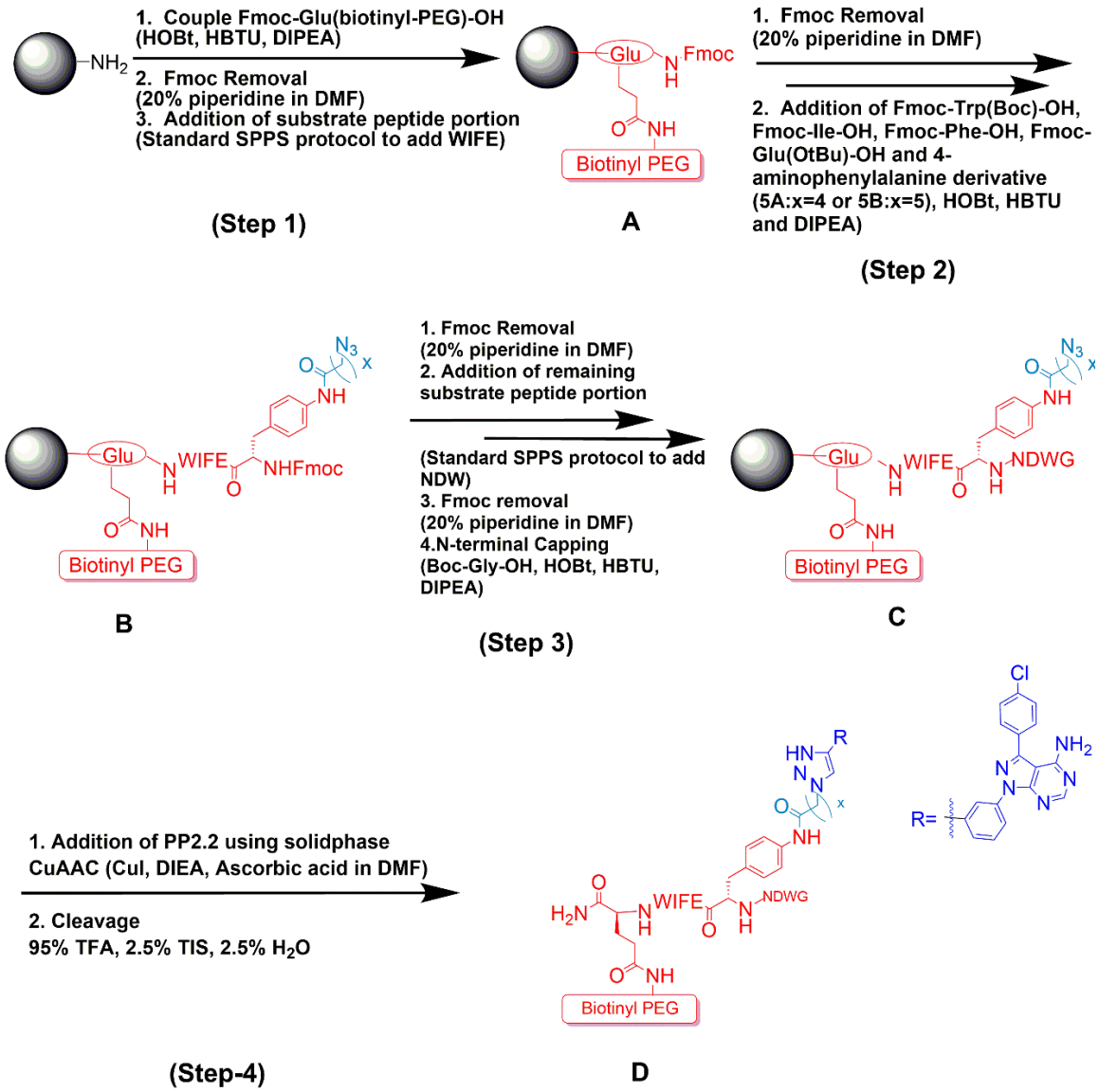

Scheme **9.** Synthesis scheme of EPHB3 series of hetero-bivalent ligands.

The hetero-bivalent ligands were synthesized using standard solid phase peptide conditions that were discussed before. Briefly, we chose NovaSyn TGR resin and couple first amino acid Fmoc-Glu(biotinyl-PEG)-OH to get compound A, which helps to detects the binding event in ELISA-like binding assays (Scheme 9, step 1). Next, we deprotect the Fmoc group with 20% piperidine in DMF and add the next amino acids, Fmoc-Trp(Boc)-OH, Fmoc-Ile-OH, Fmoc-Phe-OH, Fmoc-Glu(OtBu)-OH, and Fmoc-Phe(4-(n-azidoalkanoic)-OH to yield compound B. (Scheme 9, step 2). Next, we deprotect the Fmoc group with 20% piperidine and couple the remaining amino acids Fmoc-Asn(Trt)-OH, Fmoc-Asp(OtBu)-OH, Fmoc-Trp-OH and cap the N-terminus with Boc-Gly-OH to yield C (Scheme 9, step 3). Lastly, we introduce PP2 alkyne into the EPHS peptide side chain using CuAAC reaction. Finally, the hetero-bivalent ligands were cleaved from the resin by treating with cleaving cocktail [95% TFA, 2.5% water, 2.5% triisoproylsilane (TIS)]. (Scheme 9, step 4). Two hetero-bivalent ligands were synthesized with or without C-terminal biotinylation for *in vitro* binding and activity assays, respectively. EPHS peptide was slightly modified by substituting Tyr-4 with 4-aminophenylalanine (named as EPHB) peptide so that it can correctly resemble the peptide portion of hetero-bivalent ligand. Both biotinylated and non-biotinylated versions of EPHB peptide were synthesized using standard solid phase peptide protocol discussed in chapter 3.4.2.8.

3.5.1.2.1. ELISA-like binding studies:

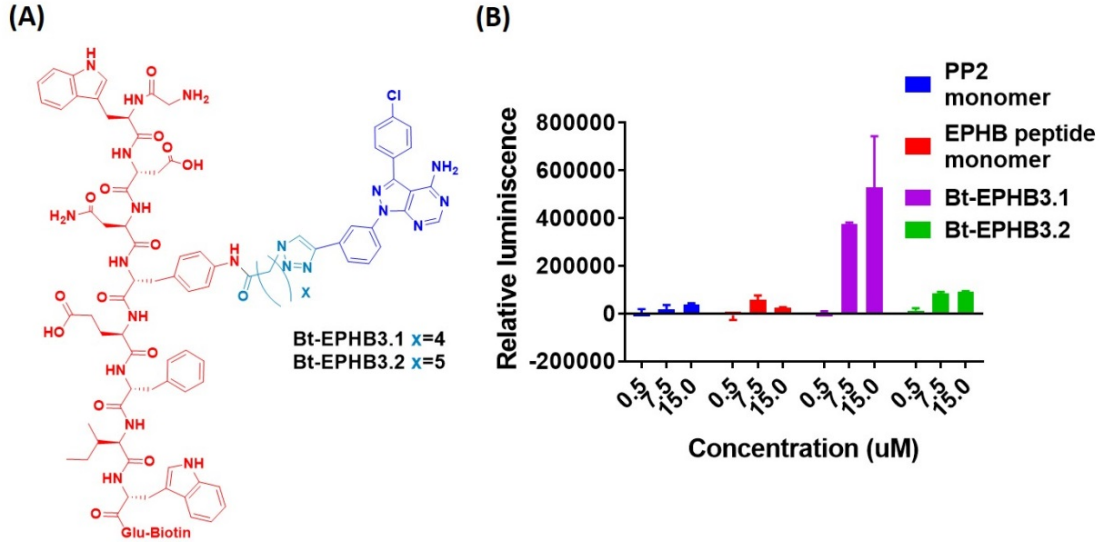

Figure 24. Binding of the biotinylated EPHB series of hetero-bivalent ligands. (A). The common chemical structure of the Bt-EPHB series of hetero-bivalent ligands. (B). ELISA-like assay results of biotinylated hetero-bivalent ligands binding to the EphA3 kinase domain at three different concentrations (0.5, 7.5, and 15 μM). Only Bt-EPHB3.1 showed high affinity.

We employed the previously established ELISA-like binding assay to select the hetero-bivalent ligand with optimal linker length. Briefly, we first coated His-tagged EphA3 kinase domain on nickel-coated plates. The biotinylated EPHB derivatives were added to each well at three different concentrations (0.5, 7.5, and 15 μM) along with monomers- PP2 and EPHB peptide. Then streptavidin-HRP enzyme was added to detect the binding event, which converts the substrate to the luminescent emission that is measured at all wavelengths. As shown in Fig. 24(B), Bt-EPHB3.1, the shortest linker containing hetero-bivalent ligand showed the greatest affinity towards the EphA3 kinase domain when compared with longer derivatives Bt-EPHB3.1, and monomers – PP2, and EPHB peptide. This indicates

that Bt-EPHB3.1 has the optimum linker, which allows both PP2 and EPHB peptides to simultaneously occupy their respective binding pockets. In contrast, Bt-EPHB3.2, the longer linker length containing hetero-bivalent ligand, showed weaker binding compared to the Bt-EPHB3.1, indicating this linker length is not optimal.

3.5.1.2.2. Kinase activity validation:

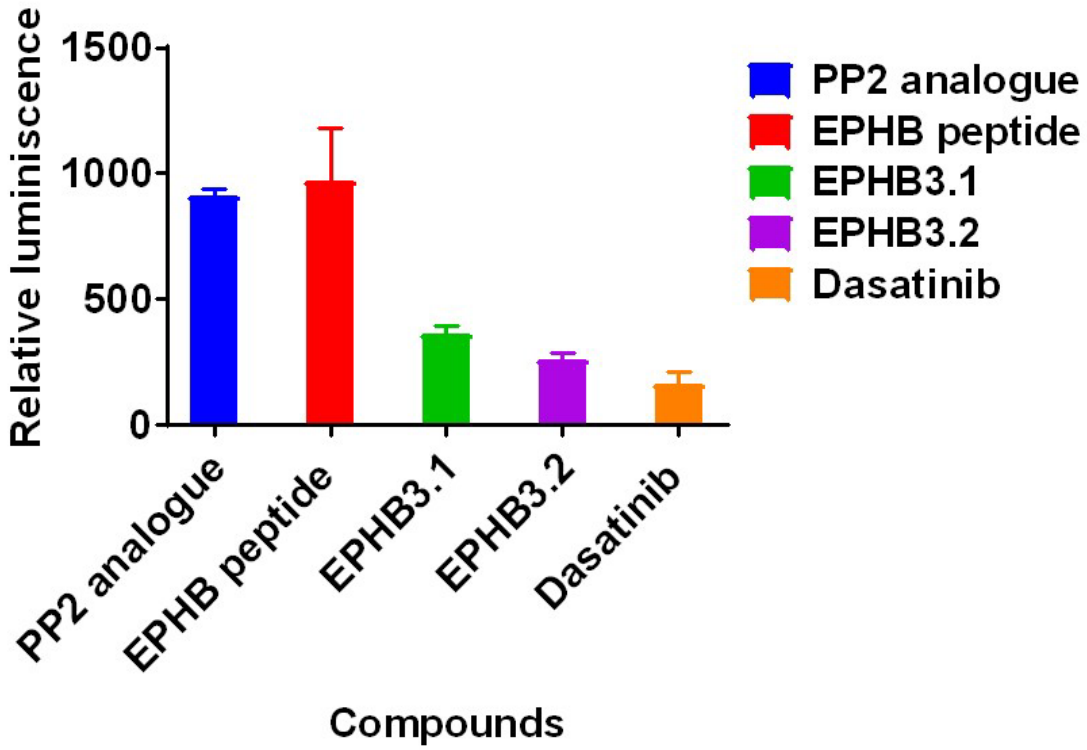

Figure 25. Results of *in vitro* kinase inhibition assay against EphA3 kinase. The ADP-Glo EphA3 kinase inhibition assay demonstrated that both hetero-bivalent ligands (EPHB3.1 and 3.2) inhibited EphA3 kinase.

The ADP-Glo kinase assay was utilized to measure the kinase inhibitory activity of these hetero-bivalent ligands. Briefly, the non-biotinylated monomers (PP2

analogue and EPHB peptide) and hetero-bivalent ligands (each at 40 μM concentration) were added to the kinase reaction consisting of EphA3 kinase (1.2 ng/μL), ATP (10 μM) and substrate peptide (200 μM). After an hour of incubation, ADP Glo kinase reagent (5 μL) was added, which stops the kinase reaction and depletes the ATP that leftover. Next, the remaining ADP that corresponds to the completed kinase reaction was probed using a kinase detection reagent (10 μL) that turns ADP to luminescence light, which can be detected at all wavelengths. As shown in Fig. 25, both monomers- PP2 analogue and EPHB peptide, did not inhibit EphA3 kinase activity (at 40 μM) but hetero-bivalent ligands EPHB3.1 and 3.2 did inhibit as comparable to dasatinib (at 100 nM), a potent EphA3 kinase inhibitor. Surprisingly, the longer linker containing hetero-bivalent ligand EPHB3.2 strongly inhibited EphA3 kinase activity when compared with EPHB3.1, a shorter linker derivative. This result contradicts the ELISA-like binding assay finding, where the biotinylated version, Bt-EPHB3.2, showed weak binding when compared with Bt-EPHB3.1. We believe this discrepancy is due to the limited solubility of Bt-EPHB3.2, as this hetero-bivalent ligand exhibited low solubility, starting to precipitate at concentrations above 15 μM during solubility testing while the shorter derivative, Bt-EPHB3.1 was soluble even up to 30 μM. Therefore, we attribute the strong binding behavior of Bt-EPHB3.1 as an artifact occurred due to the limited solubility of Bt-EPHB3.2.

3.5.1.2.3. Quantitative kinase activity studies:

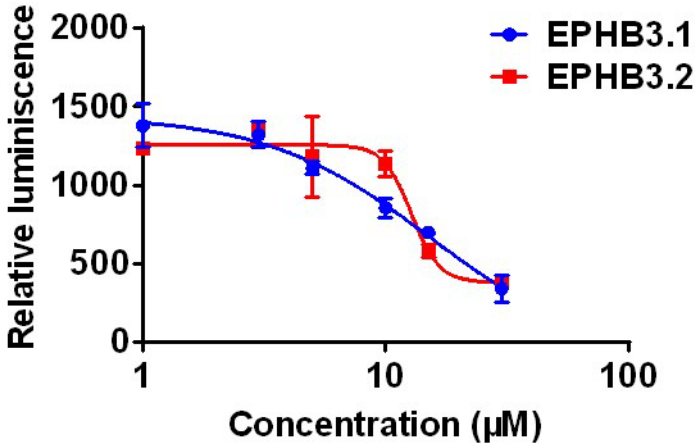

Figure 26. Concentration-gradient kinase inhibition assay. Full binding curves of EPHB3.1, EPHB3.2, evaluated using ADP- Glo EphA3 kinase inhibition assay.

The same ADP-Glo kinase assay was employed to find IC_{50} values of the hetero-bivalent ligands. As shown in Fig. 26, the two hetero-bivalent ligands exhibited full binding curves, both EPHB3.1 (IC_{50}~15 µM) and EPHB3.2 (IC_{50}~12 µM) showed similar inhibition profiles. This result was similar to a previous report of hetero-bivalent ligand targeting c-src kinase, where PP2 analogue and c-src specific substrate peptide were connected with azidoalkanoic acid linkers of varying length.[31] Among them, a 6-atom linker length between PP2 analogue and substrate peptide was more effective in inhibiting c-src kinase (IC_{50}>20 nM) when compared to either shorter or longer linker derivatives. Moreover, this report further supports ADP Glo assay findings that EPHB3.2 is the optimum linker length containing hetero-bivalent ligand and also suggests that the corresponding

contradictory binding results of ELISA-like binding assay were due to solubility artifacts.

3.6. Conclusion:

Herein was provided a novel way to design hetero-bivalent ligand targeting protein kinases, by using a short peptide sequence from the same kinase that forms unique interactions within that protein. Since the short peptide sequence was derived from the linker region that connects the kinase domain to another domain, similar sequences from crystal structures of other kinase or protein complexes can be carefully analyzed to find similar unique interactions. Moreover, the ESL peptide sequence we used in this design showed very weak binding affinity but when it was coupled to another hotspot binding unit (ATP binding site moiety in this case), using a linker that covers the distance between these two binding pockets, significant improvement in binding affinity was achieved. Most importantly, our approach does not require structural or combinatorial based design in regard to developing inhibitors because we utilize naturally existing peptide ligands. Our studies encourage the scientific community to look into existing crystal structures with a new mode of curiosity to find such readily available sequences. Moreover, there is a high possibility that these random binding events occur uniquely within a kinase. So, targeting these unique interactions can be particularly helpful in designing hetero-bivalent ligands with enhanced specificity towards the target

kinase. Here, we used very weak binding PP2 and ESL peptide monomers and employed flexible linkers, which are considered to be non-optimal starting points for hetero-bivalent ligand design. However, when these binding monomers are assembled in an optimal way into a single unit, a significant improvement in binding affinity was achieved. This suggests that, if we had started with moderate or strongly binding monomers, we would have achieved even more potent hetero-bivalent ligands.

Also, we proposed a novel approach to convert the linker portion of EPHB2.3 into an additional binding unit, using a substrate peptide is known to bind in between the ATP and ESL peptide binding sites. We planned to achieve this in two steps. First, optimizing the linker distance between ATP and EPHB peptide and next, using that hetero-bivalent ligand as a starting point to further optimize the linker connecting EPHB and ESL peptide binding pockets. We used a similar design for optimizing the linker connecting the PP2 analogue and the EPHB peptide that was previously reported for another kinase. This design was successful in producing the first hetero-bivalent ligands that can inhibit the catalytic activity of the EphA3 kinase, which indicates that these principles can be applicable to other kinases, for example, at least towards the Eph subfamily of kinases.

3.7. Future directions:

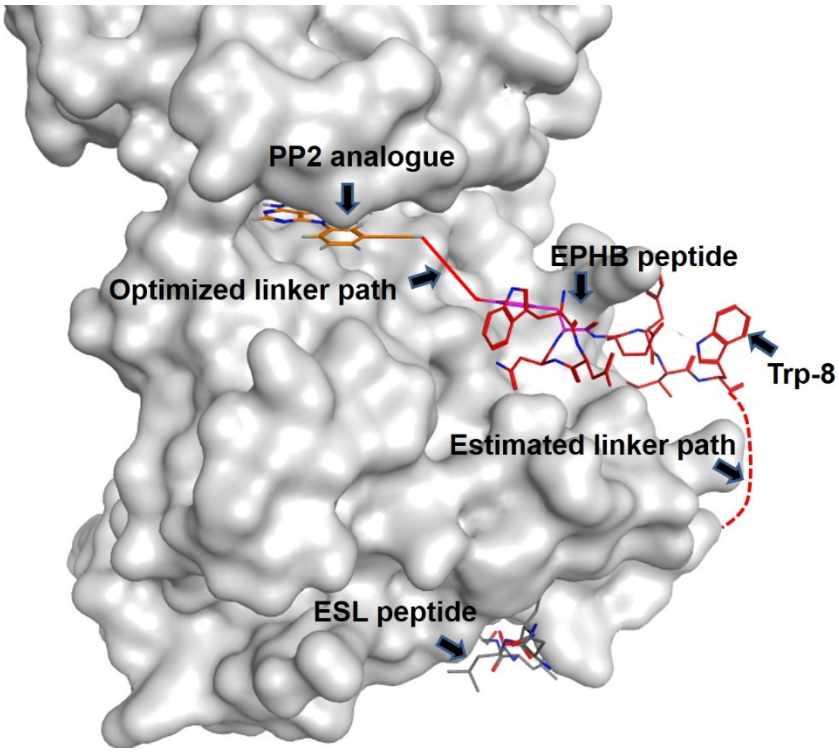

Figure 27. Future hetero-multivalent ligand design targeting EphA3 kinase domain. We have already optimized the linker region between PP2 analogue and EPHB peptide, developing improved hetero-bivalent ligand EPHB3.1 and EPHB3.2. The next step is to link the ESL peptide that binds to the bottom of this kinase to these EPHB3.1 and EPHB3.2 hetero-bivalent ligands.

The immediate future goal of this project is to optimize the linker between the EPHB and substrate peptide binding pockets. The estimated distance between the EPHB and ESL peptide binding pockets was is approximately 27 Å. Since EPHB3.2 was found to have an optimal linker length between the PP2 and EPHB peptide pockets, we can use this hetero-bivalent ligand as a starting point. Next, we plan to choose the combination of AEAAc and glycine as a linker to connect Trp-8 of EPHB3.2 and Asp-904 of the ESL peptide because this combination is

proven to be optimal for covering this linker path (as in case of EPHB2.4) (Fig. 27). We expect that the resultant hetero-multivalent ligand will show much improved affinity and selectivity towards EphA3 kinase.

Also, we plan to explore whether the linker connecting PP2 and the ESL peptide in the previously developed EPHB2.3 can be modified to interact with new hot spots along it takes as it wraps around the EphA3 kinase domain. We plan to achieve this by (i). identifying multiple binding pockets on the path of this linker region connecting ATP and ESL peptide, (ii). measuring the distance of each pocket to the linker, and (iii). docking with a library of amines to be used to incorporated into the linker region. These amines will be selected based on size, shape, charge, the the hydrophilic or hydrophobic nature of binding pocket. The best fitting amines will be selected and incorporated within the linker using straightforward peptoid chemistry. We have already identified multiple potential binding pockets on the EphA3 surface. We anticipate this approach will successfully identify additional binding hot spots along the linker path and open a new design avenue in hetero-multivalent ligand design, taking this concept into the next level.

4. REFERENCES

1. Hebert, T. E.; Bouvier, M., Structural and functional aspects of G protein-coupled receptor oligomerization. *Biochem Cell Biol* **1998,** *76* (1), 1-11.
2. Langlet, C.; Bernard, A. M.; Drevot, P.; He, H. T., Membrane rafts and signaling by the multichain immune recognition receptors. *Curr Opin Immunol* **2000,** *12* (3), 250-5.
3. Kitov, P. I.; Sadowska, J. M.; Mulvey, G.; Armstrong, G. D.; Ling, H.; Pannu, N. S.; Read, R. J.; Bundle, D. R., Shiga-like toxins are neutralized by tailored multivalent carbohydrate ligands. *Nature* **2000,** *403* (6770), 669-72.
4. Matrosovich, M. N.; Mochalova, L. V.; Marinina, V. P.; Byramova, N. E.; Bovin, N. V., Synthetic polymeric sialoside inhibitors of influenza virus receptor-binding activity. *FEBS Lett* **1990,** *272* (1-2), 209-12.
5. Xu, L.; Josan, J. S.; Vagner, J.; Caplan, M. R.; Hruby, V. J.; Mash, E. A.; Lynch, R. M.; Morse, D. L.; Gillies, R. J., Heterobivalent ligands target cell-surface receptor combinations in vivo. *Proceedings of the National Academy of Sciences of the United States of America* **2012,** *109* (52), 21295-300.
6. Kiessling, L. L.; Pohl, N. L., Strength in numbers: non-natural polyvalent carbohydrate derivatives. *Chemistry & biology* **1996,** *3* (2), 71-7.
7. Mammen, M.; Choi, S. K.; Whitesides, G. M., Polyvalent Interactions in Biological Systems: Implications for Design and Use of Multivalent Ligands and Inhibitors. *Angew Chem Int Ed Engl* **1998,** *37* (20), 2754-2794.
8. Rao, J.; Lahiri, J.; Isaacs, L.; Weis, R. M.; Whitesides, G. M., A trivalent system from vancomycin.D-ala-D-Ala with higher affinity than avidin.biotin. *Science* **1998,** *280* (5364), 708-11.
9. Vauquelin, G.; Charlton, S. J., Exploring avidity: understanding the potential gains in functional affinity and target residence time of bivalent and heterobivalent ligands. *Br J Pharmacol* **2013,** *168* (8), 1771-85.
10. Vauquelin, G., Simplified models for heterobivalent ligand binding: when are they applicable and which are the factors that affect their target residence time. *Naunyn Schmiedebergs Arch Pharmacol* **2013,** *386* (11), 949-62.
11. Vauquelin, G.; Charlton, S. J., Long-lasting target binding and rebinding as mechanisms to prolong in vivo drug action. *Br J Pharmacol* **2010,** *161* (3), 488-508.
12. Vauquelin, G., Rebinding: or why drugs may act longer in vivo than expected from their in vitro target residence time. *Expert Opin Drug Discov* **2010,** *5* (10), 927-41.
13. Lavogina, D.; Enkvist, E.; Uri, A., Bisubstrate inhibitors of protein kinases: from principle to practical applications. *ChemMedChem* **2010,** *5* (1), 23-34.
14. Kaufman, E. N.; Jain, R. K., Effect of bivalent interaction upon apparent antibody affinity: experimental confirmation of theory using fluorescence photobleaching and implications for antibody binding assays. *Cancer research* **1992,** *52* (15), 4157-67.
15. Kramer, R. H.; Karpen, J. W., Spanning binding sites on allosteric proteins with polymer-linked ligand dimers. *Nature* **1998,** *395* (6703), 710-3.
16. Manning, G.; Plowman, G. D.; Hunter, T.; Sudarsanam, S., Evolution of protein kinase signaling from yeast to man. *Trends Biochem Sci* **2002,** *27* (10), 514-20.

17. Manning, G.; Whyte, D. B.; Martinez, R.; Hunter, T.; Sudarsanam, S., The protein kinase complement of the human genome. *Science* **2002,** *298* (5600), 1912-34.
18. Schlessinger, J.; Ullrich, A., Growth factor signaling by receptor tyrosine kinases. *Neuron* **1992,** *9* (3), 383-91.
19. Cohen, P., Protein kinases--the major drug targets of the twenty-first century? *Nat Rev Drug Discov* **2002,** *1* (4), 309-15.
20. Levitzki, A., Protein kinase inhibitors as a therapeutic modality. *Acc Chem Res* **2003,** *36* (6), 462-9.
21. Fedorov, O.; Marsden, B.; Pogacic, V.; Rellos, P.; Muller, S.; Bullock, A. N.; Schwaller, J.; Sundstrom, M.; Knapp, S., A systematic interaction map of validated kinase inhibitors with Ser/Thr kinases. *Proceedings of the National Academy of Sciences of the United States of America* **2007,** *104* (51), 20523-8.
22. Krishnamurty, R.; Maly, D. J., Chemical genomic and proteomic methods for determining kinase inhibitor selectivity. *Comb Chem High Throughput Screen* **2007,** *10* (8), 652-66.
23. Gower, C. M.; Chang, M. E.; Maly, D. J., Bivalent inhibitors of protein kinases. *Crit Rev Biochem Mol Biol* **2014,** *49* (2), 102-15.
24. Ricouart, A.; Gesquiere, J. C.; Tartar, A.; Sergheraert, C., Design of potent protein kinase inhibitors using the bisubstrate approach. *Journal of medicinal chemistry* **1991,** *34* (1), 73-8.
25. Kruse, C. H.; Holden, K. G.; Pritchard, M. L.; Feild, J. A.; Rieman, D. J.; Greig, R. G.; Poste, G., Synthesis and evaluation of multisubstrate inhibitors of an oncogene-encoded tyrosine-specific protein kinase. 1. *Journal of medicinal chemistry* **1988,** *31* (9), 1762-7.
26. Traxler, P. M.; Wacker, O.; Bach, H. L.; Geissler, J. F.; Kump, W.; Meyer, T.; Regenass, U.; Roesel, J. L.; Lydon, N., Sulfonylbenzoyl-nitrostyrenes: potential bisubstrate type inhibitors of the EGF-receptor tyrosine protein kinase. *Journal of medicinal chemistry* **1991,** *34* (8), 2328-37.
27. Loog, M.; Uri, A.; Jarv, J.; Ek, P., Bi-substrate analogue ligands for affinity chromatography of protein kinases. *FEBS Lett* **2000,** *480* (2-3), 244-8.
28. Schneider, T. L.; Mathew, R. S.; Rice, K. P.; Tamaki, K.; Wood, J. L.; Schepartz, A., Increasing the kinase specificity of k252a by protein surface recognition. *Org Lett* **2005,** *7* (9), 1695-8.
29. Shen, K.; Cole, P. A., Conversion of a tyrosine kinase protein substrate to a high affinity ligand by ATP linkage. *Journal of the American Chemical Society* **2003,** *125* (52), 16172-3.
30. Parang, K.; Till, J. H.; Ablooglu, A. J.; Kohanski, R. A.; Hubbard, S. R.; Cole, P. A., Mechanism-based design of a protein kinase inhibitor. *Nat Struct Biol* **2001,** *8* (1), 37-41.
31. Brandvold, K. R.; Santos, S. M.; Breen, M. E.; Lachacz, E. J.; Steffey, M. E.; Soellner, M. B., Exquisitely specific bisubstrate inhibitors of c-Src kinase. *ACS chemical biology* **2015,** *10* (6), 1387-1391.
32. Hines, A. C.; Parang, K.; Kohanski, R. A.; Hubbard, S. R.; Cole, P. A., Bisubstrate analog probes for the insulin receptor protein tyrosine kinase: molecular yardsticks for analyzing catalytic mechanism and inhibitor design. *Bioorg Chem* **2005,** *33* (4), 285-97.
33. Stebbins, J. L.; De, S. K.; Pavlickova, P.; Chen, V.; Machleidt, T.; Chen, L. H.; Kuntzen, C.; Kitada, S.; Karin, M.; Pellecchia, M., Design and characterization of a potent and selective dual

ATP- and substrate-competitive subnanomolar bidentate c-Jun N-terminal kinase (JNK) inhibitor. *Journal of medicinal chemistry* **2011,** *54* (18), 6206-6214.
34. Bain, J.; McLauchlan, H.; Elliott, M.; Cohen, P., The specificities of protein kinase inhibitors: an update. *Biochem J* **2003,** *371* (Pt 1), 199-204.
35. Kim, J. A.; Lee, J.; Margolis, R. L.; Fotedar, R., SP600125 suppresses Cdk1 and induces endoreplication directly from G2 phase, independent of JNK inhibition. *Oncogene* **2010,** *29* (11), 1702-16.
36. Johnson, T. K.; Soellner, M. B., Bivalent Inhibitors of c-Src Tyrosine Kinase That Bind a Regulatory Domain. *Bioconjug Chem* **2016,** *27* (7), 1745-9.
37. Kedika, S. R.; Udugamasooriya, D. G., Converting a weaker ATP-binding site inhibitor into a potent hetero-bivalent ligand by tethering to a unique peptide sequence derived from the same kinase. *Organic & biomolecular chemistry* **2018,** *16* (35), 6443-6449.
38. Hill, Z. B.; Perera, B. G.; Andrews, S. S.; Maly, D. J., Targeting diverse signaling interaction sites allows the rapid generation of bivalent kinase inhibitors. *ACS chemical biology* **2012,** *7* (3), 487-495.
39. Lechtenberg, B. C.; Mace, P. D.; Sessions, E. H.; Williamson, R.; Stalder, R.; Wallez, Y.; Roth, G. P.; Riedl, S. J.; Pasquale, E. B., Structure-Guided Strategy for the Development of Potent Bivalent ERK Inhibitors. *ACS Med Chem Lett* **2017,** *8* (7), 726-731.
40. Adorno-Cruz, V.; Kibria, G.; Liu, X.; Doherty, M.; Junk, D. J.; Guan, D.; Hubert, C.; Venere, M.; Mulkearns-Hubert, E.; Sinyuk, M.; Alvarado, A.; Caplan, A. I.; Rich, J.; Gerson, S. L.; Lathia, J.; Liu, H., Cancer stem cells: targeting the roots of cancer, seeds of metastasis, and sources of therapy resistance. *Cancer research* **2015,** *75* (6), 924-9.
41. Burrell, R. A.; McGranahan, N.; Bartek, J.; Swanton, C., The causes and consequences of genetic heterogeneity in cancer evolution. *Nature* **2013,** *501* (7467), 338-345.
42. Aubry, M.; de Tayrac, M.; Etcheverry, A.; Clavreul, A.; Saikali, S.; Menei, P.; Mosser, J., From the core to beyond the margin: a genomic picture of glioblastoma intratumor heterogeneity. *Oncotarget* **2015,** *6* (14), 12094-109.
43. Hanahan, D.; Weinberg, R. A., Hallmarks of cancer: the next generation. *Cell* **2011,** *144* (5), 646-74.
44. Grove, O.; Berglund, A. E.; Schabath, M. B.; Aerts, H. J.; Dekker, A.; Wang, H.; Velazquez, E. R.; Lambin, P.; Gu, Y.; Balagurunathan, Y.; Eikman, E.; Gatenby, R. A.; Eschrich, S.; Gillies, R. J., Quantitative computed tomographic descriptors associate tumor shape complexity and intratumor heterogeneity with prognosis in lung adenocarcinoma. *PLoS One* **2015,** *10* (3), e0118261.
45. Jung, Y.; Kim, W. Y., Cancer stem cell targeting: are we there yet? *Arch Pharm Res* **2015,** *38* (3), 414-22.
46. Fulawka, L.; Donizy, P.; Halon, A., Cancer stem cells--the current status of an old concept: literature review and clinical approaches. *Biol Res* **2014,** *47*, 66.
47. Raymond, A. C.; Gao, B.; Girard, L.; Minna, J. D.; Gomika Udugamasooriya, D., Unbiased peptoid combinatorial cell screen identifies plectin protein as a potential biomarker for lung cancer stem cells. *Sci Rep* **2019,** *9* (1), 14954.

48. Pereira, D. M.; Gomes, S. E.; Borralho, P. M.; Rodrigues, C. M. P., MEK5/ERK5 activation regulates colon cancer stem-like cell properties. *Cell death discovery* **2019,** *5*, 68.
49. Tusa, I.; Cheloni, G.; Poteti, M.; Gozzini, A.; DeSouza, N. H.; Shan, Y.; Deng, X.; Gray, N. S.; Li, S.; Rovida, E.; Dello Sbarba, P., Targeting the Extracellular Signal-Regulated Kinase 5 Pathway to Suppress Human Chronic Myeloid Leukemia Stem Cells. *Stem Cell Reports* **2018,** *11* (4), 929-943.
50. Regan, C. P.; Li, W.; Boucher, D. M.; Spatz, S.; Su, M. S.; Kuida, K., Erk5 null mice display multiple extraembryonic vascular and embryonic cardiovascular defects. *Proceedings of the National Academy of Sciences of the United States of America* **2002,** *99* (14), 9248-53.
51. Wang, X.; Merritt, A. J.; Seyfried, J.; Guo, C.; Papadakis, E. S.; Finegan, K. G.; Kayahara, M.; Dixon, J.; Boot-Handford, R. P.; Cartwright, E. J.; Mayer, U.; Tournier, C., Targeted deletion of mek5 causes early embryonic death and defects in the extracellular signal-regulated kinase 5/myocyte enhancer factor 2 cell survival pathway. *Mol Cell Biol* **2005,** *25* (1), 336-45.
52. Nithianandarajah-Jones, G. N.; Wilm, B.; Goldring, C. E.; Muller, J.; Cross, M. J., ERK5: structure, regulation and function. *Cell Signal* **2012,** *24* (11), 2187-96.
53. Stecca, B.; Rovida, E., Impact of ERK5 on the Hallmarks of Cancer. *Int J Mol Sci* **2019,** *20* (6).
54. Mehta, P. B.; Jenkins, B. L.; McCarthy, L.; Thilak, L.; Robson, C. N.; Neal, D. E.; Leung, H. Y., MEK5 overexpression is associated with metastatic prostate cancer, and stimulates proliferation, MMP-9 expression and invasion. *Oncogene* **2003,** *22* (9), 1381-1389.
55. Hoang, V. T.; Yan, T. J.; Cavanaugh, J. E.; Flaherty, P. T.; Beckman, B. S.; Burow, M. E., Oncogenic signaling of MEK5-ERK5. *Cancer Lett* **2017,** *392*, 51-59.
56. Nithianandarajah-Jones, G. N.; Wilm, B.; Goldring, C. E.; Muller, J.; Cross, M. J., ERK5: structure, regulation and function. *Cell Signal* **2012,** *24* (11), 2187-2196.
57. Buschbeck, M.; Ullrich, A., The unique C-terminal tail of the mitogen-activated protein kinase ERK5 regulates its activation and nuclear shuttling. *J Biol Chem* **2005,** *280* (4), 2659-67.
58. Raviv, Z.; Kalie, E.; Seger, R., MEK5 and ERK5 are localized in the nuclei of resting as well as stimulated cells, while MEKK2 translocates from the cytosol to the nucleus upon stimulation. *Journal of cell science* **2004,** *117* (Pt 9), 1773-84.
59. Glatz, G.; Gogl, G.; Alexa, A.; Remenyi, A., Structural mechanism for the specific assembly and activation of the extracellular signal regulated kinase 5 (ERK5) module. *J Biol Chem* **2013,** *288* (12), 8596-8609.
60. Marzi, I.; Cipolleschi, M. G.; D'Amico, M.; Stivarou, T.; Rovida, E.; Vinci, M. C.; Pandolfi, S.; Dello Sbarba, P.; Stecca, B.; Olivotto, M., The involvement of a Nanog, Klf4 and c-Myc transcriptional circuitry in the intertwining between neoplastic progression and reprogramming. *Cell Cycle* **2013,** *12* (2), 353-64.
61. Kondoh, K.; Terasawa, K.; Morimoto, H.; Nishida, E., Regulation of nuclear translocation of extracellular signal-regulated kinase 5 by active nuclear import and export mechanisms. *Mol Cell Biol* **2006,** *26* (5), 1679-90.
62. Yan, C.; Luo, H.; Lee, J. D.; Abe, J.; Berk, B. C., Molecular cloning of mouse ERK5/BMK1 splice variants and characterization of ERK5 functional domains. *J Biol Chem* **2001,** *276* (14), 10870-8.

63. Gomez, N.; Erazo, T.; Lizcano, J. M., ERK5 and Cell Proliferation: Nuclear Localization Is What Matters. *Front Cell Dev Biol* **2016,** *4*, 105.
64. Honda, T.; Obara, Y.; Yamauchi, A.; Couvillon, A. D.; Mason, J. J.; Ishii, K.; Nakahata, N., Phosphorylation of ERK5 on Thr732 is associated with ERK5 nuclear localization and ERK5-dependent transcription. *PLoS One* **2015,** *10* (2), e0117914.
65. Inesta-Vaquera, F. A.; Campbell, D. G.; Tournier, C.; Gomez, N.; Lizcano, J. M.; Cuenda, A., Alternative ERK5 regulation by phosphorylation during the cell cycle. *Cell Signal* **2010,** *22* (12), 1829-37.
66. Tusa, I.; Gagliardi, S.; Tubita, A.; Pandolfi, S.; Urso, C.; Borgognoni, L.; Wang, J.; Deng, X.; Gray, N. S.; Stecca, B.; Rovida, E., ERK5 is activated by oncogenic BRAF and promotes melanoma growth. *Oncogene* **2018,** *37* (19), 2601-2614.
67. Tatake, R. J.; O'Neill, M. M.; Kennedy, C. A.; Wayne, A. L.; Jakes, S.; Wu, D.; Kugler, S. Z., Jr.; Kashem, M. A.; Kaplita, P.; Snow, R. J., Identification of pharmacological inhibitors of the MEK5/ERK5 pathway. *Biochemical and biophysical research communications* **2008,** *377* (1), 120-125.
68. Flaherty, P. T.; Chopra, I.; Jain, P.; Yi, S.; Allen, E.; Cavanaugh, J., Identification of benzimidazole-based inhibitors of the mitogen activated kinase-5 signaling pathway. *Bioorganic & medicinal chemistry letters* **2010,** *20* (9), 2892-6.
69. Nguyen, D.; Lemos, C.; Wortmann, L.; Eis, K.; Holton, S. J.; Boemer, U.; Moosmayer, D.; Eberspaecher, U.; Weiske, J.; Lechner, C.; Prechtl, S.; Suelzle, D.; Siegel, F.; Prinz, F.; Lesche, R.; Nicke, B.; Nowak-Reppel, K.; Himmel, H.; Mumberg, D.; von Nussbaum, F.; Nising, C. F.; Bauser, M.; Haegebarth, A., Discovery and Characterization of the Potent and Highly Selective (Piperidin-4-yl)pyrido[3,2- d]pyrimidine Based in Vitro Probe BAY-885 for the Kinase ERK5. *Journal of medicinal chemistry* **2019,** *62* (2), 928-940.
70. Yang, Q.; Deng, X.; Lu, B.; Cameron, M.; Fearns, C.; Patricelli, M. P.; Yates, J. R., 3rd; Gray, N. S.; Lee, J. D., Pharmacological inhibition of BMK1 suppresses tumor growth through promyelocytic leukemia protein. *Cancer Cell* **2010,** *18* (3), 258-267.
71. Lin, E. C.; Amantea, C. M.; Nomanbhoy, T. K.; Weissig, H.; Ishiyama, J.; Hu, Y.; Sidique, S.; Li, B.; Kozarich, J. W.; Rosenblum, J. S., ERK5 kinase activity is dispensable for cellular immune response and proliferation. *Proceedings of the National Academy of Sciences of the United States of America* **2016,** *113* (42), 11865-11870.
72. Deng, X.; Yang, Q.; Kwiatkowski, N.; Sim, T.; McDermott, U.; Settleman, J. E.; Lee, J. D.; Gray, N. S., Discovery of a benzo[e]pyrimido-[5,4-b][1,4]diazepin-6(11H)-one as a Potent and Selective Inhibitor of Big MAP Kinase 1. *ACS Med Chem Lett* **2011,** *2* (3), 195-200.
73. Lenart, P.; Petronczki, M.; Steegmaier, M.; Di Fiore, B.; Lipp, J. J.; Hoffmann, M.; Rettig, W. J.; Kraut, N.; Peters, J. M., The small-molecule inhibitor BI 2536 reveals novel insights into mitotic roles of polo-like kinase 1. *Curr Biol* **2007,** *17* (4), 304-15.
74. Steegmaier, M.; Hoffmann, M.; Baum, A.; Lenart, P.; Petronczki, M.; Krssak, M.; Gurtler, U.; Garin-Chesa, P.; Lieb, S.; Quant, J.; Grauert, M.; Adolf, G. R.; Kraut, N.; Peters, J. M.; Rettig, W. J., BI 2536, a potent and selective inhibitor of polo-like kinase 1, inhibits tumor growth in vivo. *Curr Biol* **2007,** *17* (4), 316-22.

75. Wang, J.; Erazo, T.; Ferguson, F. M.; Buckley, D. L.; Gomez, N.; Munoz-Guardiola, P.; Dieguez-Martinez, N.; Deng, X.; Hao, M.; Massefski, W.; Fedorov, O.; Offei-Addo, N. K.; Park, P. M.; Dai, L.; DiBona, A.; Becht, K.; Kim, N. D.; McKeown, M. R.; Roberts, J. M.; Zhang, J.; Sim, T.; Alessi, D. R.; Bradner, J. E.; Lizcano, J. M.; Blacklow, S. C.; Qi, J.; Xu, X.; Gray, N. S., Structural and Atropisomeric Factors Governing the Selectivity of Pyrimido-benzodiazipinones as Inhibitors of Kinases and Bromodomains. *ACS chemical biology* **2018,** *13* (9), 2438-2448.
76. Brandvold, K. R.; Steffey, M. E.; Fox, C. C.; Soellner, M. B., Development of a highly selective c-Src kinase inhibitor. *ACS chemical biology* **2012,** *7* (8), 1393-1398.
77. Hooks, J. C.; Matharage, J. P.; Udugamasooriya, D. G., Development of homomultimers and heteromultimers of lung cancer-specific peptoids. *Biopolymers* **2011,** *96* (5), 567-577.
78. Holub, J. M.; Jang, H.; Kirshenbaum, K., Clickity-click: highly functionalized peptoid oligomers generated by sequential conjugation reactions on solid-phase support. *Organic & biomolecular chemistry* **2006,** *4* (8), 1497-1502.
79. *Molecular Operating Environment (MOE)*, *version 2018.01*; Chemical Computing Group, Inc., Montreal, QC, Canada, **2018**.
80. Garai, A.; Zeke, A.; Gogl, G.; Toro, I.; Fordos, F.; Blankenburg, H.; Barkai, T.; Varga, J.; Alexa, A.; Emig, D.; Albrecht, M.; Remenyi, A., Specificity of linear motifs that bind to a common mitogen-activated protein kinase docking groove. *Sci Signal* **2012,** *5* (245), ra74.
81. Pavan, S.; Meyer-Schaller, N.; Diepenbruck, M.; Kalathur, R. K. R.; Saxena, M.; Christofori, G., A kinome-wide high-content siRNA screen identifies MEK5-ERK5 signaling as critical for breast cancer cell EMT and metastasis. *Oncogene* **2018,** *37* (31), 4197-4213.
82. Parang, K.; Cole, P. A., Designing bisubstrate analog inhibitors for protein kinases. *Pharmacology & therapeutics* **2002,** *93* (2-3), 145-57.
83. Hines, A. C.; Cole, P. A., Design, synthesis, and characterization of an ATP-peptide conjugate inhibitor of protein kinase A. *Bioorganic & medicinal chemistry letters* **2004,** *14* (11), 2951-4.
84. Meyer, S. C.; Shomin, C. D.; Gaj, T.; Ghosh, I., Tethering small molecules to a phage display library: discovery of a selective bivalent inhibitor of protein kinase A. *Journal of the American Chemical Society* **2007,** *129* (45), 13812-3.
85. Shomin, C. D.; Meyer, S. C.; Ghosh, I., Staurosporine tethered peptide ligands that target cAMP-dependent protein kinase (PKA): optimization and selectivity profiling. *Bioorganic & medicinal chemistry* **2009,** *17* (17), 6196-202.
86. Lim, H. S.; Archer, C. T.; Kodadek, T., Identification of a peptoid inhibitor of the proteasome 19S regulatory particle. *Journal of the American Chemical Society* **2007,** *129* (25), 7750-1.
87. Zuckermann, R. N.; Kerr, J. M.; Kent, S. B. H.; Moos, W. H., Efficient method for the preparation of peptoids [oligo(N-substituted glycines)] by submonomer solid-phase synthesis. *Journal of the American Chemical Society* **1992,** *114* (26), 10646-10647.
88. Olivos, H. J.; Alluri, P. G.; Reddy, M. M.; Salony, D.; Kodadek, T., Microwave-assisted solid-phase synthesis of peptoids. *Org Lett* **2002,** *4* (23), 4057-9.

89. Brandvold, K. R.; Santos, S. M.; Breen, M. E.; Lachacz, E. J.; Steffey, M. E.; Soellner, M. B., Exquisitely specific bisubstrate inhibitors of c-Src kinase. *ACS chemical biology* **2015,** *10* (6), 1387-91.
90. Eric, Y.; Louis, T.; Linda, G. Production of Nitro-Benzyl-DOTA via direct peptide cyclization. US patent US005847121A, December 8, **1998.**
91. Masaaki, I.; Yuji, Y.; Ashigarakami-gun; Takahiro H; Nomi-shi; W, T. Peptide compound and method for producing same, composition for screening use, and method for selecting peptide compound. US20200040039, October 4, **2019**.

.
92. Davis, T. L.; Walker, J. R.; Loppnau, P.; Butler-Cole, C.; Allali-Hassani, A.; Dhe-Paganon, S., Autoregulation by the juxtamembrane region of the human ephrin receptor tyrosine kinase A3 (EphA3). *Structure* **2008,** *16* (6), 873-84.
93. Davis, T. L.; Walker, J. R.; Allali-Hassani, A.; Parker, S. A.; Turk, B. E.; Dhe-Paganon, S., Structural recognition of an optimized substrate for the ephrin family of receptor tyrosine kinases. *FEBS J* **2009,** *276* (16), 4395-404.
94. Fox, B. P.; Tabone, C. J.; Kandpal, R. P., Potential clinical relevance of Eph receptors and ephrin ligands expressed in prostate carcinoma cell lines. *Biochemical and biophysical research communications* **2006,** *342* (4), 1263-72.
95. Herath, N. I.; Spanevello, M. D.; Doecke, J. D.; Smith, F. M.; Pouponnot, C.; Boyd, A. W., Complex expression patterns of Eph receptor tyrosine kinases and their ephrin ligands in colorectal carcinogenesis. *Eur J Cancer* **2012,** *48* (5), 753-62.
96. Janes, P. W.; Slape, C. I.; Farnsworth, R. H.; Atapattu, L.; Scott, A. M.; Vail, M. E., EphA3 biology and cancer. *Growth Factors* **2014,** *32* (6), 176-89.
97. Zuckermann, R. N.; Kerr, J. M.; Kent, S. B. H.; Moos, W. H., Efficient Method for the Preparation of Peptoids [Oligo(N-Substituted Glycines)] by Submonomer Solid-Phase Synthesis. *J. Am. Chem. Soc.* **1992,** *114* (26), 10646-10647.
98. Olivos, H. J.; Alluri, P. G.; Reddy, M. M.; Salony, D.; Kodadek, T., Microwave-assisted solid-phase synthesis of peptoids. *Org. Lett.* **2002,** *4* (23), 4057-9.
99. Unzue, A.; Dong, J.; Lafleur, K.; Zhao, H.; Frugier, E.; Caflisch, A.; Nevado, C., Pyrrolo[3,2-b]quinoxaline derivatives as types I1/2 and II Eph tyrosine kinase inhibitors: structure-based design, synthesis, and in vivo validation. *Journal of medicinal chemistry* **2014,** *57* (15), 6834-44.
100. Dong, J.; Zhao, H.; Zhou, T.; Spiliotopoulos, D.; Rajendran, C.; Li, X. D.; Huang, D.; Caflisch, A., Structural Analysis of the Binding of Type I, I1/2, and II Inhibitors to Eph Tyrosine Kinases. *ACS Med Chem Lett* **2015,** *6* (1), 79-83.
101. Karaman, M. W.; Herrgard, S.; Treiber, D. K.; Gallant, P.; Atteridge, C. E.; Campbell, B. T.; Chan, K. W.; Ciceri, P.; Davis, M. I.; Edeen, P. T.; Faraoni, R.; Floyd, M.; Hunt, J. P.; Lockhart, D. J.; Milanov, Z. V.; Morrison, M. J.; Pallares, G.; Patel, H. K.; Pritchard, S.; Wodicka, L. M.; Zarrinkar, P. P., A quantitative analysis of kinase inhibitor selectivity. *Nat Biotechnol* **2008,** *26* (1), 127-32.
102. Hubbard, S. R.; Wei, L.; Ellis, L.; Hendrickson, W. A., Crystal structure of the tyrosine kinase domain of the human insulin receptor. *Nature* **1994,** *372* (6508), 746-54.